Lehigh University
Lehigh Preserve

Fritz Laboratory Reports | Civil and Environmental Engineering

1979

Fatigue behavior of full-scale welded bridge attachments, M.S. thesis, May 1979

Bernard Barthelemy

Follow this and additional works at: http://preserve.lehigh.edu/engr-civil-environmental-fritz-lab-reports

Recommended Citation
Barthelemy, Bernard, "Fatigue behavior of full-scale welded bridge attachments, M.S. thesis, May 1979" (1979). *Fritz Laboratory Reports.* Paper 2228.
http://preserve.lehigh.edu/engr-civil-environmental-fritz-lab-reports/2228

This Technical Report is brought to you for free and open access by the Civil and Environmental Engineering at Lehigh Preserve. It has been accepted for inclusion in Fritz Laboratory Reports by an authorized administrator of Lehigh Preserve. For more information, please contact preserve@lehigh.edu.

High Cycle Fatigue of Welded Bridge Details

FATIGUE BEHAVIOR OF FULL-SCALE WELDED BRIDGE ATTACHMENTS

by

Bernard Barthelemy

A Thesis

Presented to the Graduate Committee

of Lehigh University

in Candidacy for the Degree of

Master of Science

in

Civil Engineering

LEHIGH UNIVERSITY
Bethlehem, Pennsylvania 18015

May 1979

CERTIFICATE OF APPROVAL

This thesis is accepted and approved in partial fulfillment of the requirements for the degree of Master of Science.

July 5, 1979
(date)

Professor John W. Fisher
Professor in Charge

Professor David A. VanHorn
Chairman of Department

ACKNOWLEDGMENTS

The experiments and analytical studies reported herein were conducted at Fritz Engineering Laboratory, Lehigh University, Bethlehem, Pennsylvania. Dr. Lynn S. Beedle is the Director of Fritz Laboratory and Dr. David A. VanHorn is the Chairman of the department of Civil Engineering. The work was part of a fatigue research program entitled "Fatigue Behavior of Full-Scale Welded Bridge Attachments" sponsored by the National Research Council, Transportation Research Board, under contract NCHRP 12-15(3), and directed by John W. Fisher.

The interaction with Dr. John W. Fisher, the professor in charge, was helpful in establishing the limits of the research and relating the findings to his past experience. The author is also indebted to Mr. Brian W. Price and Mr. Hajime Hosakawa for their assistance and Dr. Celal N. Kostem for his advice in computer activities.

Sincere thanks are due to various support personnel in Fritz Laboratory. Ms. Shirley Matlock typed the manuscript. Mr. John M. Gera took charge of the drafting of the figures. Mr. Richard N. Sopko provided the required photographs.

TABLE OF CONTENTS

LIST OF TABLES

LIST OF FIGURES

Figures

ABSTRACT

The fatigue resistance of gussets welded to the tension web or flange of steel bridge beams in order to provide attachments for the lateral bracing was studied. Both theoretical and experimental evaluations on 18 W27x145, W27x114 and W36x160 full-size girders was carried out, and indicated that all web gusset details yielded fatigue strengths that equaled or exceeded Category E. Only the ends of the lateral attachments developed detectable fatigue crack growth. None of the details exhibited fatigue cracking adjacent to the transverse stiffeners. The web gusset welded to one web surface with no connection to the stiffener provided good behavior with no adverse effect in web gap between stiffener and lower flange. No adverse effect was found from the lateral bracing and its imposed out-of-plane movement of the web gusset. The experimental observations were in general agreement with the theoretical model for the end of the detail. The model had a tendency to overestimate the severity of the detail. Simplified fatigue life computations were in general agreement with the experimental observations.

The theoretical calculations were carried out on a W27x145 girder using the finite element method. This permitted the stress concentration factors in high-stress locations to be evaluated. The stress intensity factor was computed from the results using the stress gradient effect. The Paris Power law was used to compute the fatigue life.

The conclusions concerning the flange gussets indicated that none of the flange details exhibited evidence of fatigue crack growth, even at very high stress range levels. The "zero" radius details had the weld end (and toe) ground smooth and this resulted in a large increase in fatigue resistance. The experimental results suggested that the ground radius details were always below the crack growth threshold as no crack growth was observed at any level of stress range. Extensive failure from other details prevented development of fatigue data for the flange gussets.

A retrofitting technique used in this experimental study was to drill holes at the crack tips. This technique was reasonably successful. No general rule concerning its efficiency was developed. Often, the fatigue crack reinitiated at the drilled hole, depending on the crack size and stress range that existed.

This study has indicated that the design criteria for lateral connections should be maintained as currently practiced. These details have exhibited a satisfactory fatigue resistance which is in agreement with the specification provisions. Consideration should be given to grinding groove welded gusset ends, since this practice can lead to a substantial improvement in fatigue behavior.

1. INTRODUCTION

Fatigue resistance of steel highway bridges has become an important problem and has been studied very intensively during the past 10 years because a lot of welded details, which are quite common in such bridges, have shown fatigue distress. Sometimes this has led to spectacular failures, like those of the King's Bridge in Australia and the Point Pleasant Bridge in West Virginia. It has been demonstrated that welded details are much more sensitive to fatigue cracking than bolted details, due to the fact that a weld has inherent discontinuities and higher stress concentration conditions which permit fatigue cracks to be easily initiated.

Extensive research in the early 70s[1,2] has shown that the fatigue life is mainly a function of the geometry of the welded detail and the stress range, S_r. The AASHTO Specifications[3] were based on these studies. The stress range values (Table 11) were derived from the 95% confidence limit of 95% survival given by experimental S_r-N curves (Figure 11). Unfortunately, these curves cannot be used in all circumstances, because in many cases the welded detail cannot be directly related to the available experimental data. Also, the stresses in the vicinity of complex details are rarely known with accuracy. Among the welded details used in steel highway bridges for which the fatigue behavior is not well known are gusset plates welded either on the lower flange or to the web of the girders (see Figure 12). In fact, almost all steel bridges require this kind of lateral attachment which is

used primarily to support lateral bracing. The bracing is used to resist forces due to wind or live loading and lateral movement. Unfortunately, field experience has shown that some details have poor fatigue resistance, mainly because of out-of-plane movements of the gusset caused by relative bending of longitudinal members. This phenomena has been discussed in detail by Fisher.[4]

It is the purpose of this study to provide more information on the fatigue behavior of such details and to develop recommendations for design. This study considers both experimental and theoretical approaches which are described hereafter in parts 2 and 3 of this report. Section 3 compares the results and develops conclusions of this research.

2. EXPERIMENTAL ANALYSIS

2.1 Description of Tests

The experimental part of this research consisted in the fatigue testing of eighteen full-size beams fabricated from A588 steel. These beams are described on Figure 21a and b. Three different profiles were selected: W27x145, W27x114 and W36x160 rolled beams. Three primary details were either fillet-welded or groove-welded on each beam. Two details were welded on the lower flange and one on the web at mid-span. The flange details were grouped as follows (see Figure 21a): Detail 1 with R = "0" (radius at end of connection), detail 2 with R = 5 cm, and detail 3 with R = 15 cm. The web details were also grouped into three types as illustrated in Figure 21b. Two beams were tested with each combination of the primary flange and web details, at two different load ranges. All welds were 0.937 cm fillet welds.

Figure 21c is a photograph of a typical web detail with the lateral bracing members bolted into place. Figure 21d shows the radiused ends of the primary groove welded flange details. Even the R = "0" detail had a small radius ground at the weld end. Since the detail was groove welded to the flange tip, the weld run-out region was ground out by the fabricator. The radius was observed to be about 5 to 10 mm.

The loads were applied in two symmetrical locations 1.5 m apart as shown schematically in Figure 22. Their magnitude and location,

as well as the location of the lateral gussets welded to the lower flange were such that the same desired nominal stress range $\Delta\sigma = \sigma_{max} - \sigma_{min}$ was achieved along the central web-to-gusset weld and at the inner corner of the lateral gussets. The load and stress ranges thus defined are given in Table 21. Since these loading ranges were within the maximum dynamic capacity of the jacks, there was no alternate loading, i.e. the stresses were only variable in magnitude but did not change from compression to tension or tension to compression at a given location. The test setup is described in Figure 22. The W27x145 and W27x114 girders were tested using an Amsler system composed of two pulsators (variable stroke hydraulic pump) and two jacks. The maximum stroke of the system with a single pulsator was lower than the deflection of the beams under the maximum load, hence it was necessary to use two pulsators to reach the maximum stress range, each of them operating one jack. The W36x160 girders were tested using an MTS system consisting of two hydraulic jacks each with a capacity of 889.60 kN. Each jack operated from a separate control unit. This system offers the following capabilities that are not available with the Amsler system:

- Increased load capacity per jack
- Variable operating frequency
- Increased stroke capacity
- Random load programming
- Various wave forms.

The girders were fully instrumented in order to provide measurements of stresses at different locations. The tests were controlled by strain measurements.

The strain gages were located as follows:

- Two gages under the lower flange at mid-span (the tests were controlled using these two gages)
- Three gages under the lower flange 162.5 cm from one support
- One gage on the web at mid-distance between stiffener and lower flange
- One gage on the web 5 cm above the web-to-gusset weld toe
- Four gages on the web gusset plate (see Figure 23).

2.2 Test Results

Since the theoretical computations were only available for the W27x145 girder, only the test results related to this shape are reported here. The entire set of results may be found in a separate report.

Two beams were tested for each detail: one was subjected to the maximum load range permitted with the two coupled Amsler pulsators, the second beam was tested at about half (details 2 and 3) or 3/4 (detail 1) of this load range.

To enlarge the scope of this research, some supplementary details were welded on web and/or lower flange of some beams. They are shown in Figures 24a and b.

Supplementary detail 1 consisted of two 40x10x5 cm plates welded on both sides of web. The distances X and Y (see Figure 24) were varied in order to achieve a given stress range at point A. Both groove and fillet welds were used to attach these plates to the beam web.

Supplementary detail 2 consisted of two 60x20x1.25 cm plates welded on the lower flange opposite the gusset plates which were already welded to the flange (R = 0). Transverse fillet welds with 0.95 cm legs were placed at each end of the plate and stopped 1.25 cm from the flange edge. There were no longitudinal welds.

Supplementary detail 3 consisted of two 60x7.5x0.95 cm plates welded together with incomplete penetration welds and then fillet welded to the web.

Supplementary detail 4 consisted of one 40x20x5 cm insert through the web at a location symmetrical of detail 1. This detail was fillet-welded on both sides of the web. The results are not presented in a chronological order.

2.2.1 W27x145, Web and Flange Detail 1

2.2.1.1 Low Stress Range

Supplementary detail 3 was welded on this beam. The theoretical stress ranges at points B and C (see Figure 24) was respectively 59 and 70 MPa, based on ΔP = 348.35 kN. The theoretical bending stress range along the web-to-gusset weld was 62.06 MPa.

The stress range measured by strain gages are given in Table 22a.

Since the two plates constituting detail 3 were welded together with incomplete penetration, only a very short time (23,000 cycles) was required to crack the plates their full width. The crack then propagated slowly into the web. At N = 1,150,000 cycles, the web surface crack was more than 5 mm above and below the longitudinal fillet welds connecting the detail to the web. At N = 2 million cycles the crack was through-thickness. Two 19 mm diameter holes were drilled 4 cm apart to stop the crack, and the test was resumed. At N = 2.85 million cycles, the crack had reinitiated from these holes. Two new holes were drilled at the crack tips, and local compression stresses were induced by installing high strength preloaded bolts in these holes. Furthermore, two plates were also clamped on top and bottom surfaces of the longitudinal plates of the cracked detail to increase its stiffness and to minimize the crack opening. The crack did not propagate further after this action was undertaken. The different stages of the propagation are illustrated in Figure 25.

At N = 4.68 million cycles a through-thickness crack was detected at the inner supplementary detail weld toe. The crack was about 50 mm long. Two 19 mm holes were drilled at the crack tips and the test was resumed. At that time a small crack was also detected at web-to-gusset weld toe. At N = 5 million cycles it was decided to stop that crack by drilling two holes at the crack tips, 25 mm apart. At N = 6.3 million cycles the crack at the supplementary detail weld toe had extended from holes. The lower crack tip was about 25 mm above the lower flange. A 25 mm hole was drilled and a high strength bolt was installed and tightened before test was resumed.

At N = 9.3 million cycles crack reinitiation was observed from holes of the crack at the web-to-gusset weld toe.

No evidence of crack growth was observed at the flange gussets and the tests were discontinued.

2.2.1.2 High Stress Range

Supplementary details 1 and 2 were fillet welded on this beam, with X = 193 cm and Y = 12.7 cm giving a theoretical stress range of 78.33 MPa at point A (see Figure 24).

The theoretical bending stress range along the web-to-gusset weld was 82.74 MPa.

The measured stress range is given in Table 22a. The test was stopped by excessive deflections at N = 782,000 cycles. A through-thickness crack had developed at the interior corner of supplementary detail 1. It ran from about 3 cm above point A down to the lower flange. Holes were drilled in the web at the crack ends in an attempt to arrest crack growth. Unfortunately further propagation was experienced and at N = 970,000 cycles the test had to be stopped and the beam removed. The crack had propagated through the lower flange thickness and was about 18 cm long and 8 cm above the upper hole. Figure 26a shows the crack after it was initially stopped. Figure 26b shows the crack at termination of the test.

2.2.2 W27x145, Web and Flange Detail 2

2.2.2.1 Low Stress Range

Supplementary detail 1 was installed at with X = 193.04 cm and Y = 12.70 cm, giving a theoretical stress range of 39.16 MPa at point A (see Figure 24). The detail was fillet-welded to the web.

The theoretical bending stress range along the web-to-gusset weld was 41.37 MPa. The actual stress ranges measured during the test are given on Table 22b.

No cracking was observed until 4.3 million cycles. At that time, very small cracks were detected by visual inspection at one

end of the supplementary detail on both sides of the web. These cracks did not exhibit appreciable growth until 14.3 million cycles. At 17.7 million cycles a through-thickness crack developed and testing was discontinued.

The crack at the lower inner corner of the supplementary detail is shown in Figure 27. The delay between crack initiation and through thickness propagation may be due to the fact the crack had to propagate through the weld on the opposite side of the beam web.

2.2.2.2 High Stress Range

Supplementary detail 1 was installed with X = 193 cm and Y = 12.7 cm giving a theoretical stress range of 78.33 MPa at point A (see Fig. 24). The detail was fillet welded to the web.

The theoretical bending stress range along web-to-gusset weld was 82.74 MPa (Fig. 23).

The measured stress range could not be obtained due to a malfunction of the oscilloscope. The test was controlled by deflection gages at mid span.

Cracks were observed at the supplementary detail weld toe after N = 1.1 million cycles. Holes were drilled at the crack ends after N = 1.4 million cycles and preloaded high strength bolts were used to induce compression stresses in the region at crack ends. After 1.8 million cycles 2 cracks were observed at the web-to-gusset weld toes. At N = 1.9 million cycles, these two cracks had reached 2.5

and 5 cm length. At N = 2 million cycles, the two cracks had developed through thickness. Holes were drilled at crack ends. After 2.3 million cycles the crack at supplementary detail reinitiated from bolt holes and propagated very quickly down through the bottom flange and up to the top flange.

Figure 28 shows the crack at its final stage.

2.2.3 W27x145, Web and Flange Detail 3

2.2.3.1 Low Stress Range

No supplementary detail was welded on this girder. The theoretical bending stress range along the web-to-gusset weld was 41.37 MPa. The actual stress ranges measured by strain gages are shown in Table 22c.

The test was discontinued after 9 million cycles without any visible cracking.

2.2.3.2 High Stress Range

Supplementary details 1 and 4 were installed at X = 193 cm and Y = 12.7 cm giving a theoretical stress range of 78.33 MPa at points A (see Figure 24). Detail 1 was groove welded to the web. Detail 4 was fillet welded on both sides of the web.

After only 1 million cycles a through-thickness crack developed at the inner weld toe of fillet-welded supplementary detail 4. The total length of the crack was about 10 cm. To stop its propagation,

a 19 mm diameter hole was drilled at its upper end and a preloaded high-strength bolt was used to induce compressive stresses at this end. The crack having already reached the lower flange, it was stopped by drilling two holes through the flange on both sides of the web, then clamping plates on top and bottom flange surfaces. After 1.5 million cycles a through-thickness crack was observed at the inner weld toe of the supplementary detail 1. Two 19 mm holes were drilled 9 cm apart to stop it. At 1.6 million cycles a through-thickness crack was noticed at one of the web-to-gusset weld toes. Two 19 mm holes were drilled 7 cm apart to stop it.

The test was discontinued after 1.8 million cycles since the crack at supplementary detail 1 reinitiated from noles and propagated down through the flange.

2.2.4 Complementary Experiment

One of the purposes of this experimental research was to investigate the effect of the gap between web and bracing member end on the fatigue behavior of that detail. One beam (W27x145, detail 3) was prepared so that two gaps (7.5 and 12.5 cm) could be obtained on the web gusset. Static tests were carried out and the deflections were recorded at three different locations as illustrated in Figure 29. Dial gage 1 was under the lower flange at mid-span. Gages 2 and 3 were located under the bracing members.

For each position of the lateral bracing system, deflections were recorded for several loads. The average of these readings is

summarized in Table 23. g_1, g_2 and g_3 are defined in Fig. 210. Δ_1, Δ_2 and Δ_3 are deflections recorded by dial gages 1, 2 and 3 respectively. The experiment confirmed that there was an out-of-plane movement of the gusset plate, since the deflections recorded under the bracing members were 89 to 96% of those recorded under the lower flange. But more important is the fact that the relative deflections, i.e. the out-of-plane movement of the gusset plate, don't change substantially when the geometry of the connection was modified. For example, the relative change of out-of-plane movement when $g_1 = g_2 = g_3 = 75$ mm and when $g_1 = g_2 = g_3 = 125$ mm was:

$$\frac{(\Delta_1/\Delta_3)_{125} - (\Delta_1/\Delta_3)_{75}}{(\Delta_1/\Delta_3)_{75}} = 0.041 = 4.1\%$$

when considering gages 1 and 3

$$\frac{(\Delta_2/\Delta_3)_{125} - (\Delta_2/\Delta_3)_{75}}{(\Delta_2/\Delta_3)_{75}} = 0.057 = 5.7\%$$

when considering gages 2 and 3. One may conclude that there is a very limited effect of the gaps on the out-of-plane movement of the gusset plate because the relative out-of-plane movement is so small.

2.3 Summary of Test Results

The fatigue tests are summarized in Table 24. Figure 211 shows fatigue lives of details that have failed during the test. The fatigue lives are based either on the number of cycles at crack initiation, when available, or on the number of cycles at through-thickness propagation.

At the web-to-gusset weld toe (critical location a), we expected a Category E behavior, mainly because of the influence of secondary bending. The test results plotted in Figure 211 indicated that under the worst condition Category E satisfactorily defines the fatigue resistance. The test data fall within the upper and lower confidence limits of the cover-plated beams used to derive the design category. The out-of-plane movement of the gusset plate was much smaller than expected. Therefore, the secondary bending was never a critical factor.

At the interior web-to-gusset weld toe (critical locaion b in details 1 and 2, Figure 31), we expected a better behavior than at critical location a, because of the more favorable stress field. The behavior of this detail was very good, since no cracking was experienced (at least no crack detectable by dye-penetrant technique).

At the gusset-to-stiffener weld toe (critical location c in detail 1 only, Figure 31), the only evidence was some reported results from Canada on Conestoga River Bridge[25] which used gusset plates of the type depicted in Figure 327. This type of gusset plate does not allow the longitudinal forces to be carried through the plate and therefore creates high stresses at location c. This particular problem has been investigated (see Chapter 3) and is discussed in the general conclusion (see Chapter 4).

The flange gussets never cracked, even when the radius was equal to zero. This is due to the fact the longitudinal groove weld toe had been ground, which is not the common practice (see Figure 21).

When fillet welded to the web, supplementary detail 1 behaves as a category E detail. One test performed with a groove-welded detail, provided a fatigue life at through-thickness propagation comparable to the fatigue life of the fillet-welded detail. Further studies are underway on this detail.

Supplementary detail 2 did not experience any fatigue crack growth at category E stress range levels. That is in good agreement with flange gusset behavior.

Supplementary detail 3 experienced very rapid fatigue crack growth in the weld between the two plates. The total life for through web thickness propagation was equivalent to category E (see Figure 21).

One beam was tested with supplementary detail 4. It provided about the same behavior as supplementary detail 1.

Further experiments are underway and should provide additional test data on these classes of details so that reasonable estimates of their behavior can be made.

3. THEORETICAL ANALYSIS

3.1 Problem Formulation

It has been recognized that the fatigue life can be analytically predicted by an empirical relationship between the crack growth per cycle da/dN and the fracture mechanics stress intensity factor ΔK. In this study the Paris Power Law[5], was used where:

$$\frac{da}{dN} = C(\Delta K)^m \tag{31}$$

where:

a = the crack length

N = the number of cycles

C,m = material constants

ΔK = stress intensity factor range $(K_{max}-K_{min})$

The stress intensity factor range ΔK may be estimated from Irwin solution of the central through crack in an infinite plate under uniaxial stress:

$$\Delta K = \Delta\sigma \sqrt{\pi a} \tag{32}$$

using four adjusting factors F_e, F_s, F_w and F_g[6] to account for the conditions that exist at actual details. This resulted in

$$\Delta K = F_e\ F_s\ F_w\ F_g\ \Delta\sigma \sqrt{\pi a} \tag{33}$$

F_e adjusts for the shape of the crack front; F_s is the free surface correction; F_w accounts for the finite plate width and F_g is related

to the stress gradient effect. The first three factors can be estimated from previous studies.[6,7] The last factor, F_g, is strongly dependent upon the geometry of the detail and the stress field in its vicinity. In a recent study, Zettlemoyer[6] developed F_g expressions for several details encountered in steel bridges (i.e. coverplates and stiffeners). They may not be generally applicable to different situations. It is the purpose of this study to compute the correction factors to be used for the details shown in Fig. 12.

F_g is a function of the detail geometry and the stress gradient. Generally, it cannot be determined in a closed-form solution since the stress field cannot be determined analytically. Numerical techniques, such as the finite element method (FEM) must be used. In this study, the SAP IV program[8] was used to determine the stress concentration contours for each critical location.

The theoretical study may be summarized in four main steps:

- computation of K_T by FEM
- computation of F_g as a function of K_T
- computation of ΔK as a function of F_g and the three other correction factors.
- computation of the fatigue life using the Paris power law.

This approach limits itself to the through-the-thickness crack propagation, which may only be a part of the total fatigue life of the structure.

3.2 Field of Investigation

Among the nine different details used for the experimental research, three were selected for the analytical examination:

Detail 1: gusset plate welded to the web of W27x145 girder. Stiffener welded to the gusset plate.

Detail 2: gusset plate welded to one web surface with no connection to the stiffener

Detail 3: idem, but stiffener welded on opposite side of the web.

These three details are shown on Figure 31. Also shown in this figure are the high stress locations where fatigue cracks are likely to be initiated.

The computations were performed assuming a load range of 464.46 kN. This resulted in a stress range of 82.74 MPa along the weld between web and gusset plate.

Young's modulus and Poisson's ratio were respectively 2×10^5 MPa and 0.30.

3.3 FEM Investigation Procedure

The finite element method and substructuring techniques were used in the sequence shown in Figure 32 to estimate the critical stress conditions. The procedure is schematically illustrated in Figure 33 for the case of the critical location a in detail 1.

Three two-dimensional (2D) discretizations using the substructuring technique (each mesh considering only a small part of the previous one) were necessary before a more accurate three-dimensional (3D) analysis was carried out. It was not possible to perform a single analysis of the whole half-beam (it is obvious that by symmetry a discretization of the whole beam is not necessary) fine enough to give stresses or displacements directly that could be input in the 3D mesh of the selected detail. In fact, two unfruitful attempts were made using 598 and 262 nodal points: in each case the computation time exceeded 400 SS! In order to avoid excessive computation time, the first three steps of the analysis were as follows:

(1) First a very crude analysis of the whole half-beam was performed, as shown in Figure 34. Plate bending elements were used in the web, the lower flange and the gusset plates. Plane stress elements were used in the stiffener and the upper flange. The lateral bracing members discretized by beam elements, were connected to external corners of the gusset plates and fixed at the other end. The effects of the type of connection between the gusset plate and the lateral bracing, as well as those of an elastic support of the

other end, were studied separately.

(2) The second 2D mesh only considered the part of the beam between the cross section under the load and the mid-span. The lateral bracing members connected to the central gusset were suppressed and the displacements and rotations computed in the first analysis were induced through boundary elements at external corners of the gusset plate. The displacements and rotations were applied to the nodal points of the cut-off sections. These meshes are shown in Figure 35.

(3) The third step was a 2D analysis of the most critical areas for each detail, based on experience. These locations are shown in Figure 31. For detail 4 three critical locations were selected at web-to-gusset and gusset-to-stiffener welds. In case of detail 2, only the critical locations along the web-to-gusset remain, since the stiffener is no longer welded to the gusset plate. For the third detail, there is only one critical location, at the web-to-gusset weld toe. However, the whole weld length was examined for out-of-plane movement in order to check other possible high stress locations. These meshes are shown in Figure 36.

The effect of the weld size, which is one of the most important factors influencing the stress concentration was not taken into account by the earlier discretizations. It was obvious it has to be included in the analysis by describing each critical location in a

3D analysis. This was done using 8-nodes bricks of SAP IV program.[8] Figure 37 shows the discretized details.

The displacements along the cut-off lines, given by the previous 2D analysis, were induced at mid-thickness of the web and the gusset plate. Also the weld was idealized as shown in Figure 38. The use of very skewed elements can decrease the reliable of the FEM analysis. Unfortunately there is no way to avoid these problems. Another practical problem that had to be solved for these 3D discretizations was the consistency between the numbering patterns of cubic and skewed elements. After several tests on a small auxilliary structure, a numbering pattern was developed that avoided the negative diagonal warning. The results of this pilot study are summarized in Figure 39 and Table 31. The numbering pattern of a prism and a pyramid is illustrated and related to a cubic.

Once these 3D analysis had been performed, the next step (see Figure 32) was to go back to a 2D analysis of each critical location by discretizing a section of the previous 3D mesh. This procedure is illustrated in Figure 310 for critical location a. The section was selected between cubic elements in order to contain enough nodal points for the displacements input. Only a small part of the section near the critical location was discretized. For example, in case of critical location a, half of the web thickness and 1.25 cm length were used. The longest and the smallest element sides were respectively 0.125 and 0.03125 cm. These meshes are shown in Figure 311.

For the small part of the structure discretized, the out-of-plane movement was previously accounted for and hence plane stress elements were used instead of plate bending in the previous 2D discretizations.

The last 2D analysis was performed discretizing a very small area near the weld toe. For example, the last mesh in case of critical location "a" considered only three elements adjacent to the weld toe of the previous mesh. The smallest elements in this mesh were 0.039 mm plane stress elements. At this stage, the element size was smaller than most initial discontinuities in the structure (see 361). Any finer analysis would have been unreliable.

3.4 Results of Analysis

3.4.1 Stress concentration factor (SCF) definition

3.4.1.1 Web nominal stress range and SCF at critical locations a and b

Most texts define the stress concentration factor as the actual stress at a point in a given direction divided by the nominal stress at the same point and in the same direction.

During the computation of the specimen loading range, it has been assumed that the stress range along the web-to-gusset weld should be 82.74, 62.06 or 41.37 MPa. The FEM analysis has been conducted for the case $\Delta\sigma$ = 82.74 MPa by applying a load range ΔP = 464.46 kN.

The stresses calculated by the FEM analysis were somewhat different from the assumed values. Table 32 gives the stresses in the web around critical locations a and b. Elements 1 to 4 are 65 mm square elements counted clockwise around the critical location, number 1 being at the upper left corner. The average stresses range between 52.52 and 62.61 MPa and never reach 82.74 MPa.

On the other hand, the measured stresses were in good agreement with the assumed values, as shown in Table 32.

The discrepancy between FEM analysis and strength of material bending formulas is likely due to the size of the elements around the critical locations. Only average values in the element result from such large elements.

Therefore, the computations were conducted with the assumed value of the web nominal stress range, i.e. 82.74 MPa. The SCF was defined as:

$$SCF = \frac{1}{82.74} \text{ (actual stress at weld toe)} \qquad (34)$$

3.4.1.2 Gusset nominal stress range and SCF at critical location c

The definition of the nominal stress range is difficult in case of critical location c, since no easily usable strength of material's formula can be applied. The FEM analysis showed that the stresses varied from zero to about 40 MPa at distances ranging between zero and 17 cm from the gusset-to-stiffener weld toe, without any obvious trend. The strain gage measurements also show this high variability (see Table 22) with no obvious trends.

3.4.2 Results of analytical studies

The SCF contours are shown in Figures 312 to 317. An important comment about these SCF contours concerns the physical meaning of values higher than σ_y/σ_n, i.e. actual stresses larger than the yield strength of the material. Such a situation could not be avoided since SAP IV is a linear elastic program. The actual stress field in the vicinity of the weld toe should exhibit a small plastic zone, whose size effects the whole stress field. The SCF given by the FEM analysis often exceeds 3.0 (i.e. $\sigma > \sigma_y$) at distances from the weld toe smaller than 0.25 mm. That distance is of the same order of magnitude as the initial crack size and the accuracy of the weld discretization. Furthermore, it is much smaller than the final critical crack size, which appeared to be several millimeters. The effects of the plastic zone on the stress field at the weld toe vicinity were neglected. It is demonstrated (see 355) that the propagation of this plastic zone as the crack grows does not affect the fatigue life computation. In case of critical location c, the SCF contours were not defined, since no nominal stress at that location could be obtained either from FEM analysis or from strain measurements. Therefore Figure 314 only shows stress contours without any reference to a nominal stress value.

3.5 Stress Intensity Factor

3.5.1 General expression of ΔK

As stated in Art. 21, the stress intensity factor K_I can be expressed using the well-known value of K_I for a central through crack in an infinite plate under uniaxial stress ($K_I = \sigma\sqrt{\pi a}$) adjusted by four correction factors F_e, F_s, F_w and F_g, which take into account the shape of the crack, the free surface and the finite width effects, and the stress concentration at the crack vicinity. The stress gradient factor, F_g, may be computed from the previous finite element analysis. A brief literature survey provides expressions for the three other correction factors.

3.5.2 Crack shape correction factor

The stress intensity factor at any point along the perimeter of an elliptical crack embedded in an infinite body subjected to uniform tensile stress (see Fig. 318) is given by:[9]

$$K_I = \sigma\sqrt{\frac{\pi a}{Q}}\left(\sin^2\beta + \frac{a^2}{b^2}\cos^2\beta\right)^{1/4} \qquad (35)$$

where $Q = [E(k)]^2$

E(k) is the complete elliptical integral of the second kind:

$$E(k) = \int_0^{\pi/2} (1-k^2\sin^2\theta)^{1/2}\, d\theta \quad \text{with} \quad k^2 = 1 - a^2/b^2 \qquad (36)$$

K_I is maximum at the minor axis end of the ellipse ($\beta = 90^\circ$). This is why the minor axis length a has been chosen as the crack length in Eq. 35. The crack shape correction factor is therefore:

$$F_e = \frac{1}{E(k)} \quad \text{for} \quad \beta = 90^\circ \qquad (37)$$

It varies between 1.0 and $\pi/2$ as the ratio a/b varies between zero and 1.0.

The actual crack shape is a semiellipse submitted to a complex stress field due to the bending of the girder, the out-of-plane movement of the gusset plate and the stress concentration caused by the crack itself. Although several studies have been performed,[10] they cannot be directly used in this particular situation. The crack shape correction factor does not vary substantially

for different loading configuration. Therefore we used $F_e = 1/E(k)$ in our fatigue computations.

Since the crack shape experiences a variation during the growth, it is necessary to know the equation linking major and minor axis lengths in order to compute F_e at each stage of crack propagation.

Several experimental reports[2,11,12] provide measurements on the size and shape of cracks growing from coverplates and stiffener fillet weld toes and from gusset plates groove welded to flange tips. There is only one investigation applicable to the type of details studied here. Maddox[12] investigated a gusset plate which was fillet welded to a plate subjected to tension force. Cracks grew from the toe of the short transverse fillet at either end of the gusset. Maddox developed the following equation from the experimental data.

$$b = 3.355 + 1.29\ a \qquad (38)$$

The validity of this equation has been discussed in details by Zettlemoyer.[6] Although it may have some deficiencies, it is rather well correlated to experiments. It was used to describe the crack shape in this study.

According to this equation, the visible crack lengths when the crack has propagated through the web or the gusset plate are respectively 22.71 and 19.48 mm

3.5.3 Front free surface correction

A front free surface is of course only necessary for edge cracks since the stress is zero on the free boundary. In actual situations, such as the ones studied here, displacement is generally restricted on the free surface. The magnitude of this restriction is not known to any specific degree although it is estimated to be quite modest.[6] Thus we can neglect it and consider we have simple edge cracks.

Zettlemoyer[6] summarized the work of Tada and Irwin[13] who tabulated the variation of F_s with the distribution of stress applied to the crack for the extreme conditions of through ($a/b = 0$) and circular ($a/b = 1$) crack fronts. Table 33 shows the variability for the types of stress distributions common to bridge details. It must be pointed out that some values have been extrapolated from positions other than the free surface, since the existing solutions are not accurate there.

According to Zettlemoyer, the following simplified formula

$$F_s = 1.0 + 0.12\left(1 - \frac{a}{b}\right) \tag{39}$$

provides a reasonable estimate and was adopted for use in this study.

3.5.4 Back free surface correction

The correction factor, F_s, takes into account the front free surface effect, but assumes an infinite half space. Since the space is not infinite, another correction factor must be introduced. Nevertheless, during a large part of the fatigue life, the crack depth is small enough by comparison to the plate thickness so that the back surface correction can often be neglected. F_w is approximately equal to 1.0 for a large range of a/t_p (a = crack depth, t_p = thickness of plate) when the crack shape is near semi-circular.[12]

The finite width correction, or back free surface correction was therefore assumed to equal 1.0 for this study.

3.5.5 Plastic zone effect

In fracture problems, the plastic zone at the crack tip has considerable importance, because it modifies the stress distribution in the vicinity of the crack (see Figure 319).[14] In fatigue problems, we generally disregard this effect since small stress ranges and reverse yielding cause the plastic zone to be very small. We have neglected it in the computations presented here.

3.5.6 Stress gradient correction

As previously stated, the stress gradient correction takes into account the actual stress field in the vicinity of the critical location. More precisely, it is computed from the stress

gradient along the potential crack path. The finite element analysis provides SCF in any direction and at any distance from the weld toe. To use these results we have to know the crack path through the web or the gusset plate thickness.

3.5.6.1 Crack path

It is well known that a crack generally originates at the maximum tensile stress location and propagates along the minimum principal stress trajectory through that origin. That trajectory can be defined by using the results of the finite element analysis. The minimum principal stress trajectory represents the probable crack path only in cases where the propagation is of the unstable, catastrophic variety.[6] During fatigue crack propagation, the stress field has time to redistribute itself with each increment of crack growth and may result in a directional change. Determining the actual crack path would require a finite element analysis for each increment of crack growth, which could not be economically done here. We can only say that the minimum stress trajectory and a crack line constantly perpendicular to the applied stress represent the physical limits of the path. It has been shown by Zettlemoyer[6] that in most cases the actual crack does not vary greatly from a straight line through the point of maximum concentration and perpendicular to the direction of applied stress. Further, the difference in perpendicular stress (Mode I) is not great. The crack path was assumed to be the perpendicular one illustrated in Figure 320.

The computation of fatigue life was done using the values of the SCF along that assumed crack path.

3.5.6.2 Stress gradient correction

As it has been demonstrated by Tada, Paris and Irwin,[15] the stress intensity factor can be evaluated by simply considering the crack submitted to traction forces equal to those of the stress distribution in the uncracked solid. Since the distribution and magnitude of these traction forces are usually irregular for real structural details. The concept suggested by Irwin and used by Albrecht,[7] (see Figure 321) can be used. The stress intensity for this configuration is:

$$K = \frac{2P}{\sqrt{\pi a}} \frac{a}{\sqrt{a^2 - \rho^2}} \tag{310}$$

The force P can be broken into stress over an incremental length ($P = \sigma_e \times d\rho$) in order to get the stress intensity along the entire crack length as follows:

$$K = \sqrt{\pi a} \times \frac{2}{\pi} \int_0^a \frac{\sigma_e \, d\rho}{\sqrt{a^2 - \rho^2}} \tag{311}$$

If the stress on element ℓ is expressed in terms of the nominal stress σ_n, the stress ratio σ_e/σ_n is the SCF at the distance P, namely $K_{T\ell}$.

Since $\sigma_n\sqrt{\pi a}$ is the SCF for a through crack in an infinite plate under uniform uniaxial stress, the balance of the

expression for K is the correction factor $F_g(a)$, as a function of the crack size a:

$$F_g(a) = \frac{2}{\pi} \int_o^a \frac{K_{T\rho}}{\sqrt{a^2-\rho^2}} \, d\rho \tag{312}$$

Equation 312 can be solved either by assuming an analytical expression for SCF,[6] or by using numerical values as suggested by Albrecht:[7]

$$F_g(a) = \frac{2}{\pi} \sum_{j=1}^{m} K_{Tj} \left[\arcsin\left(\frac{\rho_{j+1}}{a}\right) - \arcsin\left(\frac{\rho_j}{a}\right) \right] \tag{313}$$

where K_{Tj} = SCF in element j of the FE analysis or the average between two adjacent elements, both of equal distance along the decay line

ρ_j, ρ_{j+1} = distances from crack origin to the near and far sides of element j

m = number of elements to crack length a

Equation 313 is partly a numerical solution of Eq. 312 and partly an exact one, because the integration is carried out over the element width, and the summation over the number of elements from the center of the crack to the crack tip.

$$F_g(a) = \frac{2}{\pi} \sum_{j=1}^{m} \frac{\sigma_{bj}}{\sigma} \int_{b_j}^{b_{j+1}} \frac{d\rho}{\sqrt{a^2-\rho^2}} \tag{314}$$

If the stress distribution along the crack path is given in function form, integration of Eq. 312 by parts yields:

$$K = \sqrt{\pi a}\left[\sigma_a - \frac{2}{\pi}\int_0^a \arcsin\left(\frac{\rho}{a}\right)\frac{d\sigma}{d\rho}\,d\rho\right] \qquad (315)$$

where σ_a is the value of the applied stress at $\rho = a$.

3.6 Predicted Fatigue Life

The Paris power law was used to compute crack growth, knowing the stress field in each critical area and the various correction factors taking into account the actual geometry of the detail.

The use of Paris' power law requires knowledge of the following factors:

- the initial crack size, which may be approximated by the size of the largest possible defect in the high stress location
- the final crack size, which is a function of the fracture toughness of the material
- the material coefficients C and m

3.6.1 Weld defects

Welds are never completely defect-free. On the contrary, they generally contain discontinuities which may be classified as follows:[16]

A. Geometrical

1. Undercut
2. Overlap
3. Poor fit-up, mismatch
4. Exessive reinforcement
5. Stress concentrations in general
6. Nature of weld dressing

B. Weld character

1. Lack of penetration
2. Lack of fusion
3. Slag inclusions
4. Oxide films
5. Delaminations
6. Tungsten inclusions in GTA welds
7. Gas porosity
8. Microsegregation during cellular or dendritic growth
9. Shape of weld puddle
10. Arc strikes
11. Entrapped weld spatter

C. Metallurgical

1. Stress relief cracking
2. HAZ hydrogen embrittlement (cold cracking)
3. Weld metal solidification cracking
4. HAZ liquidation cracking (low melting int segregates)
5. Delamination of plate

D. Residual stresses

1. Constraint
2. Repair welding

It is necessary to differentiate between internal discontinuities inside the weld and smaller ones at the weld toe. In case of welded bridge structures, we are primarily concerned by small, sharp intrusions of slag emanating from the welding flux and leading to crack initiation and growth at the weld toe.[17,18] Inspection

of the origin regions of fatigue cracks has suggested that the initial defect size may be in the range of 0.05 to 0.5 mm.[19]

It is very difficult to establish a definite size of the initial defect. A range of initial crack values from 0.05 to 0.5 mm was used in this study.

3.6.2 Final crack size

It is also difficult to determine the final crack size, since this value is related to the fracture toughness of the steel and the geometry of the detail. Furthermore, the FEM analysis only concerns the SCF through the web or gusset plate thickness and therefore can only be used for the propagation through that thickness (Phase A). This phase of propagation is only a part of the total fatigue life. (see Figure 322). Phases B and C cannot be accounted for by using the expression of ΔK obtained in 35. As a first approximation, we can assume the failure is complete when the crack has grown through the plate thickness. It can be shown that the fatigue life is almost exhausted at this stage. However, experimental data has demonstrated that most of the fatigue resistance is exhausted once the crack has propagated through the plate thickness

3.6.3 Weld Shape

Based on Maddox's work[12] a correction factor for 30° fillet weld was introduced in order to study the effect of the weld slope. This correction factor is defined as the ratio of the stress intensity factors for 30° and 45° fillet welds, as a function of the ratio of the crack length a to the plate thickness W (see Table 35).

3.6.4 Paris Power Law Coefficients

The coefficients C and m have been determined from experimental results. These coefficients are primarily material constants. They are affected by environment and loading conditions. Barsom[20] has established an upper bound on the crack growth rate for ferrite-pearlite steels as follows:

$$C = 2.18 \times 10^{-13} \quad m = 3.0 \quad \text{(SI units)}$$

Hirt and Fisher[22] used an average value of C equal to 1.21×10^{-13} with m = 3.0. That C value is within the range of variation given by Maddox[23,24] i.e. 0.9 to 3×10^{-13}.

The average value of $C = 1.21 \times 10^{-13}$ and m = 3.0 was used in this study.

3.6.5 Fatigue lives computations

The computation of the fatigue life of each detail was made with the previously selected values of initial and final crack lengths and coefficients C and m. The stress intensity factor range ΔK was computed for two assumed values of the nominal stress range - 41.37 MPa and 82.74 MPa.

3.6.6 Results of computations

The results of these computations are presented in Table 36.

3.7 Complementary Investigations

The previously described general analysis does not include the effect of several important parameters. These include the size of the girder, the type of connection between bracing and gusset plate, the stiffness of an adjacent girder (in the general analysis the bracing ends were assumed fixed) and gussets welded to the lower flange. In order to take these factors into account, additional studies were performed. They are described hereafter.

3.7.1 Effect of web thickness

The effect of the girder size is mainly due to the web thickness. The thicker the web, the more rigid the girder when considering out-of-plane movements induced by the lateral bracing system. Instead of modifying all the geometrical properties of the girder, only the web thickness was considered to vary between 2/3 and 4/3 of the actual web thickness of the W27x145 beam, i.e. 1 and 2 cm. The results of these computations were compared to those from the analysis of the W27x145 beam in terms of vertical displacements and rotations around the longitudinal axis at the web-to-gusset weld toe and at the gusset at the mid-span cross-section. These two locations correspond to critical locations a, b and c. The comparison indicated (see Table 37) that the displacements and rotations decreased when the web thickness increases. The amount of the decrease was not the same for displacements and rotations. Here the question arises of which one is the best measure of the SCF variation. The rotation

around the longitudinal axis seems to be a more critical parameter (as far as the fatigue behavior of the weld is concerned) than the vertical displacement. In addition, the larger values are more conservative than those considering the vertical displacement. Hence the rotation around the longitudinal axis was used to assess the SCF variation. The SCF values from previous computations (t_w = 1.5 cm) were used to estimate the influence of web thickness. Figure 323 shows the resulting change in SCF assuming it is proportional to the change in rotation.

3.7.2 Influence of flange connections

In order to check whether or not the gussets welded on the lower flange have an effect on the behavior of the web gusset, the first three FEM analysis were repeated without these gussets on the girder. The results are compared with those obtained with the flange gussets in place.in Table 38. It appears that the gusset welded to the lower flange has an opposite effect on detail 1 than on details 2 and 3. In the first case, the vertical displacements increased where the gusset is suppressed. They slightly decrease in the two other cases. This study has indicated that the attachment of gussets to the flange have a negligible influence on the behavior of the web gussets.

3.7.3 Effect of the type of connection

Since the out-of-plane movement of the gusset plate is induced by the bending rigidity of the bracing members, the type of connection between the bracing members and the gusset plate is of major importance. The following factors appear to be the main parameters influencing this connection:

- the length of the connection and the gap between the end of the bracing member and the web plane
- the type and the size of the fasteners (bolts or welds)
- the angle between the bracing members and the girder axis.

These parameters are illustrated in Figure 324. Unfortunately, the FEM does not allow the precise introduction of these factors without the use of a very complex 3D mesh. A 2D mesh was used to examine the effect of the type of connection by changing the attachment points of the bracing members discretized by use of beam elements. These attachments points are numbered 1 to 10 in figure 325 showing the gusset plate discretization. Two different conditions were considered as follows:

Type 1: gusset plate and stiffener are welded together on the same side of the web.

Type 2: gusset plate and stiffener are each on one side of the web.

For each type, four different connection lengths were considered. They were denoted cases 1 to 4, as follows:

Case	Connecting Points	Gap (cm)
1	1, 6	5.84
2	3, 8	10.92
3	4, 9	13.46
4	5, 10	21.08

In addition, the behavior of the type 1 connection was studied with a zero gap. The largest displacements were always obtained at the web-to-gusset weld toe. Table 39 gives the displacements and rotations at that point. Examination of these results showed that none of the cases examined were significantly different. This parameter is not sensitive to the position of the stiffener or to the gap between the web and the bracing member end.

A comparison was also made of the out-of-plane bending moments along the web-to-gusset weld. These moments are shown in Figure 326. Elements E1 to E6 are the six plate bending elements along the web-to-gusset weld toe (see Figure 325). They indicate that the smaller gaps result in smaller bending moment. The stresses induced by the out-of-plane movement stay at a very low level in the gap. Thus there is no major advantage of a reduction of the gap.

This is in agreement with the experiment described in section 224. None of the beam tests gave any indication of fatigue crack growth along the web-to-gusset weld connection as a result of distortion.

In order to evaluate the behavior of more flexible (or weaker) connections (see Figure 327), two complimentary FEM analyses were

conducted for the type 2 connection case, by removing part C alone and parts A, B, C respectively (see Figure 325). The results of these studies were compared to the previous ones in terms of out-of-plane bending stresses and stresses in the direction transverse to the weld. Both web-to-gusset and the stiffener-to-gusset welds were considered (see Tables 310 and 311). When analyzing the web-to-gusset connection, bending stresses and axial stresses perpendicular to the web are of primary concern. When considering the behavior of the stiffener-to-gusset connection stresses perpendicular to the stiffener are of interest. The bending stresses along the web-to-gusset weld were not drastically altered by the cut-outs (see Table 310). On the other hand, the transverse stresses along the stiffener-to-gusset weld increase substantially when part C or parts A, B and C are cut out. One may therefore expect location c (stiffener-to-gusset weld toe) to be more critical in these special gussets than in those previously studied.

3.7.4 Effect of adjacent girder stiffness

The last parameter examined was the stiffness of the adjoining girder which was parallel to the main girder to which the ends of lateral bracing members were attached. The study was conducted on a very elementary discretization of the system using beam elements and neglecting the gusset plates and stiffener. This simplification is reasonable, since there is a linear relationship between the relative vertical displacements of the two girders and the out-of-plane movement of the gusset plate. This is the critical factor in the fatigue behavior of these details. The discretization is presented in

Figure 328. The parameter selected was a function of the rotation of the bracing member 6-7 due to the deflections and rotations of nodes 6 and 7. The definition of that critical parameter, called φ, is illustrated in Figure 329.

Several investigations were conducted. The end stiffness was varied from zero (no adjoining girder) to infinity (fixed ends). The results are plotted on Figure 330. They are somewhat surprising, since the critical parameter φ was found to increase with decreasing torsional stiffness J at constant bending inertia I. This suggests that the situation is getting worse (from the standpoint of the out-of-plane movement of the gusset plate) when the adjoining girder twists more easily.

3.8 Estimate fatigue life

As discussed in Article 356 an accurate computation of the stress intensity factor at the web-to-gusset weld toe requires a knowledge of the stress field in its vicinity. Of primary interest is the web thickness variation when only considering the through-thickness crack propagation.

Hereafter is described a less accurate computation which doesn't require any computer work and therefore may be easily performed in any circumstance.

Crack propagation must be split into three phases as shown in Figure 222. These phases must be analyzed separately, since the

propagation mechanisms are substantially different and may not be formulated in the same way. Only fatigue crack propagation will be considered and initiation and the final fracture stage will be ignored. This simplification can be justified by the fact that the majority of steel components contain initial discontinuities or defects (see 361) which have a negligible crack initiation phase. Fracture is not a major concern since prior to reaching it, the useful life of the structural component has been essentially exhausted with through thickness propagation. Furthermore, the crack growth rate is so high during that stage that any computation would be both difficult and inaccurate.

Propagation type 1

For a part-through thumbnail crack, the stress intensity factor is given by Eq. 35 (see 352). Its maximum value is reached at the minor axis end ($\beta = \pi/2$):

$$K_I = \sigma\sqrt{\pi a/Q}$$

This expression has to be corrected by a front surfact correction factor $F_s \simeq 1.12$ and a stress concentration factor F_g which is about 2.5, according to Popov[26] who gives a stress concentration factor of approximately 2.4 for a flat plate in tension having a fillet with the ratio of curvature of fillet to plate thickness being zero. zero.

Furthermore, assuming $\sigma/\sigma_y = 0.9$, which is a very conservative value, we get $Q = 1.7$[23].

Using Paris' Power law and integrating between a_i and a final crack size equal to the web thickness (a_f = 15 mm), we get:

$$\int_{a_i}^{a_f} a^{-3/2}\, da = 1.21\times10^{-13}\ \ 1.12\times2.5\sqrt{\frac{\pi}{1.7}}^{3}\ \Delta\sigma^3\ N_1$$

Thus

$$N_1 = \frac{3\times10^{11}}{(\Delta\sigma)^3}\ \ \frac{1}{\sqrt{a_i}} - \frac{1}{\sqrt{15}}$$

Propagation types 2 and 3

The contribution to fatigue life corresponding to these stages of propagation is much more difficult to estimate. The main difficulties are:

- in stage 2, a through-thickness crack in a plate of variable thickness
- in stage 2, we have no idea of the SCF at crack tip
- in stage 3, the crack is propagating in a variable stress field due to the bending stress gradient and SCF
- the computation of the final crack size requires the knowledge of K_{IC} (or K_c if the plate is not thick enough to be in a plane strain condition) and the stress at the crack tip, which is unknown.

Nonetheless, a crude estimate of the contribution to the fatigue life corresponding to these stages of crack growth can be made by assuming the crack at the end of the first stage is a through thickness crack with length 2a equal to the crack length at mid-thickness (see Figure 331).

Since the actual crack shape is a semiellipse, i.e.

$$\frac{x^2}{a^2} + \frac{y^2}{b^2} - 1 = 0$$

with $b = 3.355 + 1.29\ a$

the length of the assume through thickness crack is:

$$a' = \frac{\sqrt{3}}{2}\ b = \frac{\sqrt{3}}{2}\ (3.355 + 1.29\ t)$$

where t is the plate thickness, being 15 mm in the case here investigated.

Therefore $a' \simeq 20$ mm.

Assuming this through-thickness crack behaves as in an infinite plate in tension, we have:

$$\frac{da}{dN} = 1.21 \times 10^{-13}\ (\Delta\alpha\sqrt{\pi a})^3$$

The number of cycles required to propagate to a given length a_f is therefore:

$$N_{2,3} = \frac{3 \times 10^{+12}}{(\Delta\sigma)^3}\ \frac{1}{\sqrt{20}} - \frac{1}{\sqrt{a_f}}$$

Fatigue lives

Assuming an initial flaw of size $a_i = 0.1$ mm and a crack length at discovery $a_f = 30$ mm, the following fatigue lives ($N = N_1 + N_{2,3}$) result (for Phases 1, 2 and 3)

N = 14.40 million cycles at $\Delta\sigma = 41$ MPa

N = 4.12 million cycles at $\Delta\sigma = 62$ MPa

N = 1.77 million cycles at $\Delta\sigma = 83$ MPa

This is in good agreement with the experimental fatigue data for critical location a which are 17.7, 4.2 and 1.3 million cycles respectively at these three stress ranges.

4. CONCLUSIONS AND RECOMMENDATIONS

4.1 Basic web details

The experimental and analytical studies on the basic web details indicated that the following conclusions could be made.

1. All web gusset details yielded fatigue strengths that equaled or exceeded category E.

2. Only the ends of the lateral attachments developed detectable fatigue crack growth. None of the details exhibited fatigue cracking adjacent to the transverse stiffeners.

3. The web gusset welded to one web surface with no connection to the stiffener provided good behavior with no adverse effect in web gap between stiffener and lower flange.

4. No adverse effect was found from the lateral bracing and its imposed out-of-plane movement of the web gusset.

5. The experimental observations were in general agreement with the theoretical model for the end of the detail. The model had a tendency to overestimate the severity of the detail.

6. Simplified fatigue life computations were in general agreement with the experimental observations.

4.2 Flange gussets

The conclusions concerning these details are as follows:

1. None of the flange details exhibited evidence of fatigue crack growth, even at very high stress range levels.

2. The "zero" radius details had the weld end (and toe) ground smooth. This resulted in a large increase in fatigue resistance.

3. The experimental results suggest that the ground radius details were always below the crack growth threshold as no crack growth was observed at any level of stress range.

4. Extensive failure from other details prevented development of fatigue data for the flange gussets.

4.3 Special details

Several special details were added to most of the test girders in order to develop experimental data on their behavior and strength. These tests provided the following results:

1. Supplementary detail 1 simulated heavy flanges either groove or fillet welded to the test girder web. All of these test details provided fatigue resistance that was in agreement with category E.

2. Supplementary detail 2 consisted of two plates welded on the lower flange opposite the gusset plates which were already

welded to the flange. No cracking was observed at the stress range level of 83 MPa. Further tests are underway on this detail.

3. Supplementary detail 3 consisted of two plates welded together with incomplete penetration and then fillet welded to the web as a longitudinal stiffener. The detail quickly cracked to the web, but the growth through the web was not as quick as anticipated. A subsequent test yielded much less fatigue resistance.

4. Supplementary detail 4 consisted of an insert through the web. The only test exhibited category E behavior. Additional experiments are being made on this detail and are currently underway.

4.4 Retrofitting techniques

The only retrofitting technique used in this experimental study was to drill holes at the crack tips. Generally, the cracks that developed at the special details could not be arrested by any other method. This technique was reasonably successful (see Table 42). No general rule concerning its efficiency was developed. Often, the fatigue crack reinitiated at the drilled hole, depeneding on the crack size and stress range that existed. When the crack was longer than 20 mm, it was advisable to use tightened high strength bolts to induce compression stresses at bolt holes.

This technique should be used with caution in actual structures. It is primarily an interim procedure that only temporarily arrests the growth of the original crack. Such repairs should be inspected frequently because the crack may reinitiate under the bolt and washer. It is then difficult to detect crack initiation and growth from the hole. This can result in very rapid propagation and lead to failure.

4.5 Recommendations

This study has indicated that the design criteria for lateral connections should be maintained as currently practiced. These details have exhibited a satisfactory fatigue resistance which is in agreement with the specification provisions. Consideration should be given to grinding groove welded gusset ends, since this practice can lead to a substantial improvement in fatigue behavior.

5. TABLES

Table 11 AASHTO Allowable Stress Range, MPa

Detail Category	Cycles			
	100,000	500,000	2,000,000	over 2,000,000
A	413.7	248.2	165.5	165.5
B	310.3	189.6	124.1	110.3
C	220.6	131.0	89.6	69.0, 82.7*
D	186.2	110.3	69.0	48.3
E	144.8	86.2	55.2	34.5
F	103.4	82.7	62.1	55.2

*For transverse stiffener welds on webs or flanges

Table 21 Load and Stress Ranges

Girder	Load Ranges (kN)	Stress Ranges (MPa)
W27x145	464.46	82.74
	348.35	62.06
	232.23	41.37
W27x114	343.83	82.74
	257.88	62.06
	171.92	41.37
W36x160	462.59	82.74
	346.95	62.06
	231.30	41.37

Table 22a Stress Record during Test of W27x114 Girder, Detail 1

Gage Location	Average Stress Range (MPa) Low S_r	High S_r
Under lower flange at 162.5 cm from support	82.38	122.75
Under lower flange at mid span (pilot gages)	105.26	143.00
On web below stiffener end	85.43	120.00
On web above web-to-gusset weld toe	61.00	80.00
On web above internal web-to-supplementary detail weld toe	44.24	49.00
On web gusset plate 11	Not Available	114.50
On web gusset plate 12	Not Available	77.50
On web gusset plate 14	Not Available	13.00
On web gusset plate 16	Not Available	75.00

Table 22b Stress Record during Test of S27x145 Girder, Detail 2

Gage Location	Average Stress Range (MPa) Low S_r	High S_r
Under lower flange at 162.5 cm from support	58.00	NOT AVAILABLE
Under lower flange at mid span (pilot gages)	72.15	
On web below stiffener end	56.67	
On web above web-to-gusset weld toe	31.67	
On web above internal web-to-supplementary detail weld toe	17.33	
On web gusset plate 21	25.00	
On web gusset plate 22	28.00	
On web gusset plate 23	22.67	
On web gusset plate 24	18.00	

Table 22c Stress Record during Test of W27x145 Girder, Detail 3

Gage Location	Average Stress Range (MPa) Low S_r	High S_r
Under lower flange at 162.5 cm from support	55.00	104.00
Under lower flange at mid span (pilot gages)	68.10	137.00
On web below stiffener end	60.00	122.00
On web above web-to-gusset weld toe	32.00*	Not Available
On web above internal web-to-supplementary detail weld toe	Not Available	43.00
On web gusset plate 31	20.00	27.50
On web gusset plate 32	14.00	30.50
On web gusset plate 33	26.50	39.50
On web gusset plate 34	7.00	Not Available

Table 23 Out-of-Plane Movements

Gaps (mm)			Relative Deflections %	
g_1	g_2	g_3	Δ_1/Δ_3	Δ_2/Δ_3
75	75	75	88.70	90.52
125	75	75	89.89	92.27
125	75	125	90.08	93.35
125	125	125	92.33	95.70
125	125	75	90.56	93.46
75	125	75	89.14	94.20

Table 24 Experimental Fatigue Lives

Detail	Critical Location or Supplementary Detail	Stress Range (MPa)		Number of Million Cycles at	
		Theory	Nearest Gage	Visible Crack Initiation	Through-Thickness Propagation
1	a	62	61	4.6	NA
		83	80	> 0.78	
	b	62	61	> 9.3	
		83	80	> 0.78	
	c	62	61	> 9.3	
		83	80	> 0.78	
	1 fillet welded	78	49	NA	0.78
	2	78	49	> 0.78	
	3	70	NA	1.1	2.0
		59	44	NA	4.6
2	a	41	32	>17.7	
		83	NA	1.8	2.0
	b	41	32	>17.7	
		83	NA	> 2.3	
	1 fillet welded	39	17	4.3	17.7
		78	NA	1.1	1.4
3	a	41	32*	> 9.0	
		83	NA	NA	1.6
	1 groove welded	78	43	NA	1.5
	4	78	NA	NA	1.0

*Strain gage not balanced

NA - Not Available

Table 31 Numbering Pattern for Cubic and Skewed Elements

Element Number	Connected Nodes							
	1	2	3	4	5	6	7	8
1	1	4	5	2	10	13	14	11
2	2	5	6	3	11	14	15	12
3	4	7	8	5	13	16	17	14
4	5	8	9	6	14	17	18	15
5	11	14	15	12	19	21	22	20
6	19	21	22	20	23	25	26	24
7	11	14	21	19	10	13	25	23
8	14	15	22	21	17	18	26	25
9	14	17	17	21	13	16	16	25

Table 32 Stresses in the Web around Critical Locations a and b

Detail	Critical Location	Stresses (MPa)				
		Element 1	Element 2	Element 3	Element 4	Average
1	a	52.20	41.09	59.85	73.29	56.61
	b	40.34	47.99	67.92	53.85	52.52
2	a	57.00	45.56	67.01	80.88	62.61
	b	41.85	57.09	79.84	63.78	60.64
3	a	57.16	44.89	66.74	66.95	58.94

Table 33 Comparison between Assumed and Measured Nominal Stress Ranges

Detail	Assumed Stress Range (MPa)	Measured Stress Range (MPa)
1	82.74	80
	62.06	61
2	82.74	Not Available
	41.37	32
3	82.74	
	41.37	32*

*Not balanced

Table 34 Front Free Surface Correction

Type of Crack	Stress Distribution	Front Free Surface Correction F_s
Through crack	a	$F_s = 1.122$
	b	$F_s = 1.210$
	c	$F_s = 1.300$
	d	$1.210 < F_s < 1.300$
Half circular crack	a	$F_s = 1.025$
	b	$F_s = 1.085$
	c	$F_s = 1.145$ (estimated)
	d	$1.085 < F_s < 1.145$
Quarter circular crack	a	$F_s = 1.380$ (estimated)
	b	$F_s = 1.067$ (estimated)
	c	$F_s = 0.754$ (estimated)
	d	$0.754 < F_s < 1.067$

a: uniform stress over the crack length

b: linear stress variation to zero at the crack tip

c: concentrated load at the crack origin

d: decreasing stress distribution more rapid than linear variation to zero at the crack tip

Table 35 Weld Slope Correction Factor

$\frac{a}{w}$	$\frac{K(30^\circ)}{K(45^\circ)}$
0	0.56
0.01	0.72
0.02	0.76
0.04	0.79
0.05	0.82
0.08	0.88
0.10	0.90
0.12	0.92
0.14	0.925
0.16	0.93
0.18	0.95
0.20	0.96
0.30	1.00
1.00	1.00

Table 36 Computed Fatigue Lives

Detail	Critical Location	Stress Range (MPa)	Weld Slope (°)	Initial Crack Size (mm)	Fatigue Life (million cycles)
1	a	62	30	0.05	3.4
				0.5	3.0
			45	0.05	2.5
				0.5	2.6
		83	30	0.05	1.4
				0.5	1.3
			45	0.05	1.1
				0.5	1.1
	b	62	30	0.05	3.6
				0.5	3.2
			45	0.05	2.7
				0.5	2.7
		83	30	0.05	1.5
				0.5	1.3
			45	0.05	1.1
				0.5	1.1
2	a	41	30	0.05	19.1
				0.5	15.9
			45	0.05	13.2
				0.5	13.1
		83	30	0.05	2.3
				0.5	1.9
			45	0.05	1.6
				0.5	1.6
	b	83	30	0.05	11.9
				0.5	6.6
			45	0.05	6.0
				0.5	4.7
3	a	41	30	0.05	10.8
				0.5	9.5
			45	0.05	8.0
		83	30	0.05	1.3
				0.5	1.2
			45	0.05	1.0
				0.5	1.0

Table 37 Effect of Web Thickness on Displacement of Weld Toes

Location	Web Thickness mm	Vertical Displacement mm	Relative Variation	Rotation around Longitudinal Axis radians	Relative Variation
Web to gusset weld toe	0.4	-0.29242	1.13	-0.0056199	1.20
	0.6	-0.25869	1.00	-0.0046727	1.00
	0.8	-0.23567	0.91	-0.0037675	0.81
Mid-span x-section at gusset level	0.4	-0.29323	1.12	-0.0064307	1.25
	0.6	-0.26014	1.00	-0.0051572	1.00
	0.8	-0.23735	0.91	-0.0039523	0.77

Table 38 Effect of Gussets Welded to the Lower Flange

Location	Detail	Gusset on Lower Flange	Vertical Displacement mm	Relative Variation
Web-to-gusset weld toe	1	yes	-0.25869	
	1	no	-0.28219	1.09
	2	yes	-0.28216	
	2	no	-0.26026	0.92
	3	yes	-0.28216	
	3	no	-0.26489	0.94
Mid-span x-section at gusset level	1	yes	-0.26014	
	1	no	-0.28536	1.10
	2	yes	-0.28418	
	2	no	-0.26243	0.92
	3	yes	not available	
	3	no		
External corners of gusset plate	1	yes	-0.13503	
	1	no	-0.28038	1.44
	2	yes		
	2	no	-0.16089	
	3	yes	-0.19794	
	3	no	-0.18575	0.94
Mid-length external side of gusset plate	1	yes	-0.16832	
	1	no	-0.28340	1.68
	2	yes		
	2	no	-0.082326	
	3	yes	-0.089008	
	3	no	-0.068492	0.77

Table 39 Displacements and Rotations at Web-to-Gusset Weld Toe

Case	Type	Displacements (μm)			Rotations	
		X	Y	Z	X	Y
1	1	43.18	-91.44	6553.20	-0.0004	-0.0038
	2	60.96	-88.90	6553.20	-0.0003	-0.0033
2	1	45.72	-91.44	6553.20	-0.0004	-0.0041
	2	96.52	-88.90	6553.20	-0.0003	-0.0035
3	1	45.72	-91.44	6578.60	-0.0004	-0.0042
	2	101.60	-88.90	6553.20	-0.0003	-0.0035
4	1	45.72	-88.90	6553.20	-0.0004	-0.0042

Table 310 Out-of-Plane Bending Stresses at Web-to-Gusset Weld (special gusset plates)

Element	No Cut-Out	Part C Cut-Out	Parts A,B,C Cut-Out
E1	0.189	0.152	-
E2	-0.118	-0.099	-0.045
E3	-0.024	-0.035	-0.047
E4	-0.023	-0.039	-0.041
E5	-0.028	-0.038	-0.026
E6	-0.018	-0.021	-

Table 311 Transverse-to-Weld Stresses along Gusset-to-Stiffener Weld (special gusset plates)

Element	No Cut-Out	Part C Cut-Out	Parts A,B,C Cut-Out
E1	6.645	7.367	-
E7	4.666	6.382	8.508
E8	3.759	6.457	6.802
E9	2.933	-	-
E10	1.679	-	-

Table 41 Comparison between Experimental and Computed Fatigue Lives (at through-thickness propagation)

Detail	Critical Location	Stress Range (MPa)	Fatigue Life (million cycles)	
			Experimental	Estimated
1	a	62	4.2**	2.9
		83	> 0.8	1.2
	b	62	> 9.3*	3.1
		83	> 0.8*	1.3
	c	62	> 9.3*	N.A.
		83	> 0.8*	N.A.
2	a	41	17.7	15.4
		83	1.8**	1.8
	b	41	>17.7*	N.A.
		83	> 2.3*	7.3
3	a	41	> 9.0*	9.1
		83	1.3**	1.2

*Failure elsewhere prevented further testing

N.A.: not available

**Fatigue life at through-thickness propagation estimated from crack length at time of observation

Table 42 Retrofitting Results

Web Detail	Stress Range	Crack Location	Stress Range (MPa)	Crack Length (mm)	Holes Dia. (mm)	Bolts	Rein-itiation
1	Low	Central weld of supp. detail 3	59	40	19	No	Yes
1	Low	Inner weld toe of supp. detail 3	70	50	19	No	Yes
1	Low	Web gusset weld toe	62	25	19	No	Yes
1	High	Supp. detail 1 weld toe	78	157	19	No	Yes
2	High	Web-to-gusset weld toes	83	59 112	19 19	No No	No No
2	High	Supp. detail 1 weld toe	78	50	19	Yes	Yes
3	High	Supp. detail 4 weld toe	78	10	19	Yes	No
3	High	Supp. detail 1 weld toe	78	90	19	No	Yes

6. FIGURES

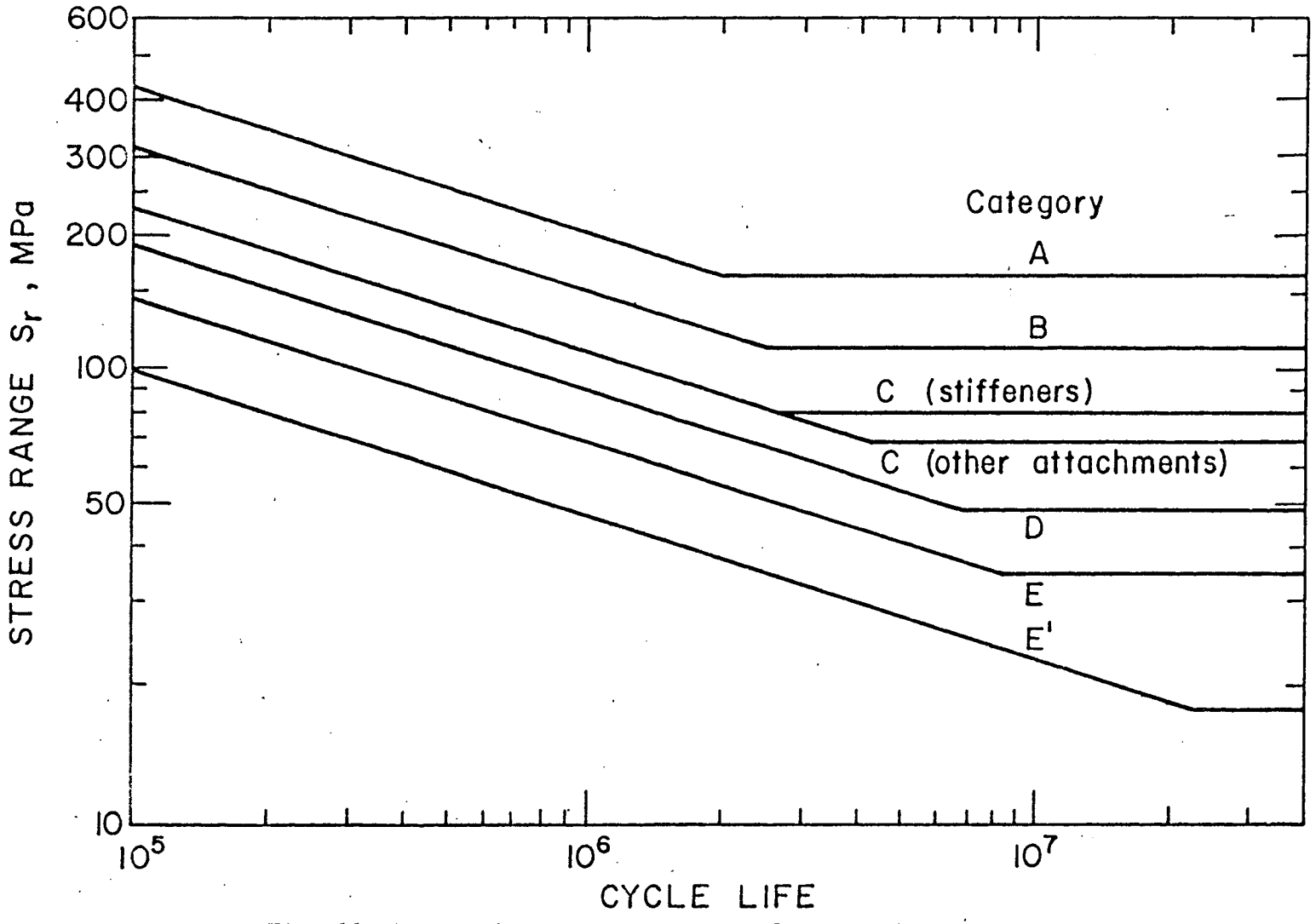

Fig. 11 Design Stress Range Curves for Details A to E

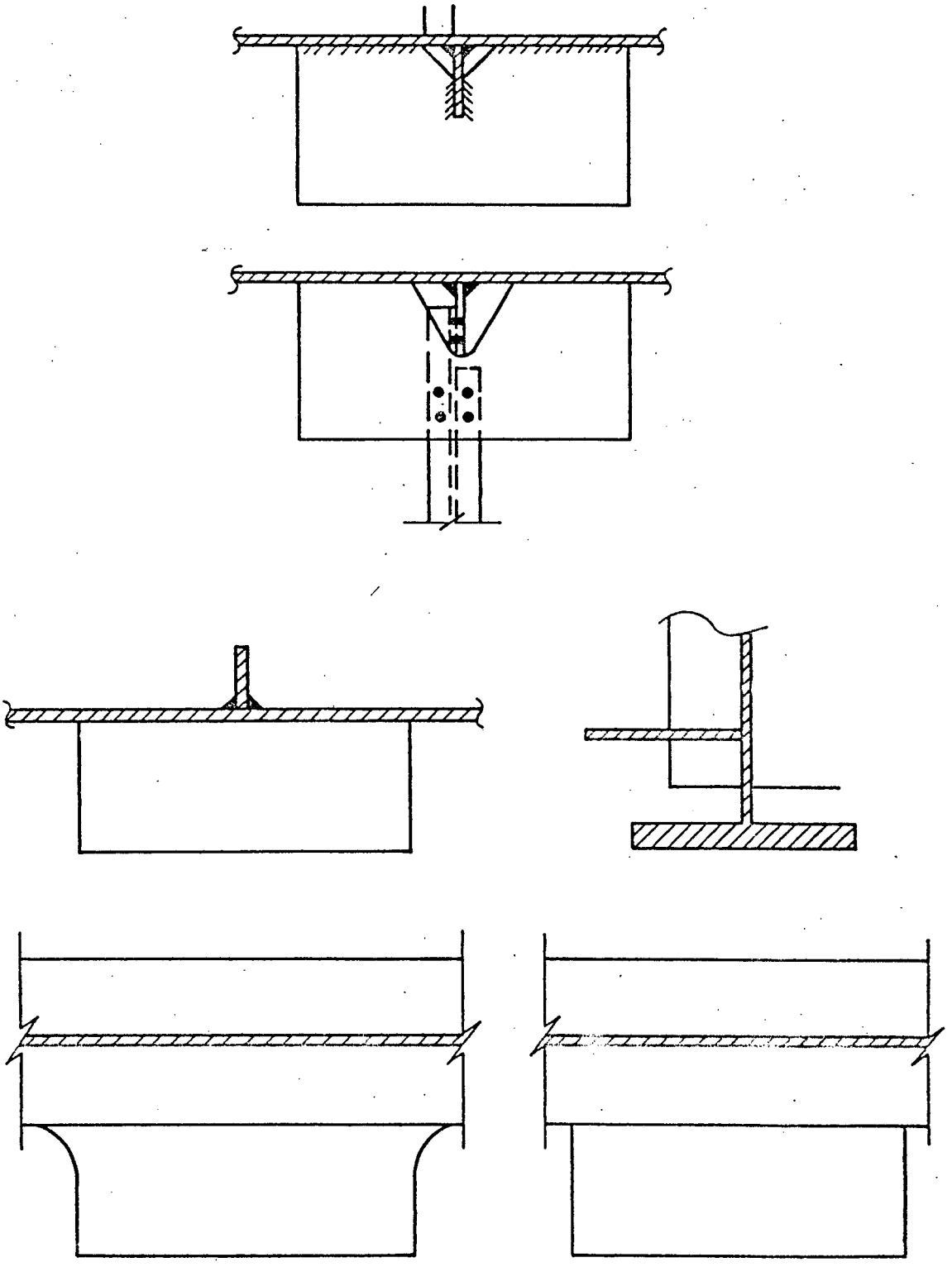

Fig. 12 Typical Lateral Attachments

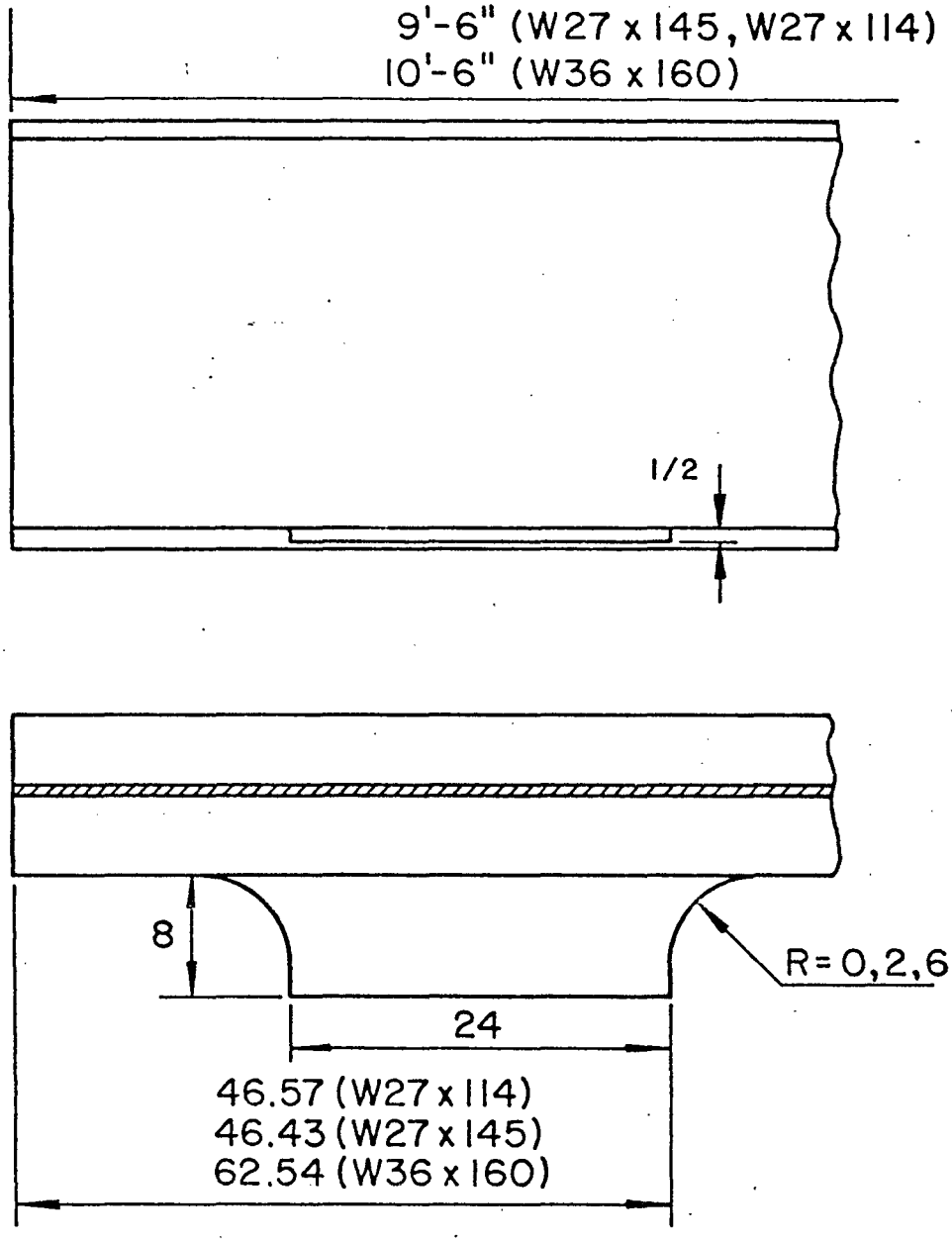

Fig. 21(a) Test Specimens in Shear Span

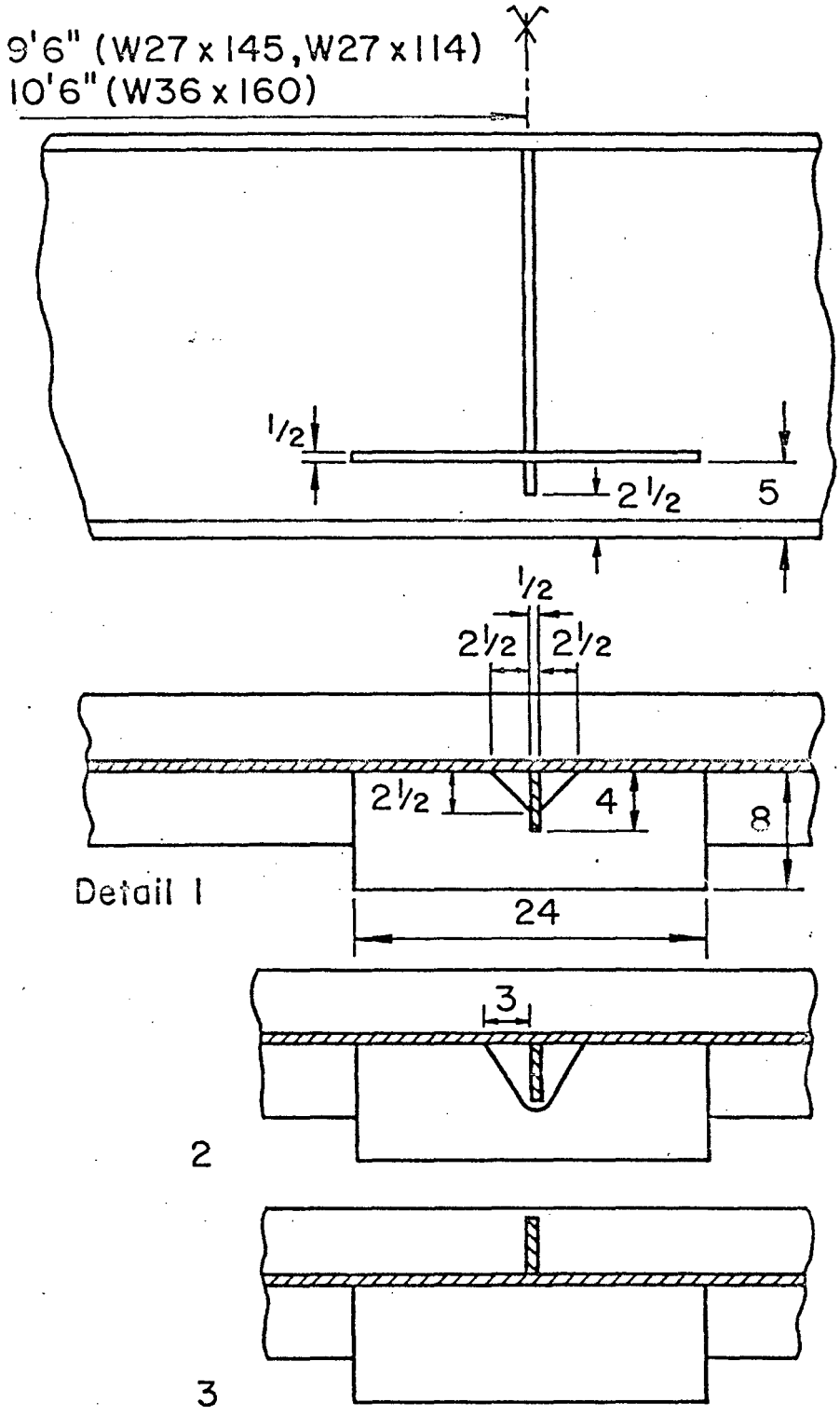

Fig. 21(b) Test Specimens Near Centerline
Note: Dimensions are English units

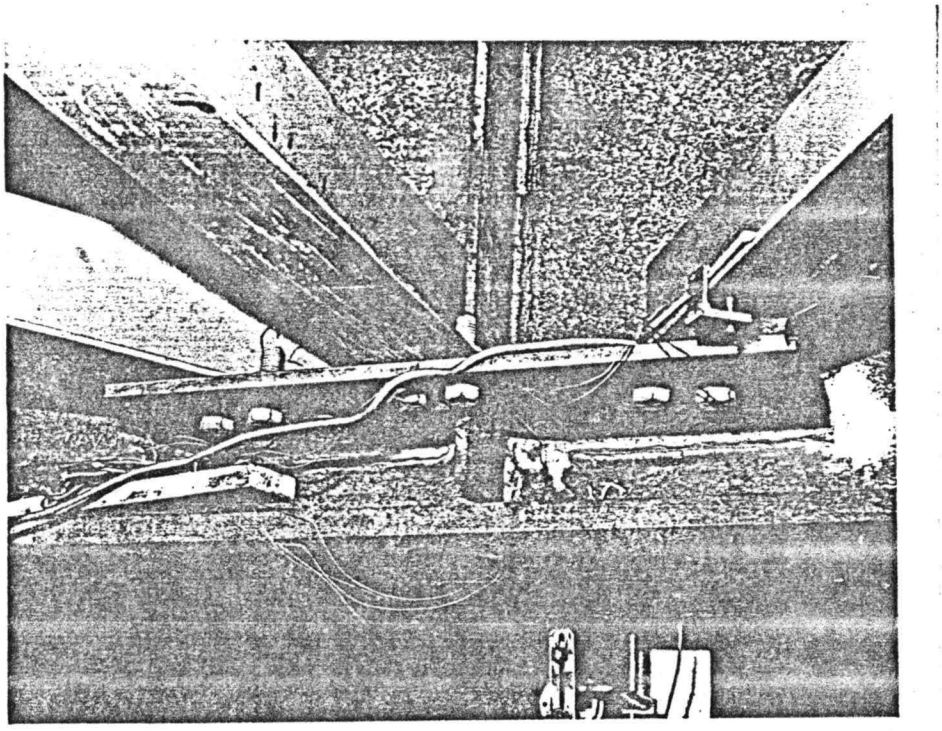

Fig. 21(c) Typical Lateral Attachment

(Web Detail 1)

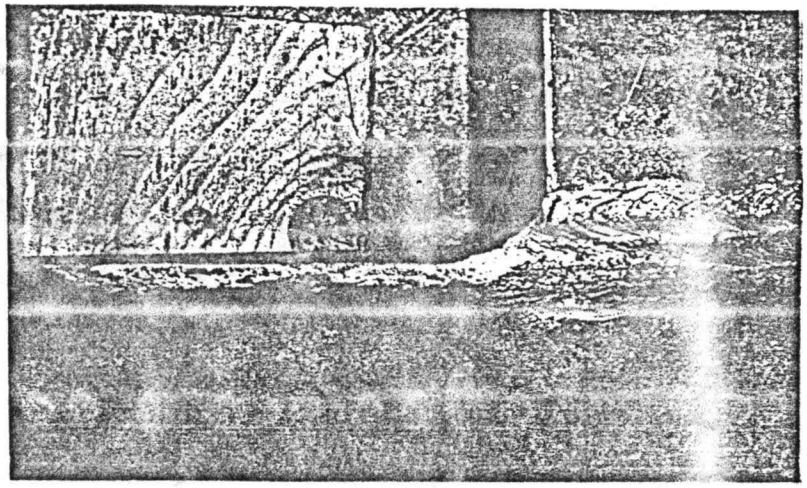

(a) R = "0"

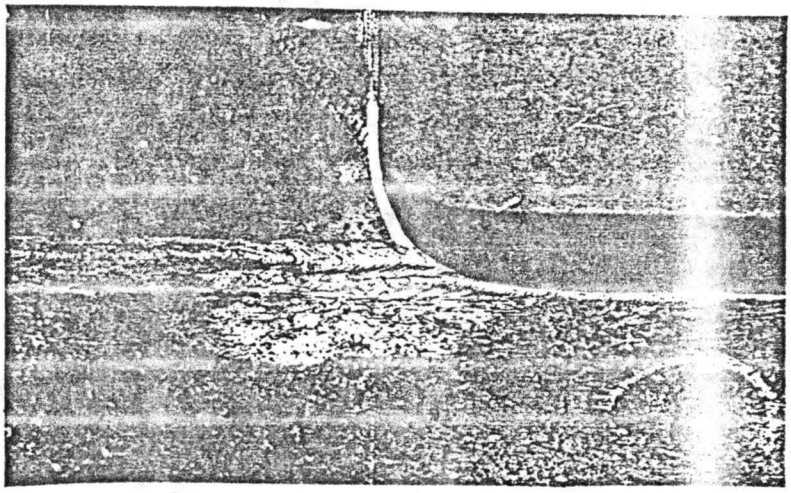

(b) R = 5 cm

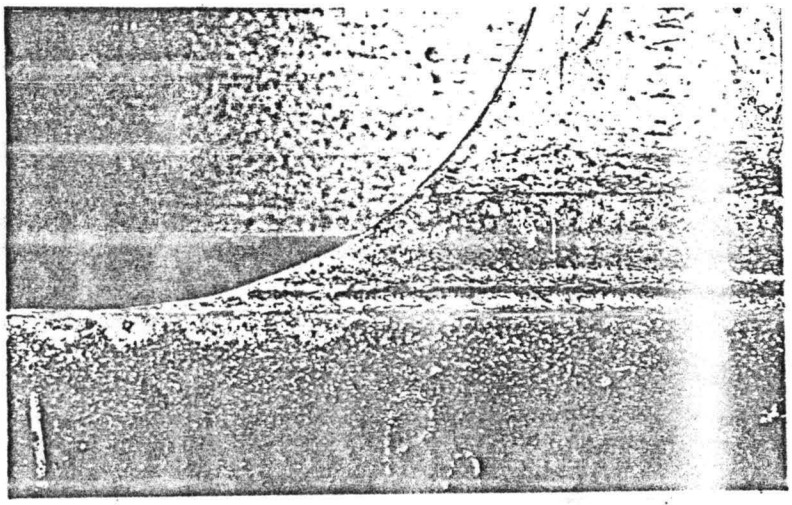

(c) R = 15 cm

Fig. 21(d) Radii at Primary Flange-to-Gusset Attachments

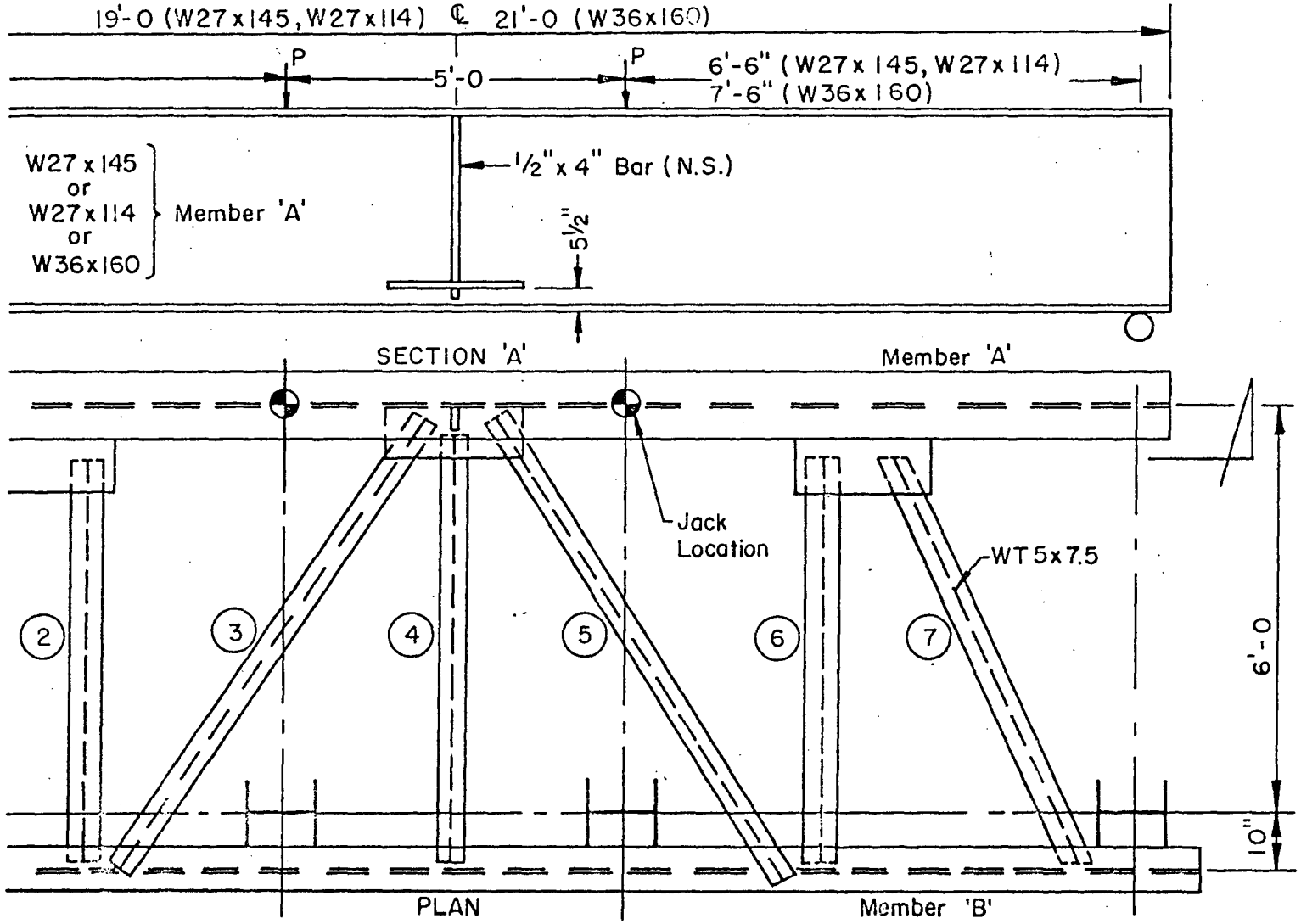

Note: Dimensions are in English units

Fig. 22 Test Setup

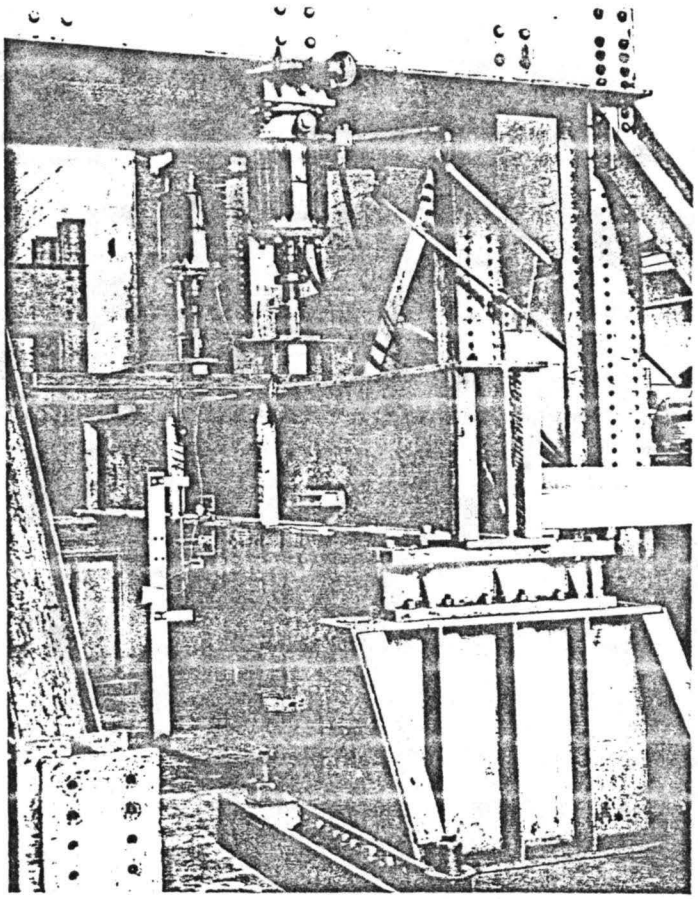

Fig. 22 (continued) Test Setup

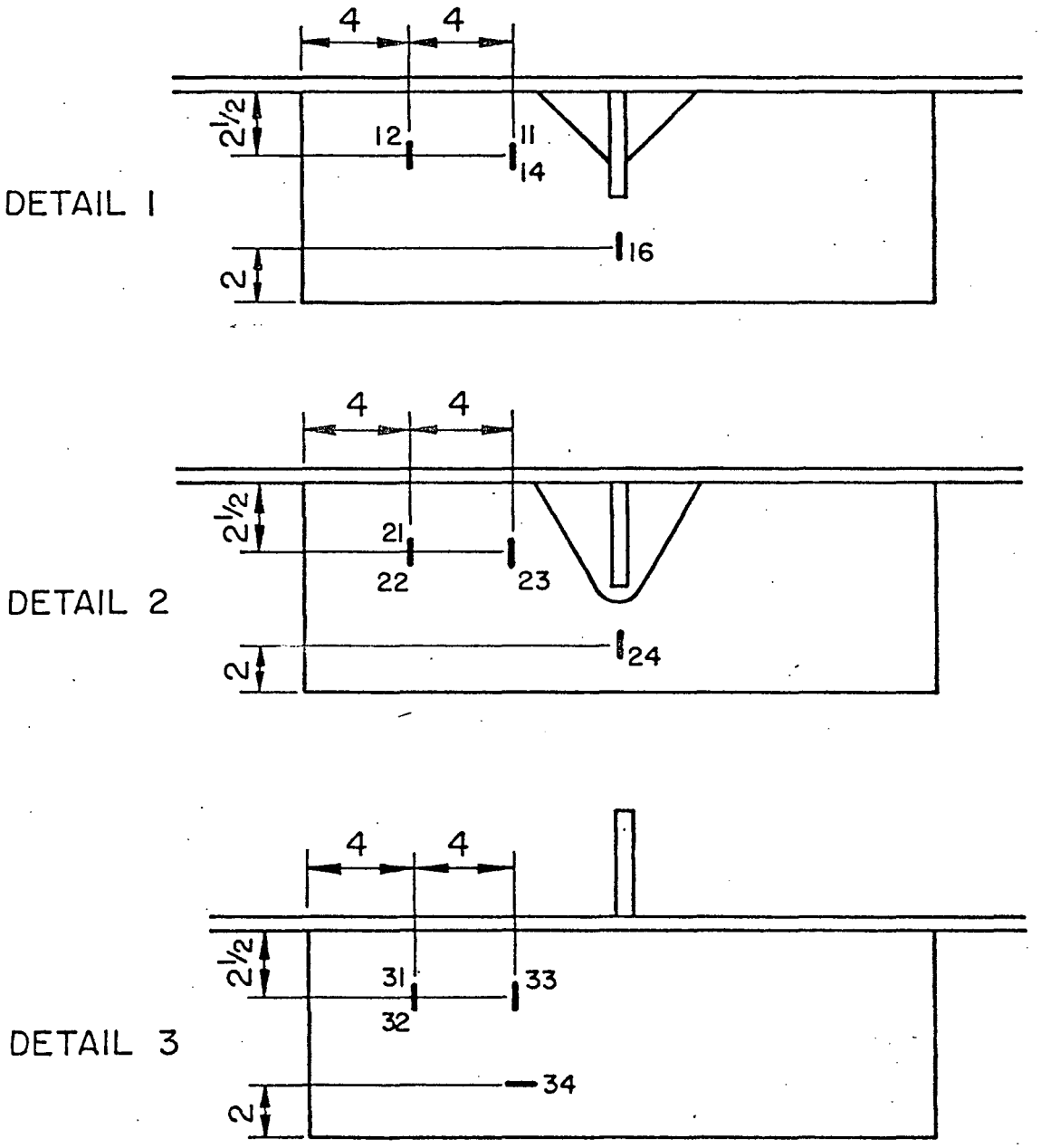

Fig. 23 Gage Locations on the Central Gusset Plate
Numbering pattern: 1st digit: detail number (1,2,3)
2nd digit: gage number
odd: on upper face
even: on lower face

Note: dimensions are in English units (in)

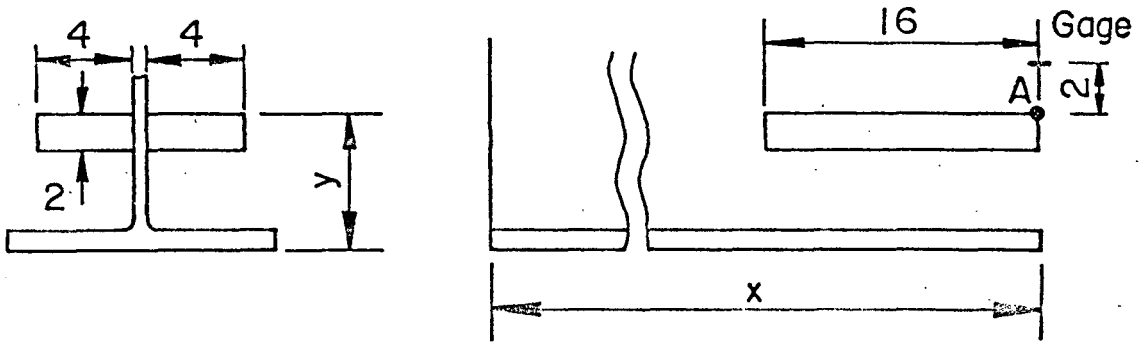

Supplementary Detail 1

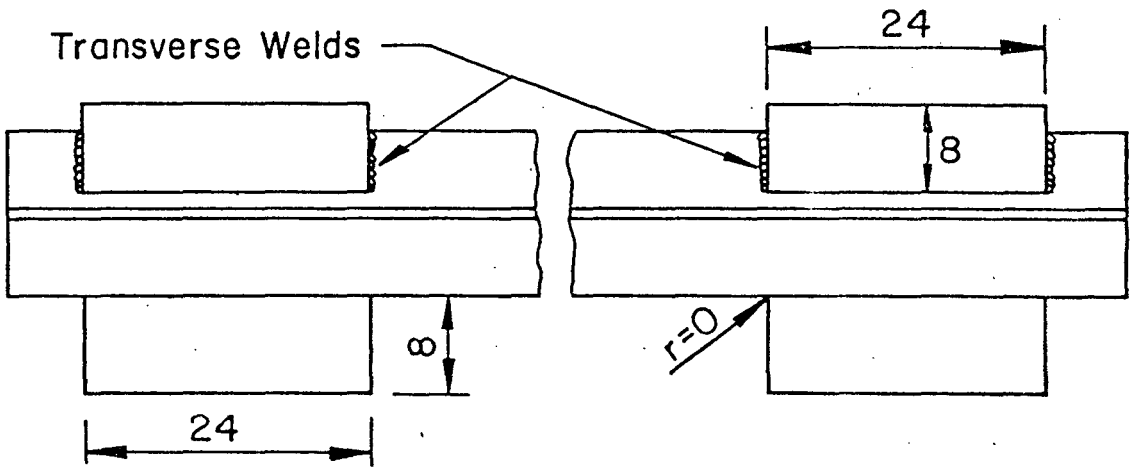

Supplementary Detail 2

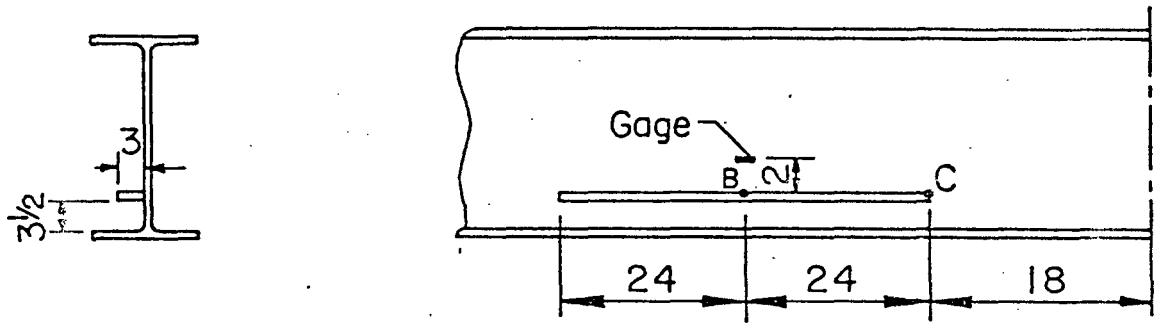

Supplementary Detail 3

Fig. 24(a) Supplementary Details

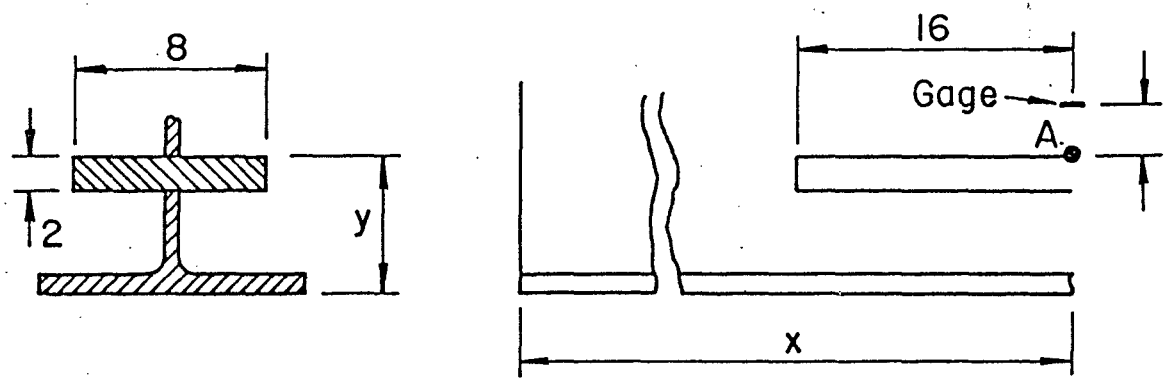

Supplementary Detail 4

Fig. 24(b) Supplementary Details

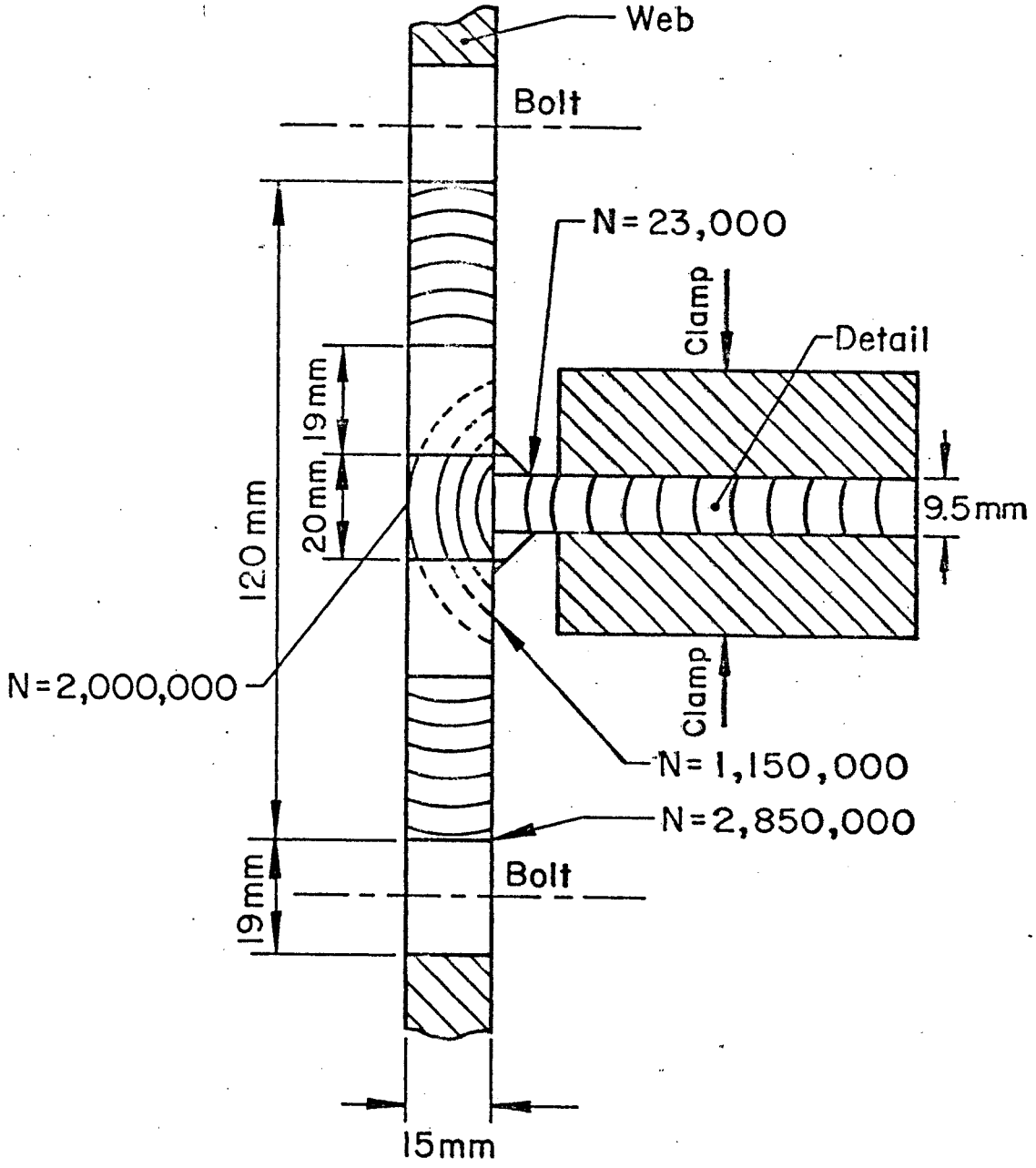

Fig. 25 Crack Growth at Supplementary Detail 3 (W27x145, Detail 1, Low Stress Range)

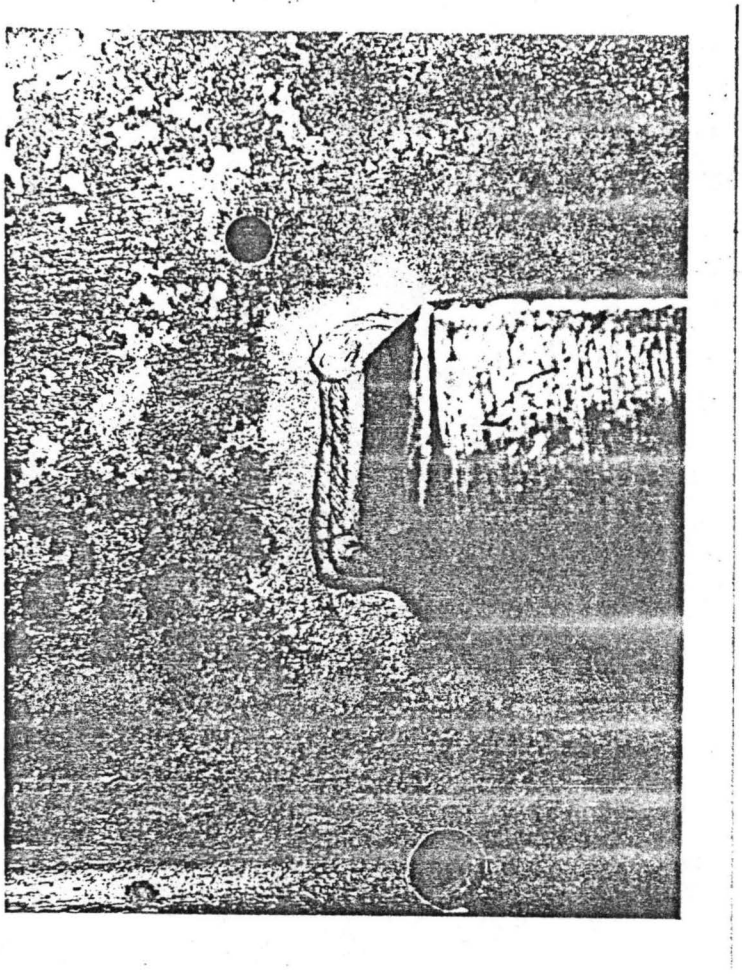

Fig. 26(a) First State of Crack Growth
at Supplementary Detail 1 Toe
(W27x145, detail 1, high stress range)

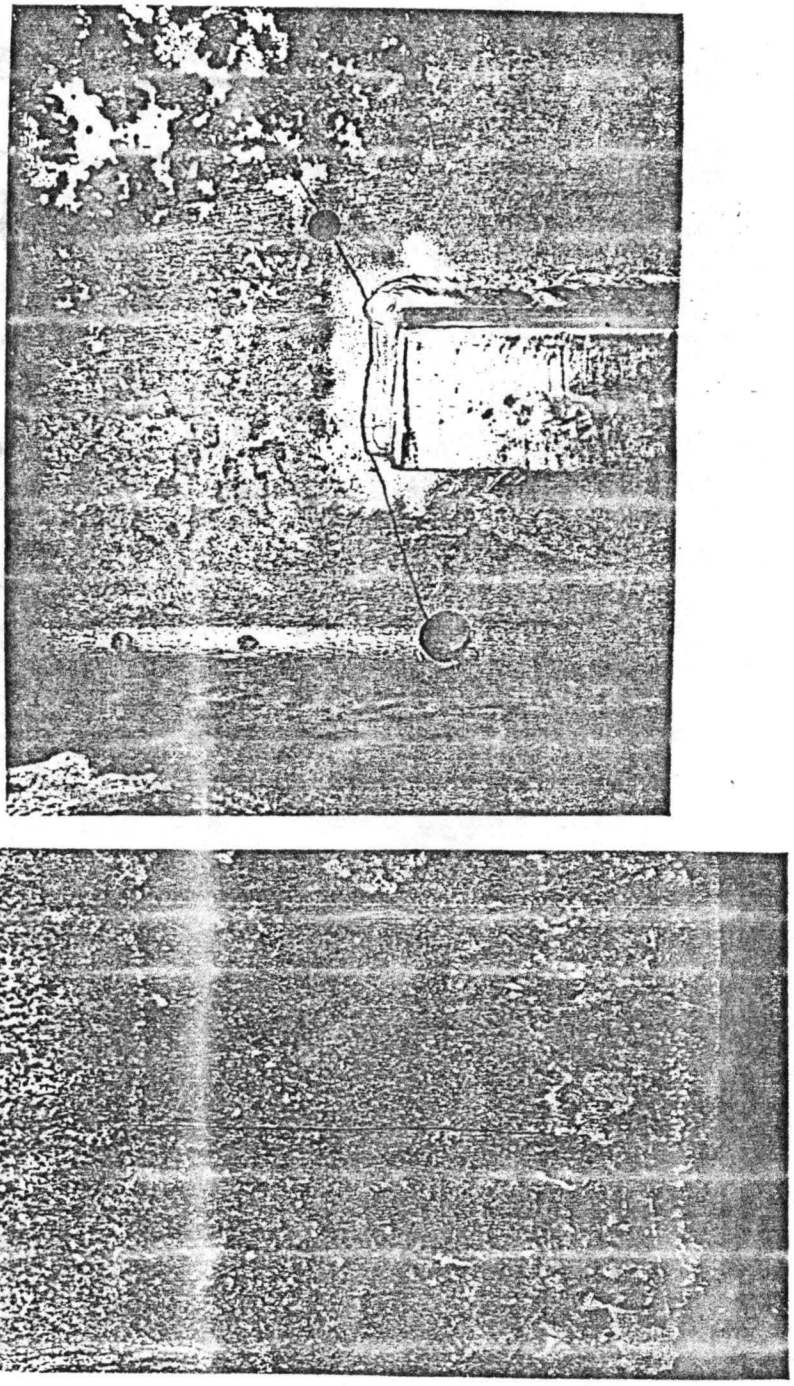

Fig. 26(b). Second Stage of Propagation
a) crack in web
b) crack through lower flange

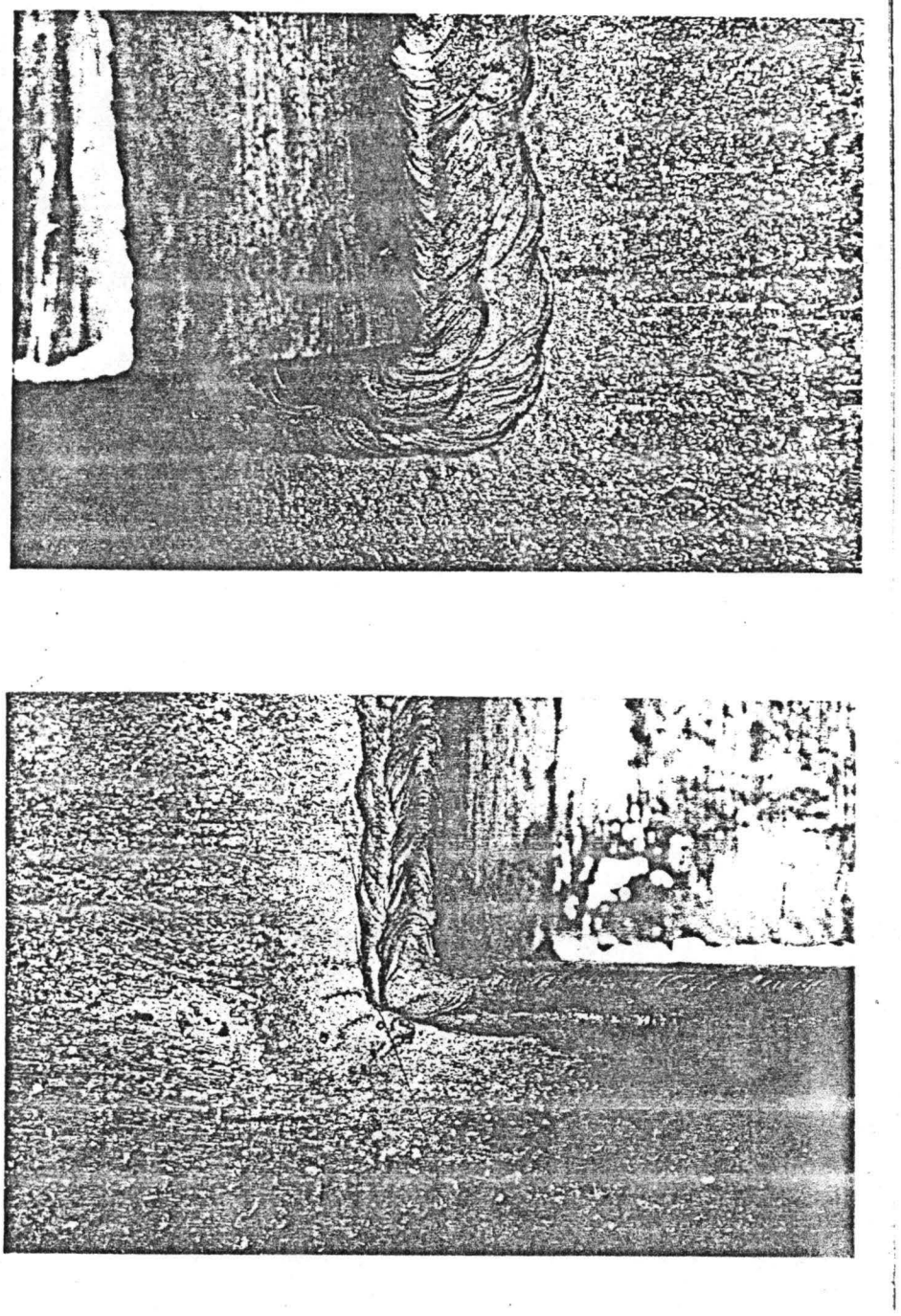

Fig. 27 Through-Thickness Propagation at Weld Toe of Supplementary Detail 1 (W27x145, detail 2, low stress range)

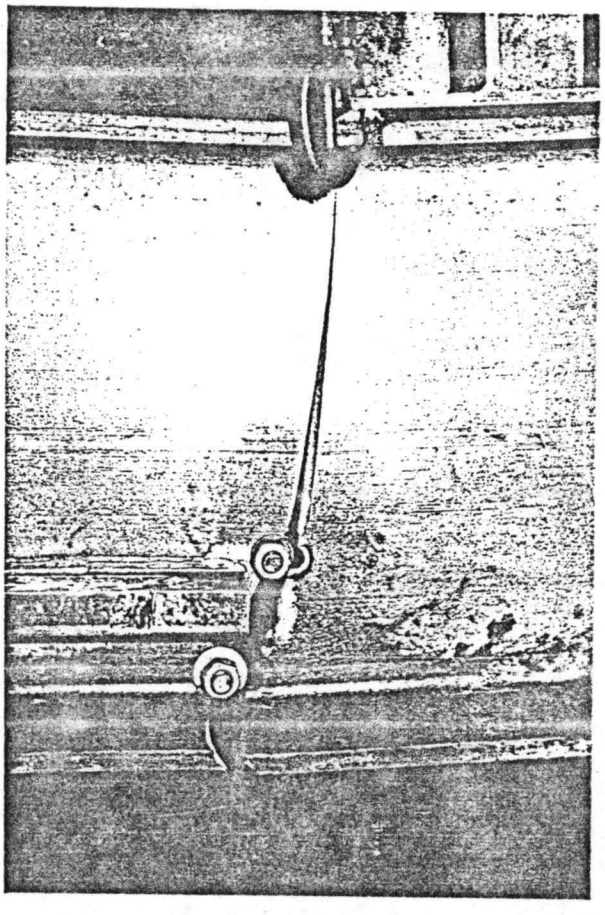

Fig. 28 Cracks at Web-to-Supplementary Detail 1 Weld Toe
(27x145, detail 2, high stress range)

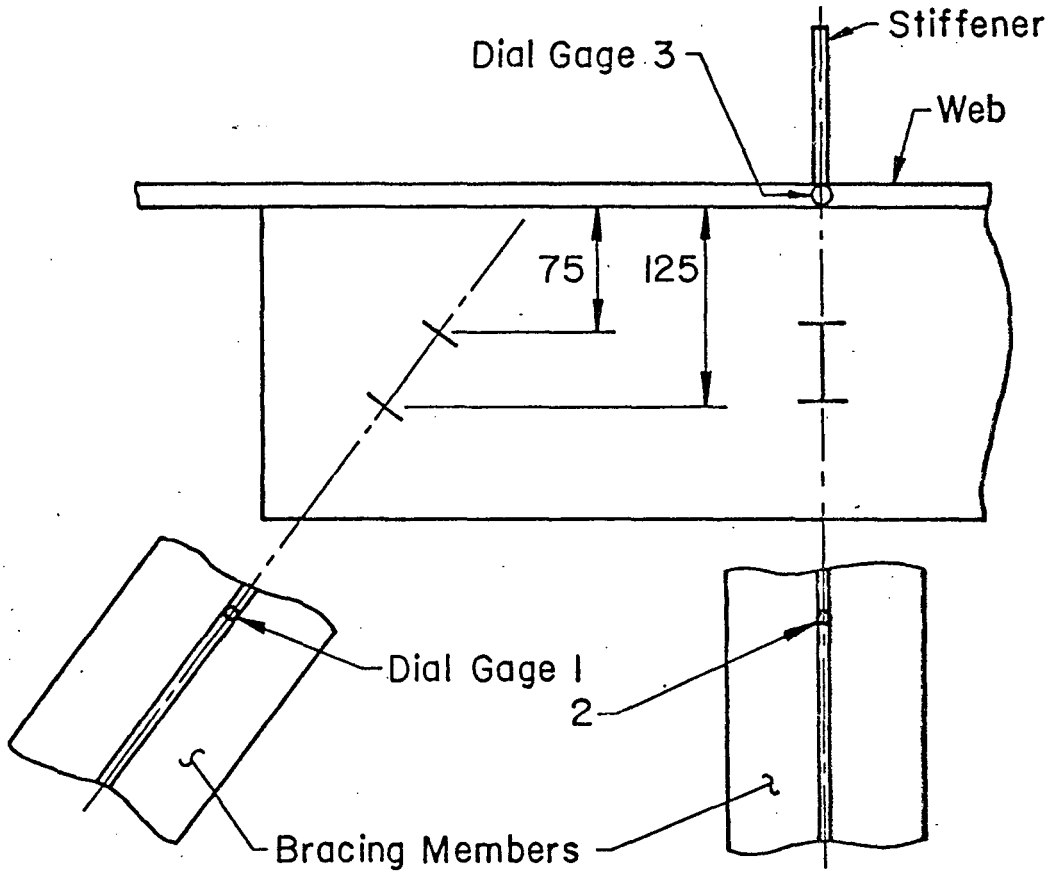

Fig. 29 Experimental Study of Gap Effect

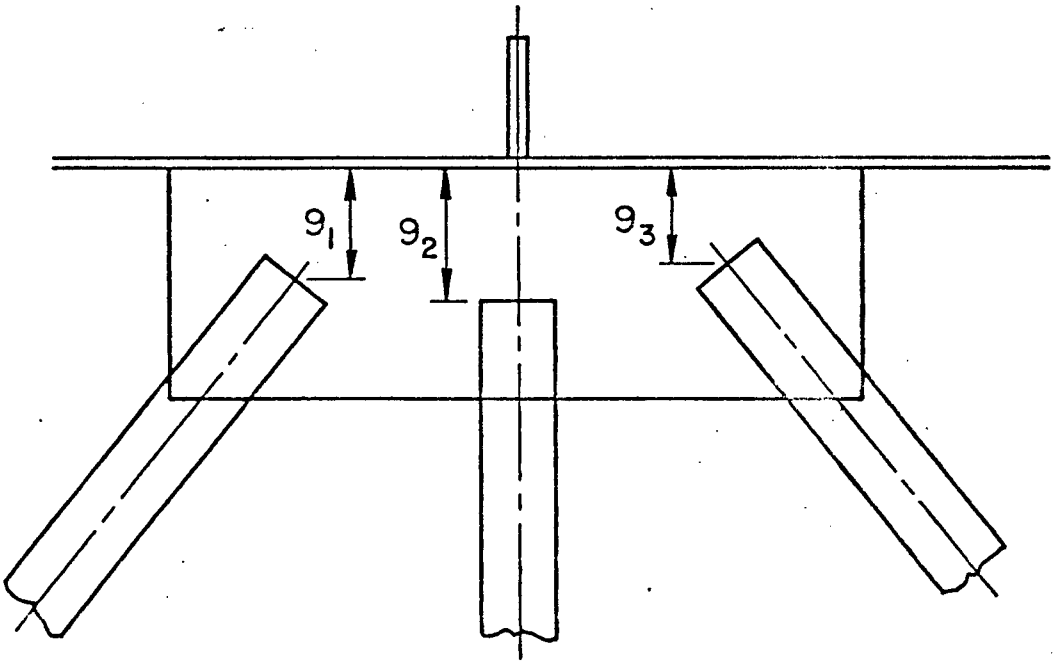

Fig. 210 Measured Gaps

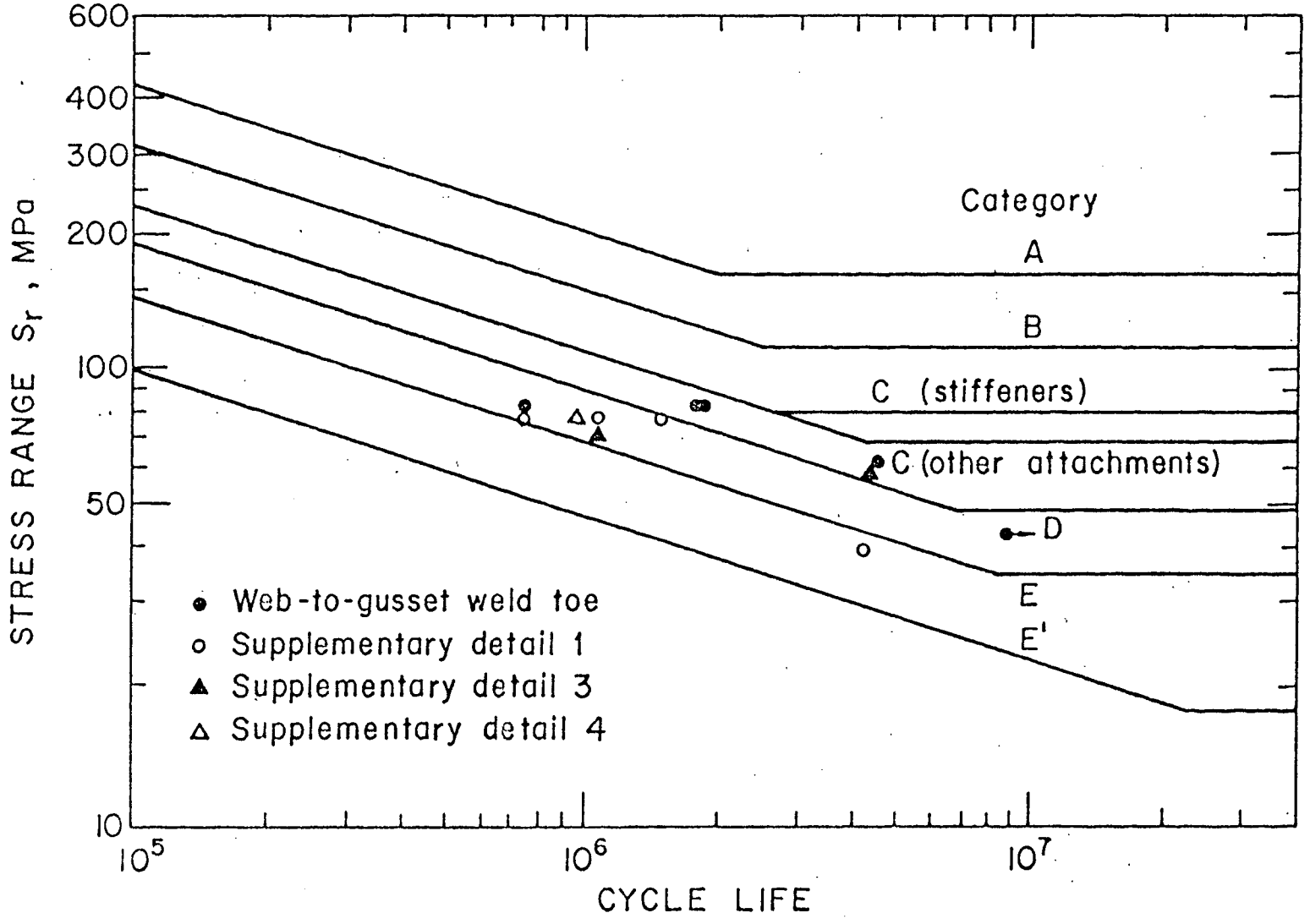

Fig. 211 Experimental Fatigue Lives

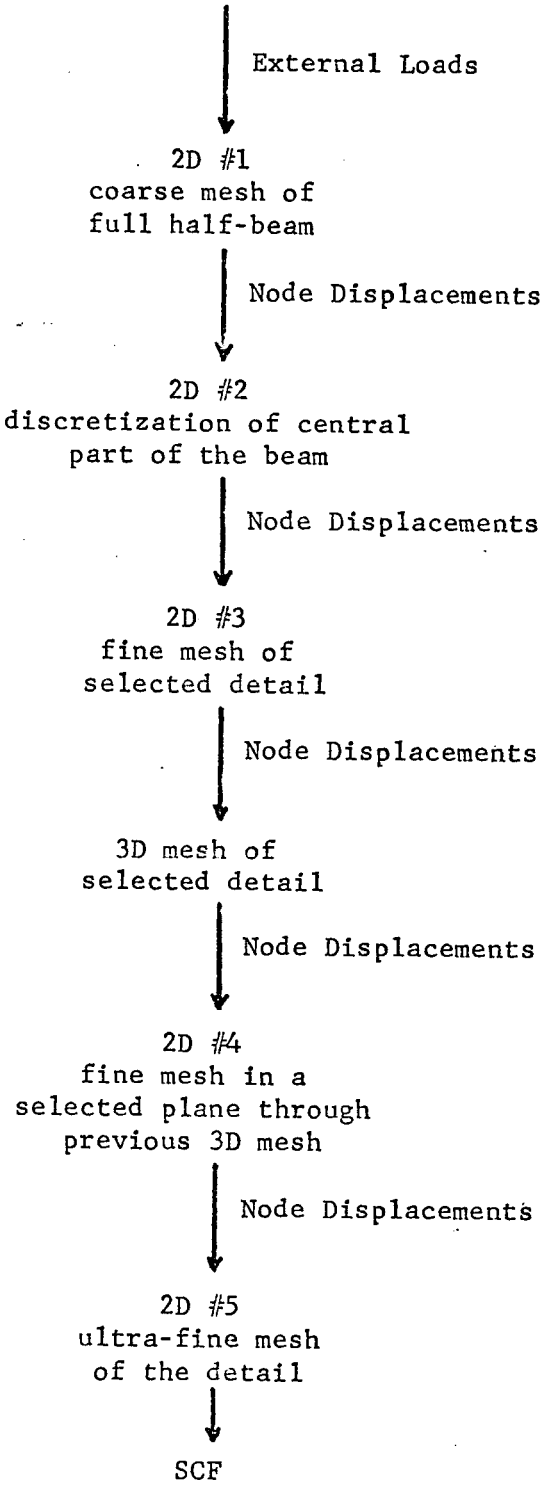

Fig. 32 Theoretical Investigation Procedure

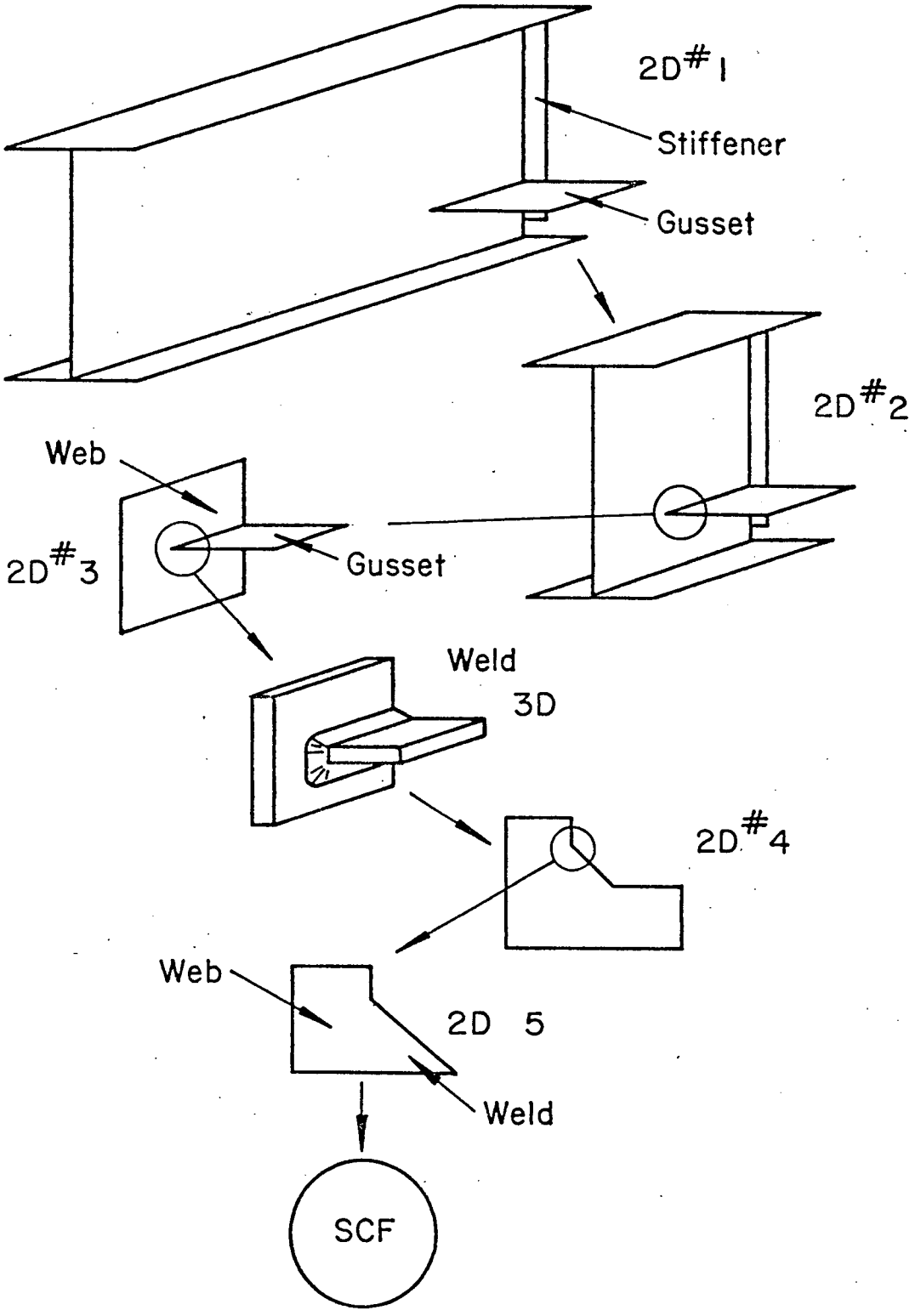

Fig. 33 Schematic Illustration of the Theoretical Investigation Procedure

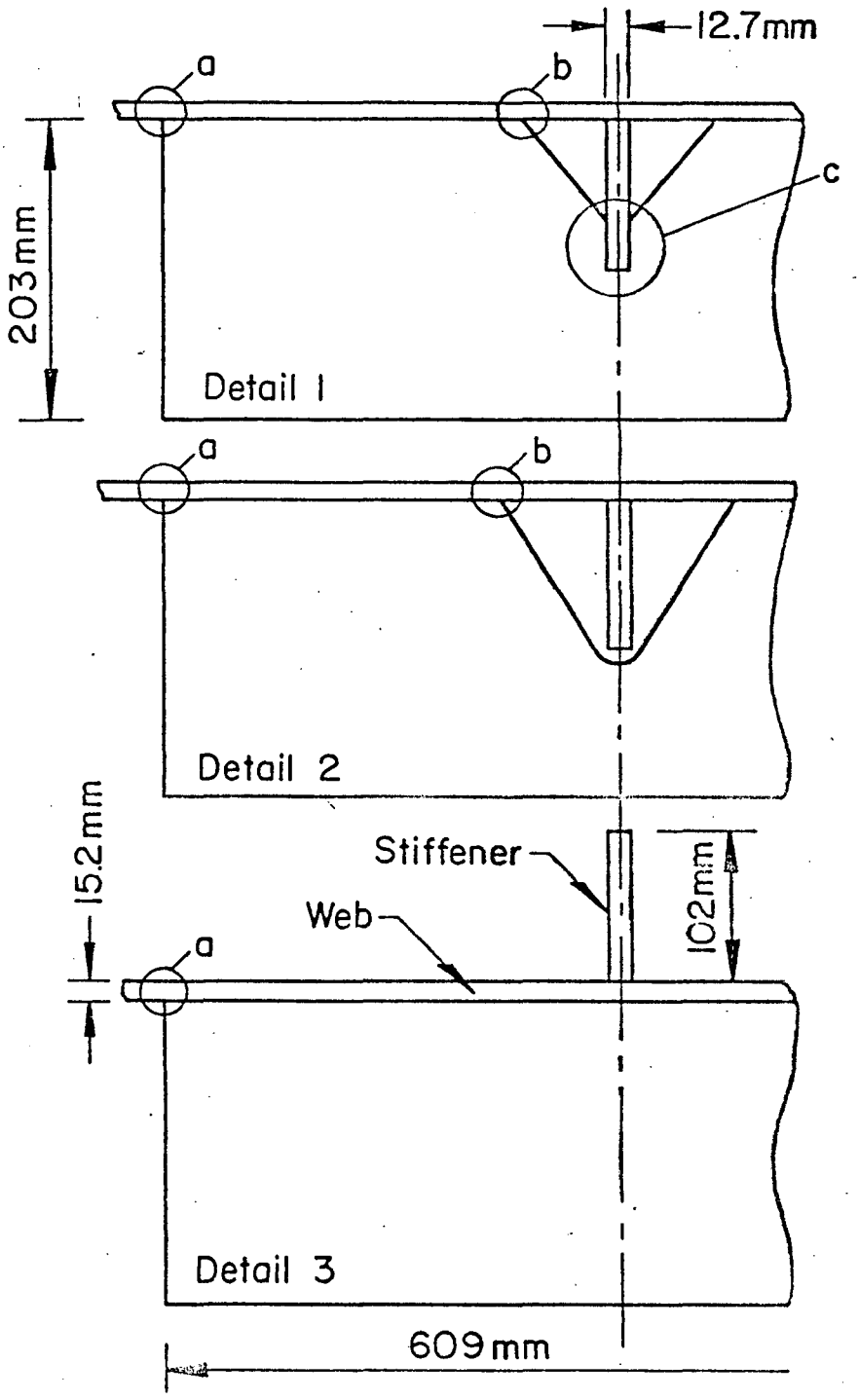

Fig. 31 Selected Details and Critical Locations

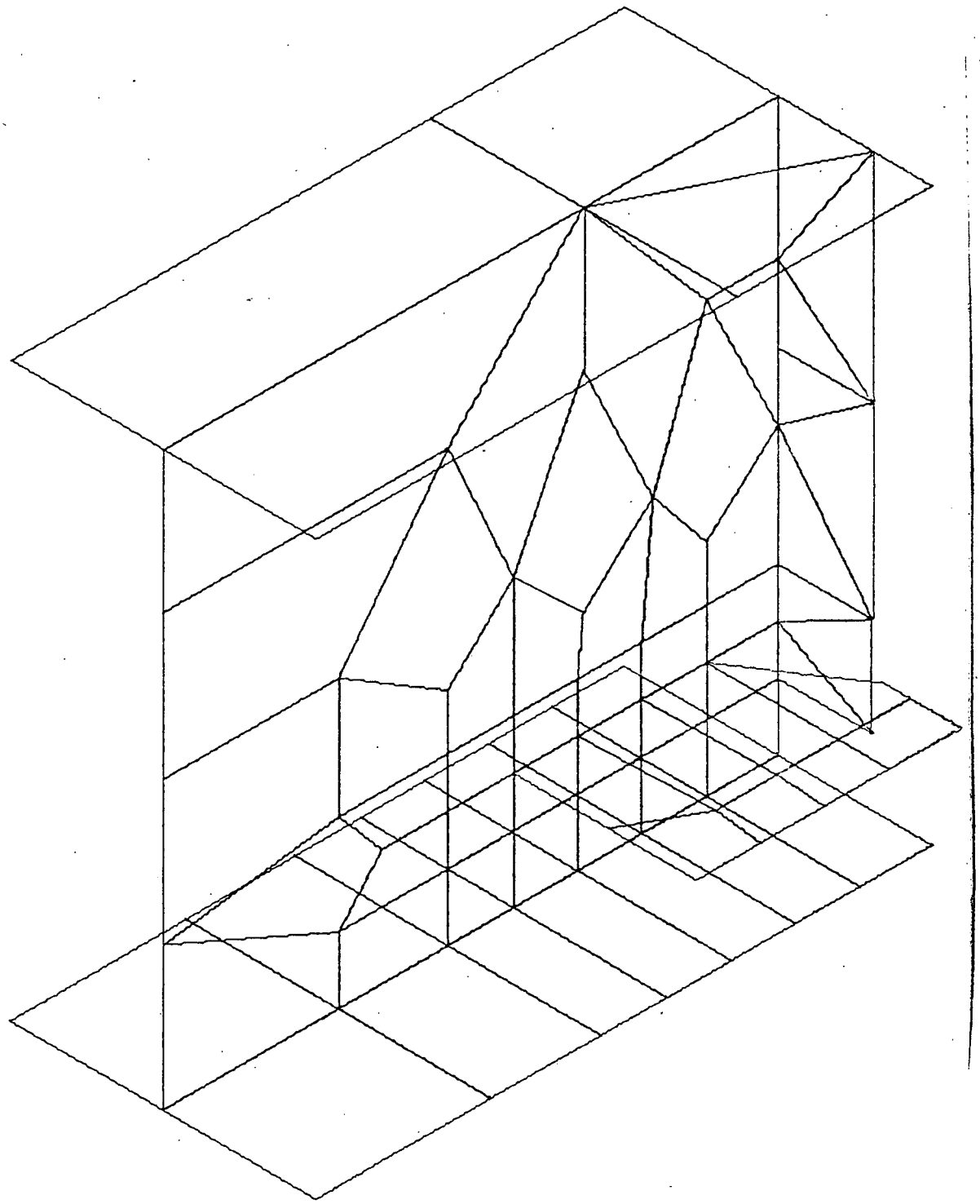

Fig. 35 (continued) Two-Dimensional Analysis of the Girder Central Part in Case of Detail 2

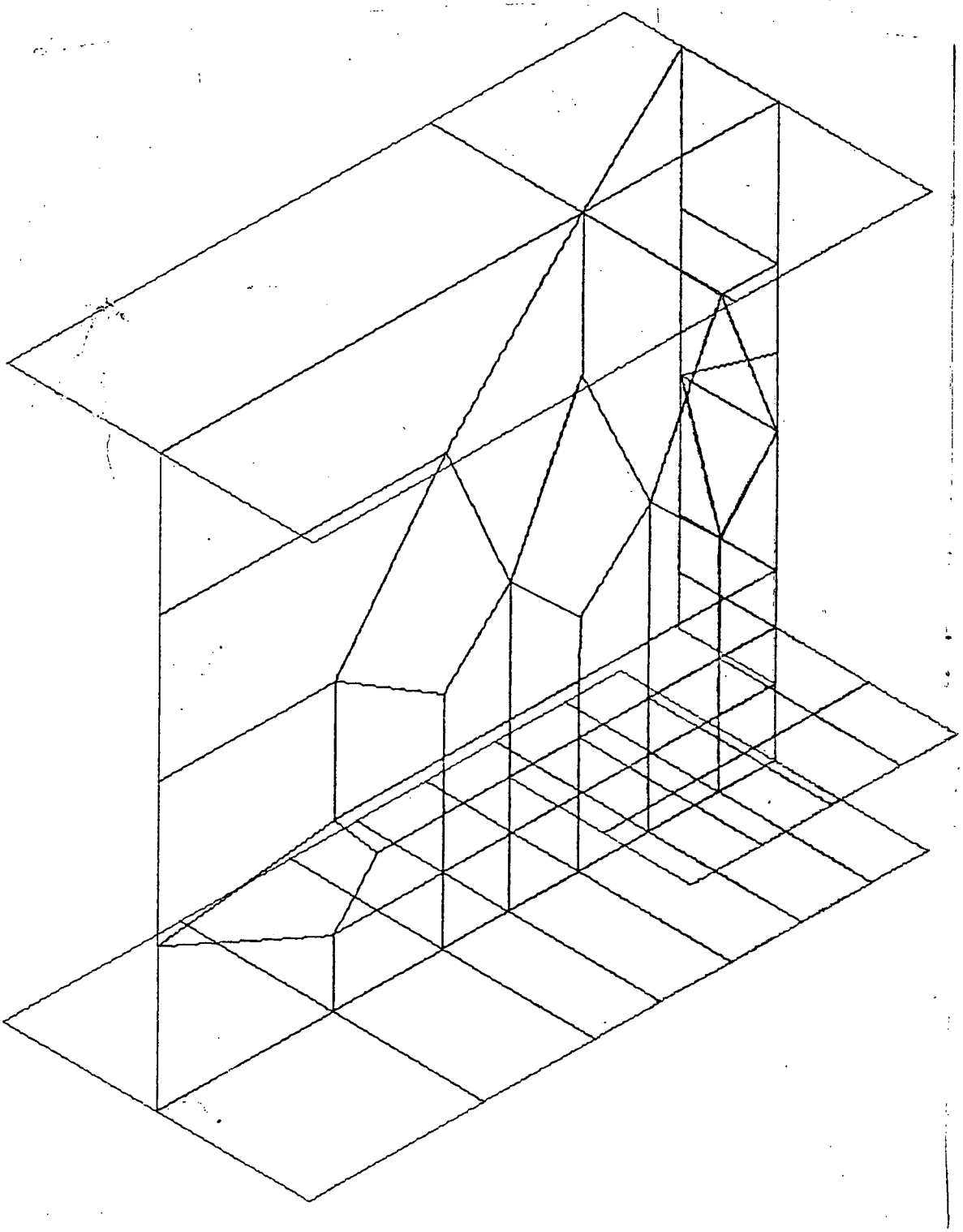

Fig. 35 (continued) Two-Dimensional Analysis of the Girder Central Part in Case of Detail 3

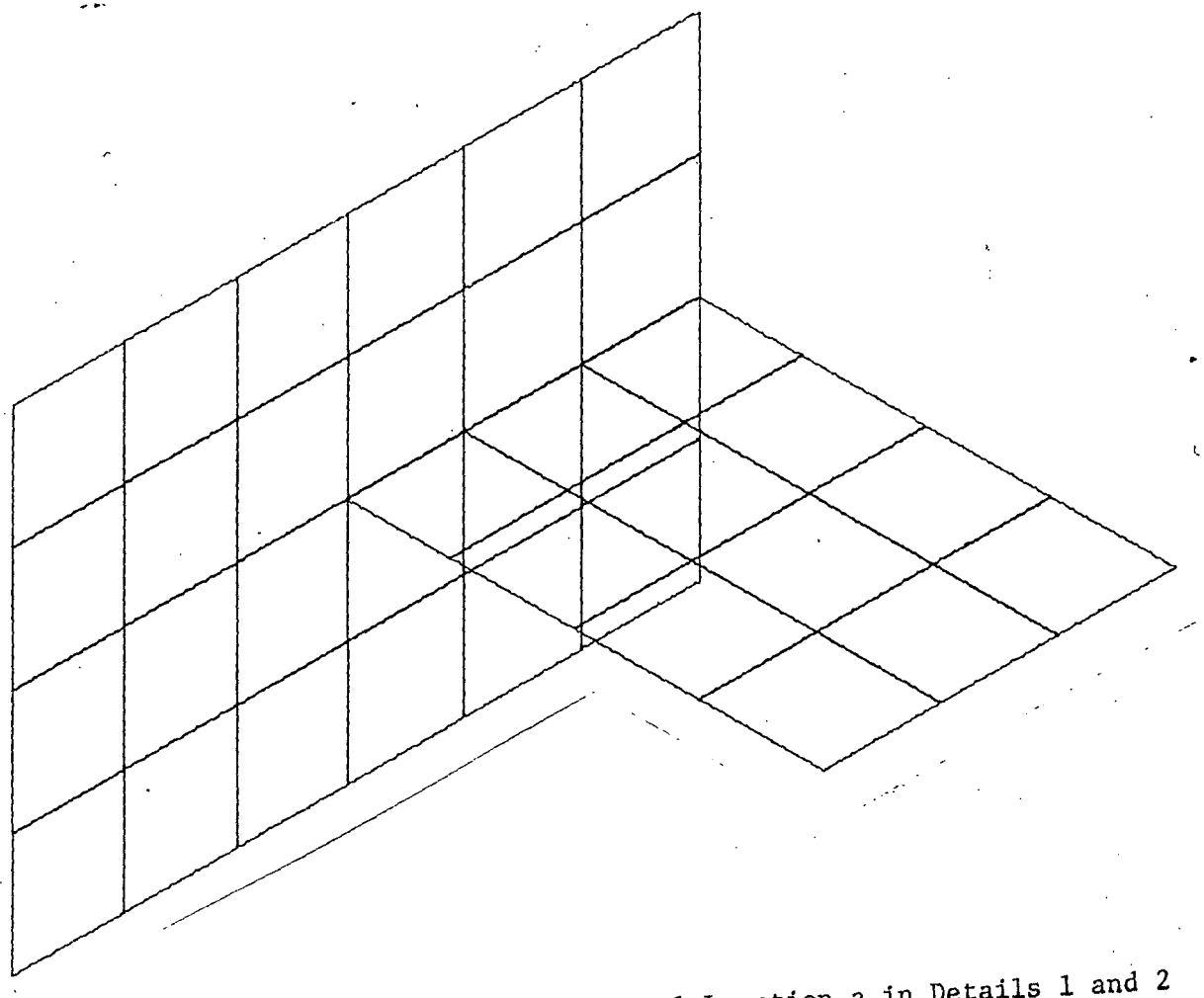

Fig. 36 Two-Dimensional Analysis of Critical Location a in Details 1 and 2

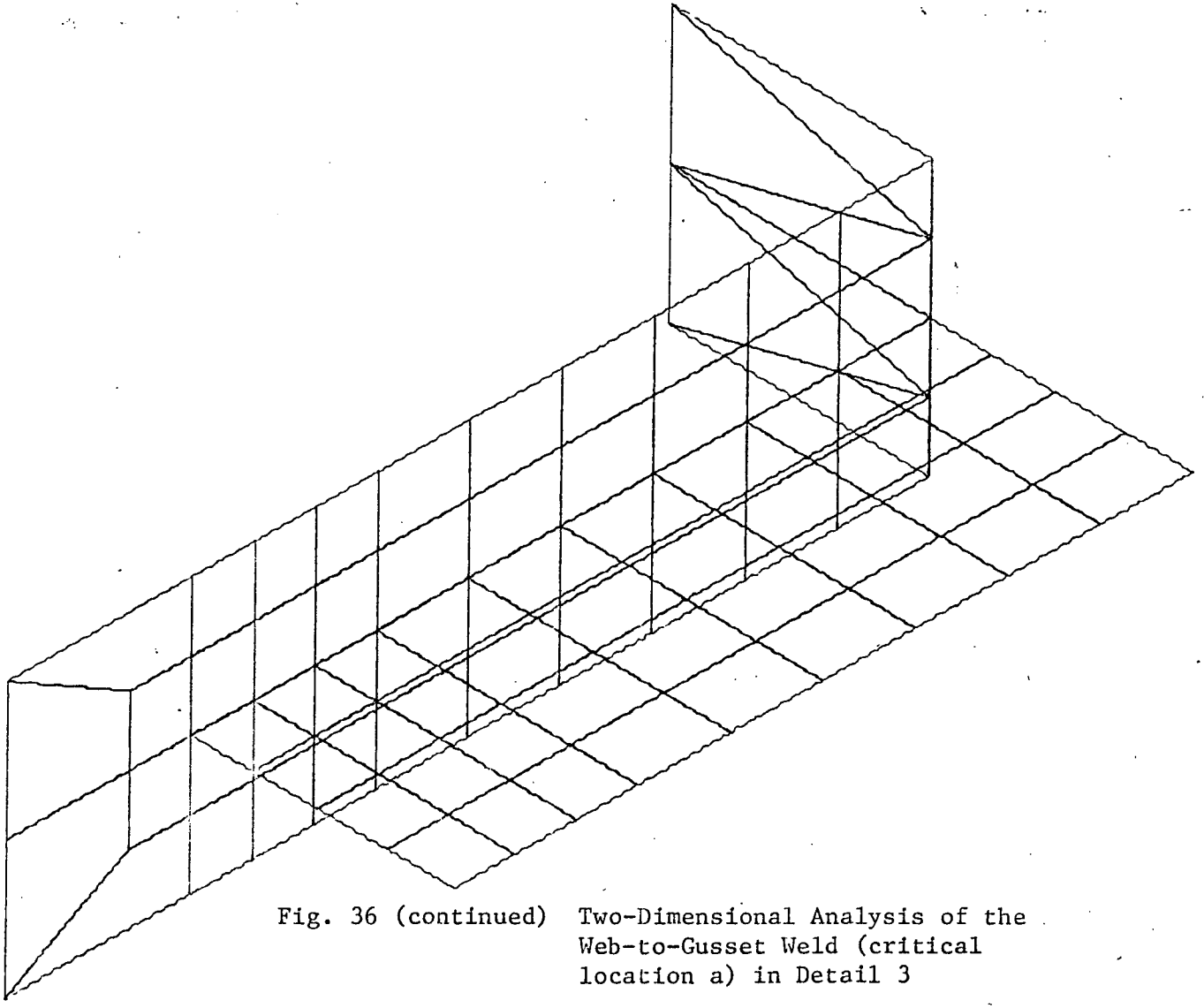

Fig. 36 (continued) Two-Dimensional Analysis of the Web-to-Gusset Weld (critical location a) in Detail 3

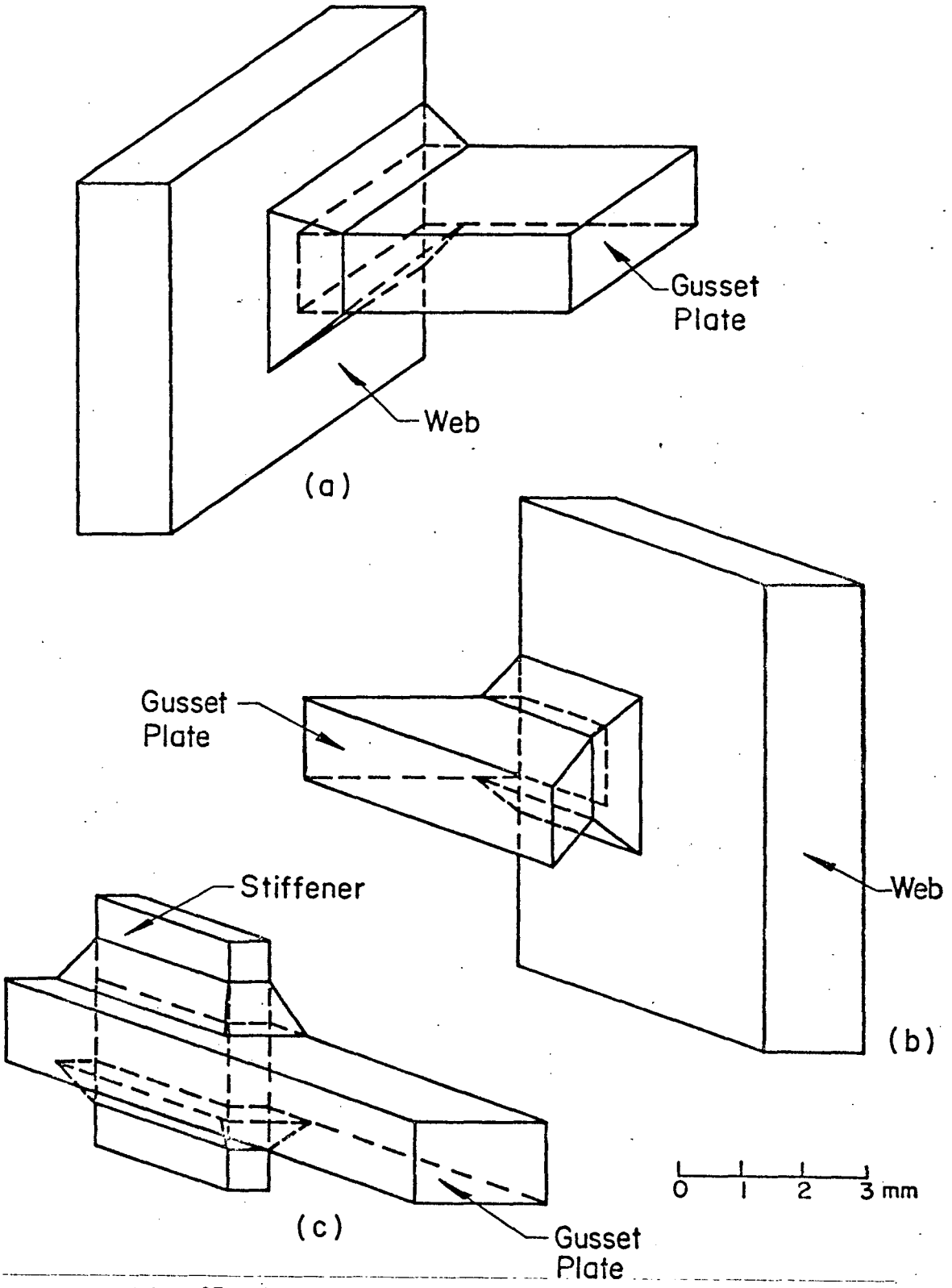

Fig. 37 Three-Dimension Analysis
(a) Critical Location a, details 1,2,3
(b) Critical Location b, details 1,2
(c) Critical Location c, details 3

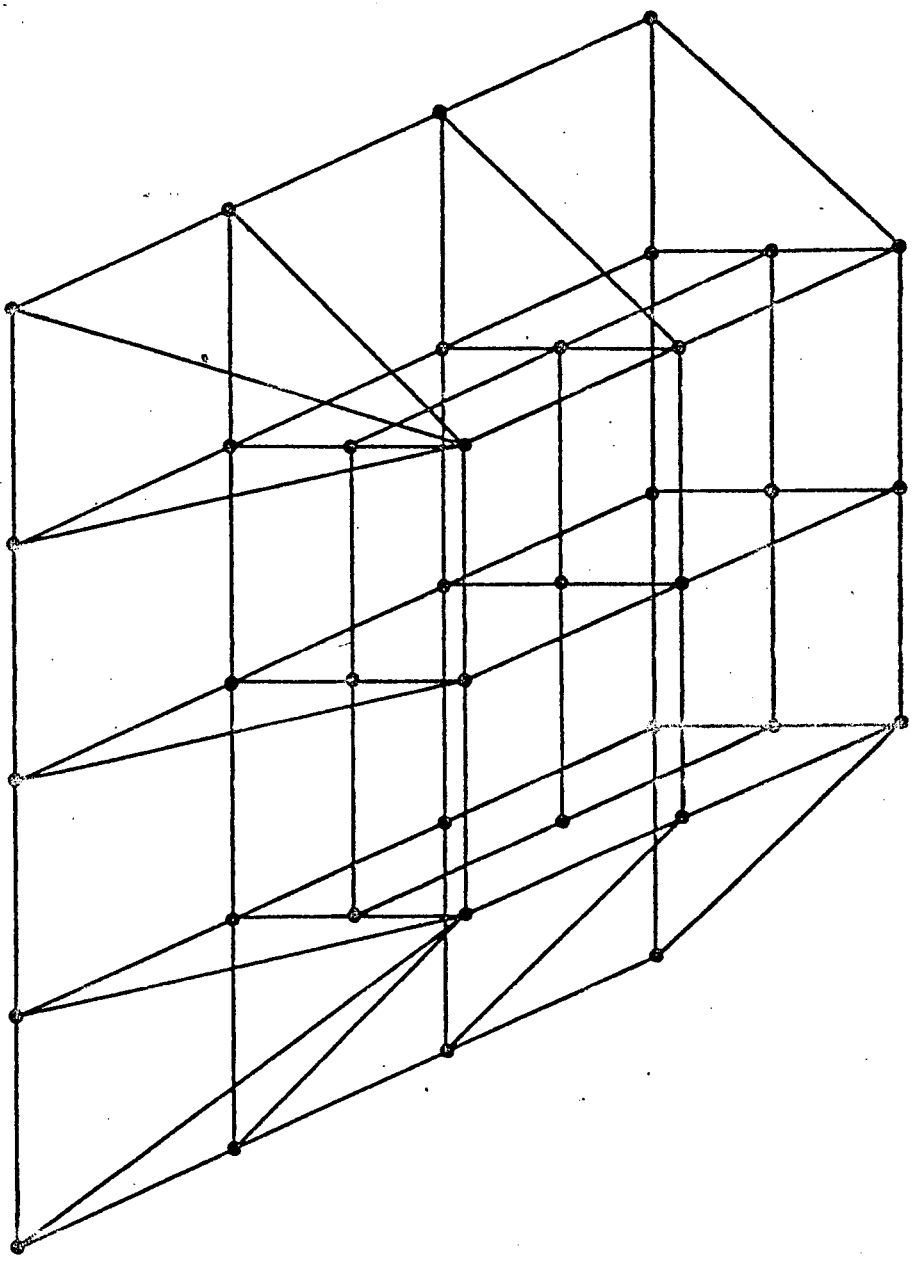

Fig. 38 Idealization and Discretization of a Weld Toe

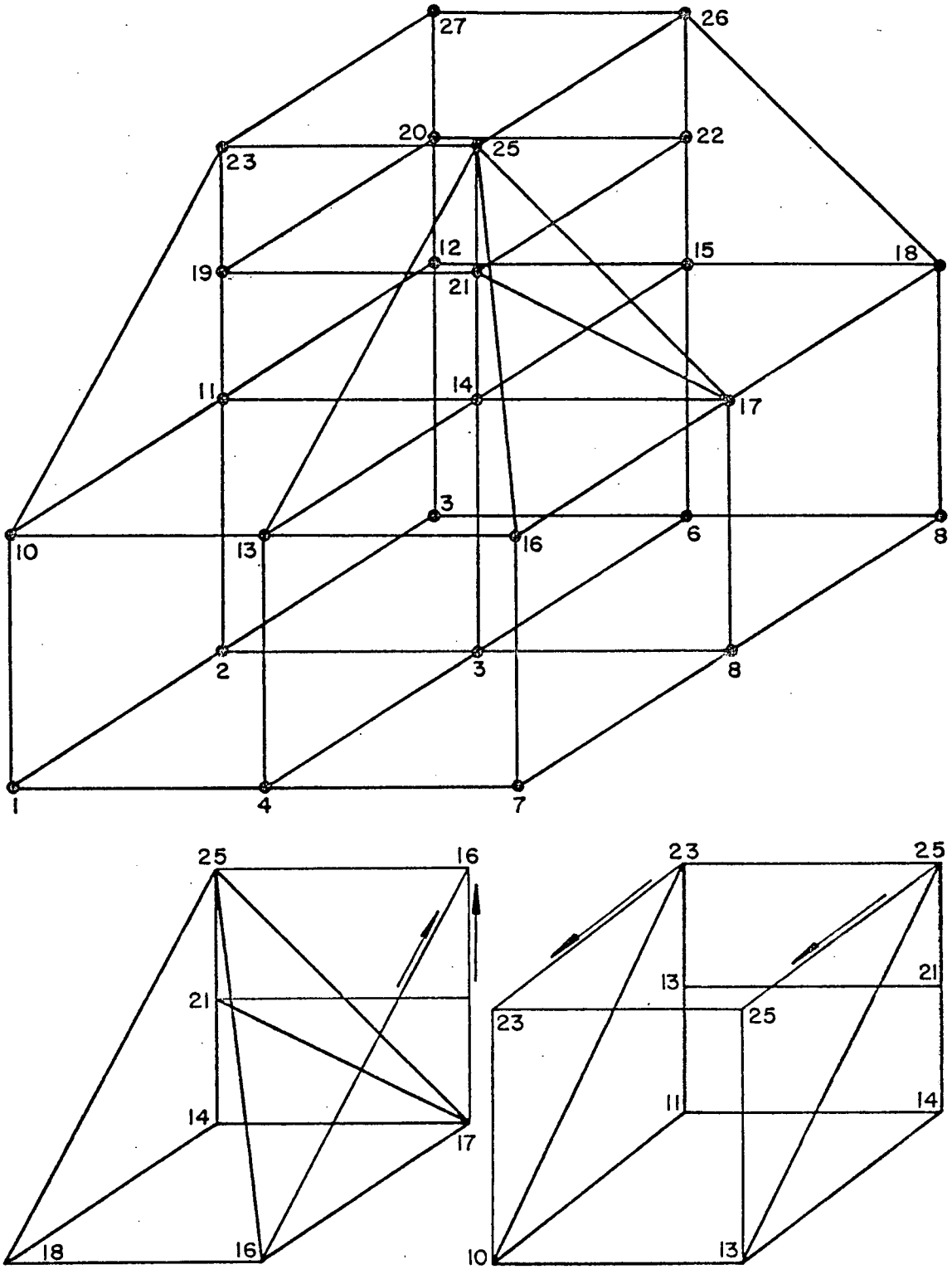

Fig. 39 Numbering Pattern for Cubic and Skewed Elements

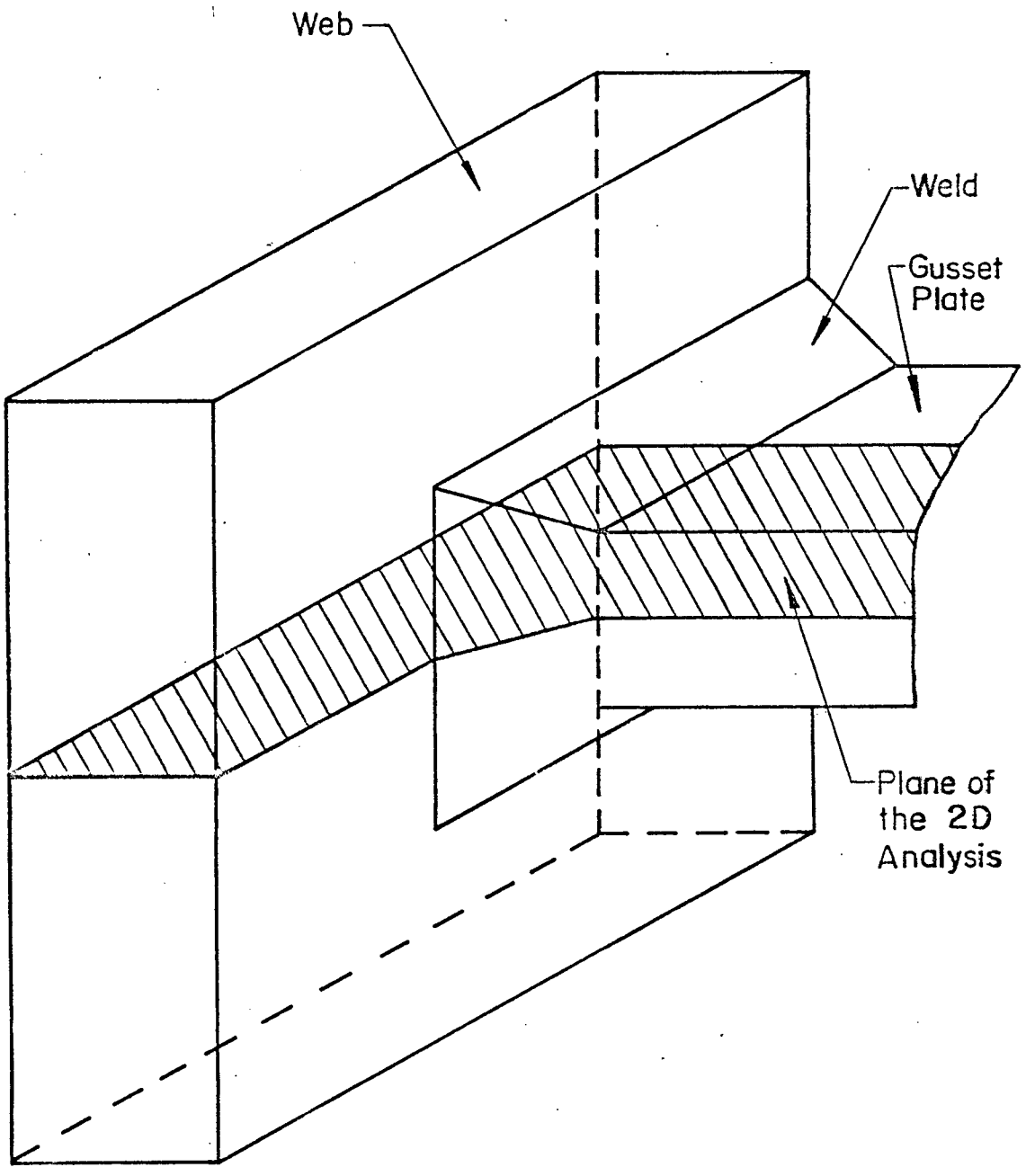

Fig. 310 Example of Selection of a Section in a 3D Discretization for further 2D Analysis

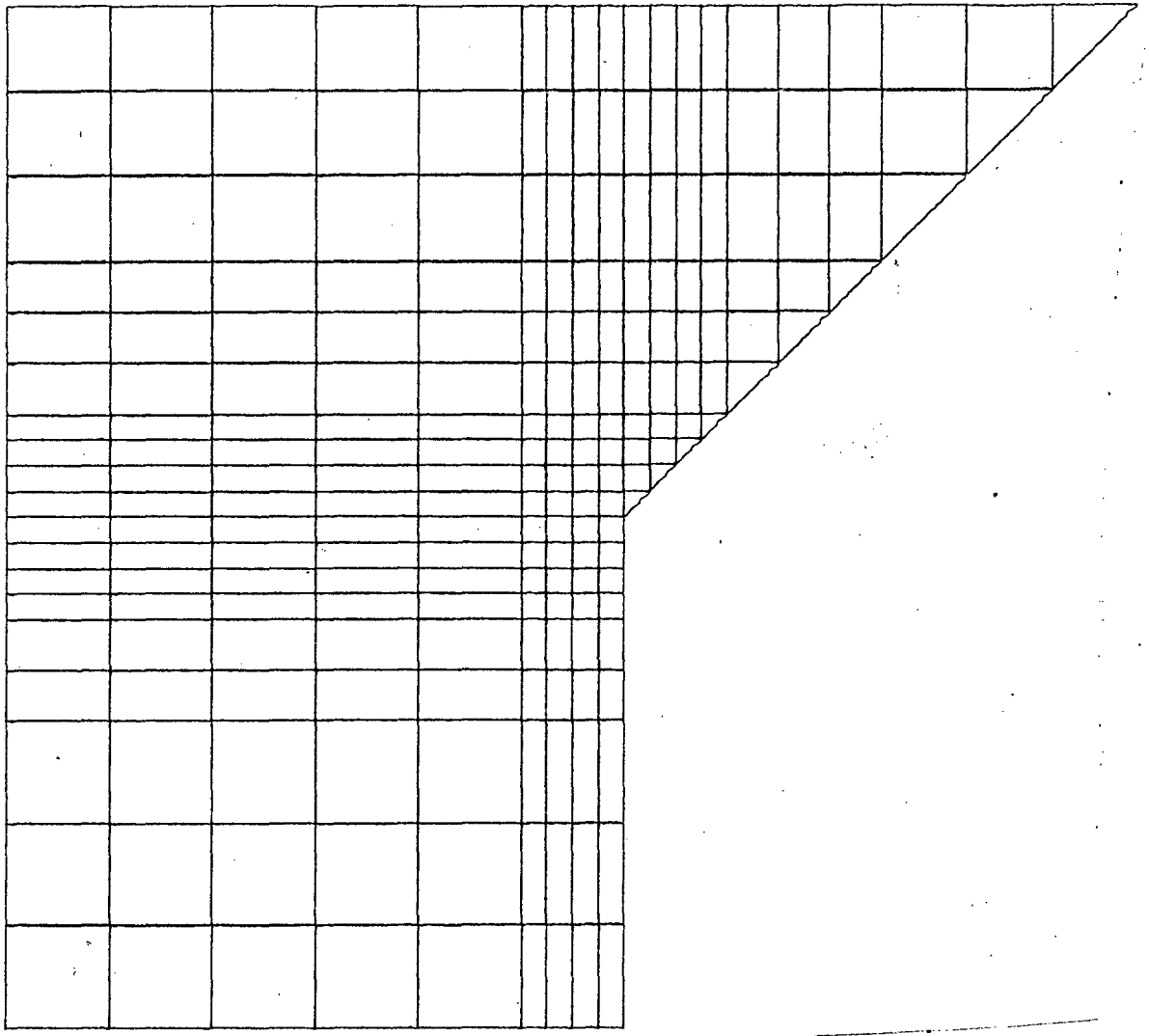

Fig. 311 Two-Dimensional Analysis of Critical Locations a and b

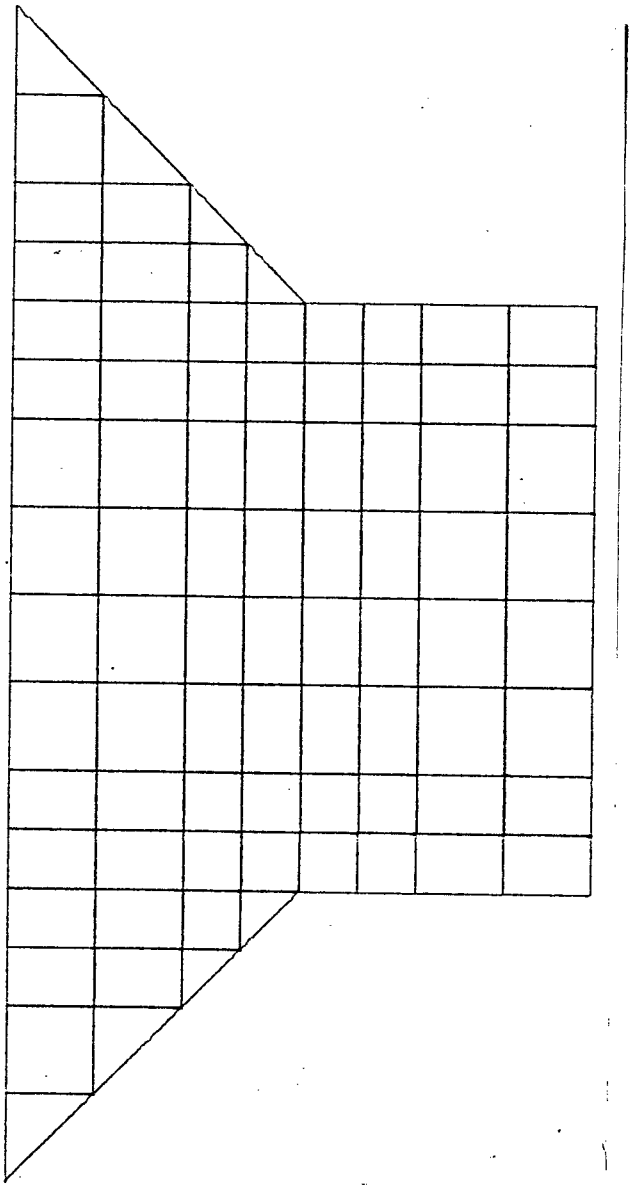

Fig. 311 (continued) Two-Dimensional Analysis of Critical Location c

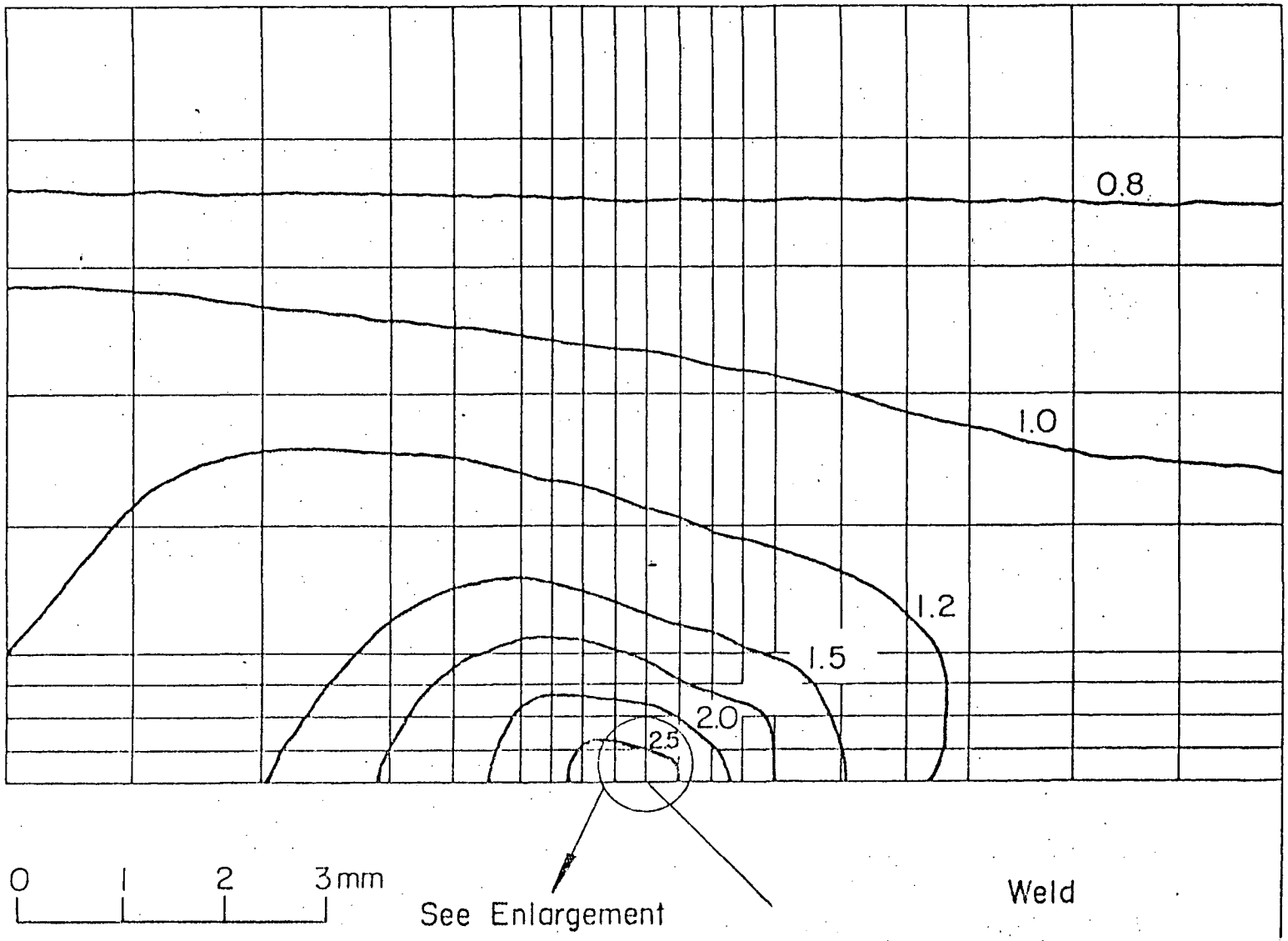

Fig. 312 SCF Contours for Critical Location a in Detail 1 (large scale)

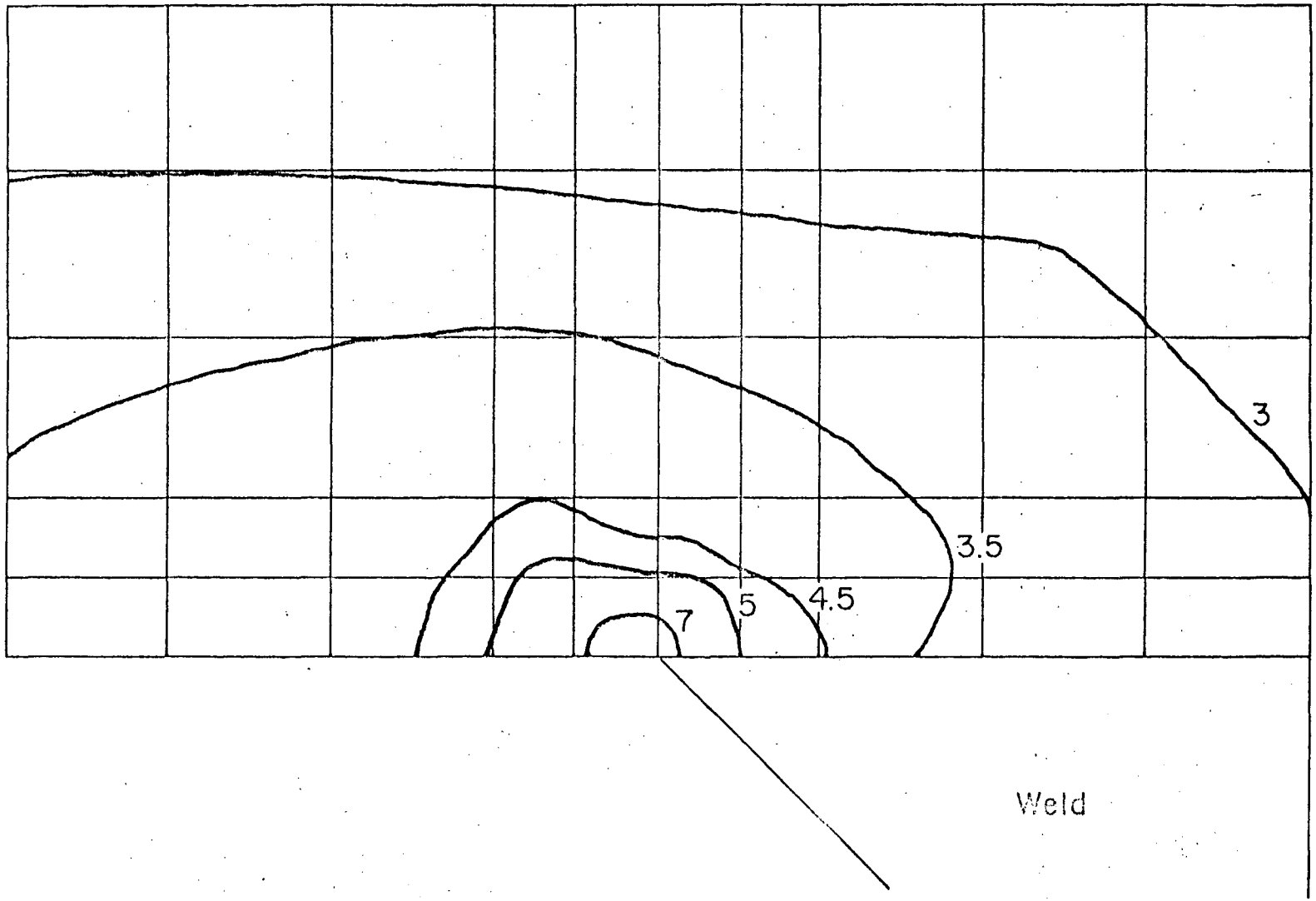

Fig. 312 (continued) SCF Contours for Critical Location a in Detail 1 (small Scale)

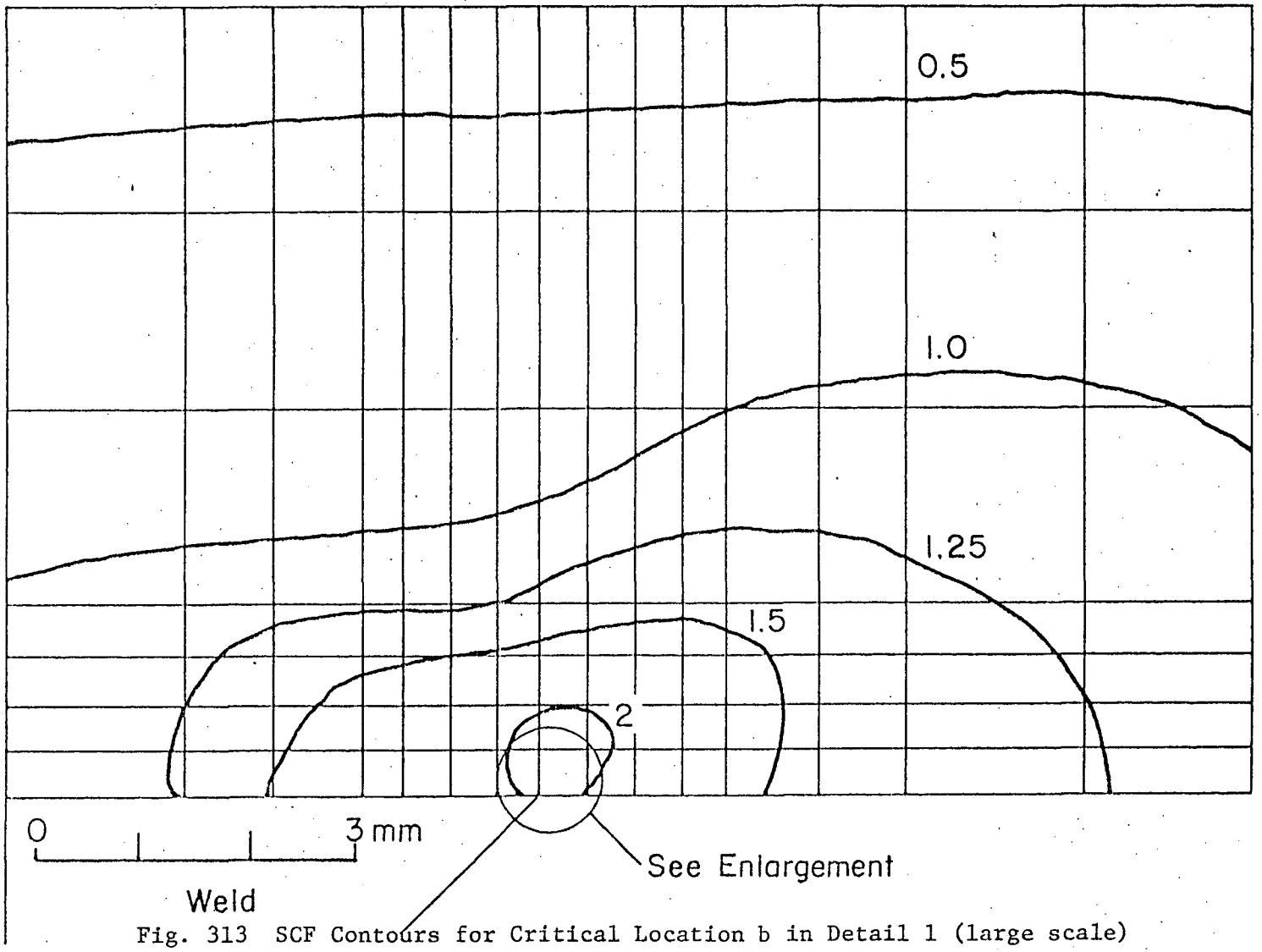

Fig. 313 SCF Contours for Critical Location b in Detail 1 (large scale)

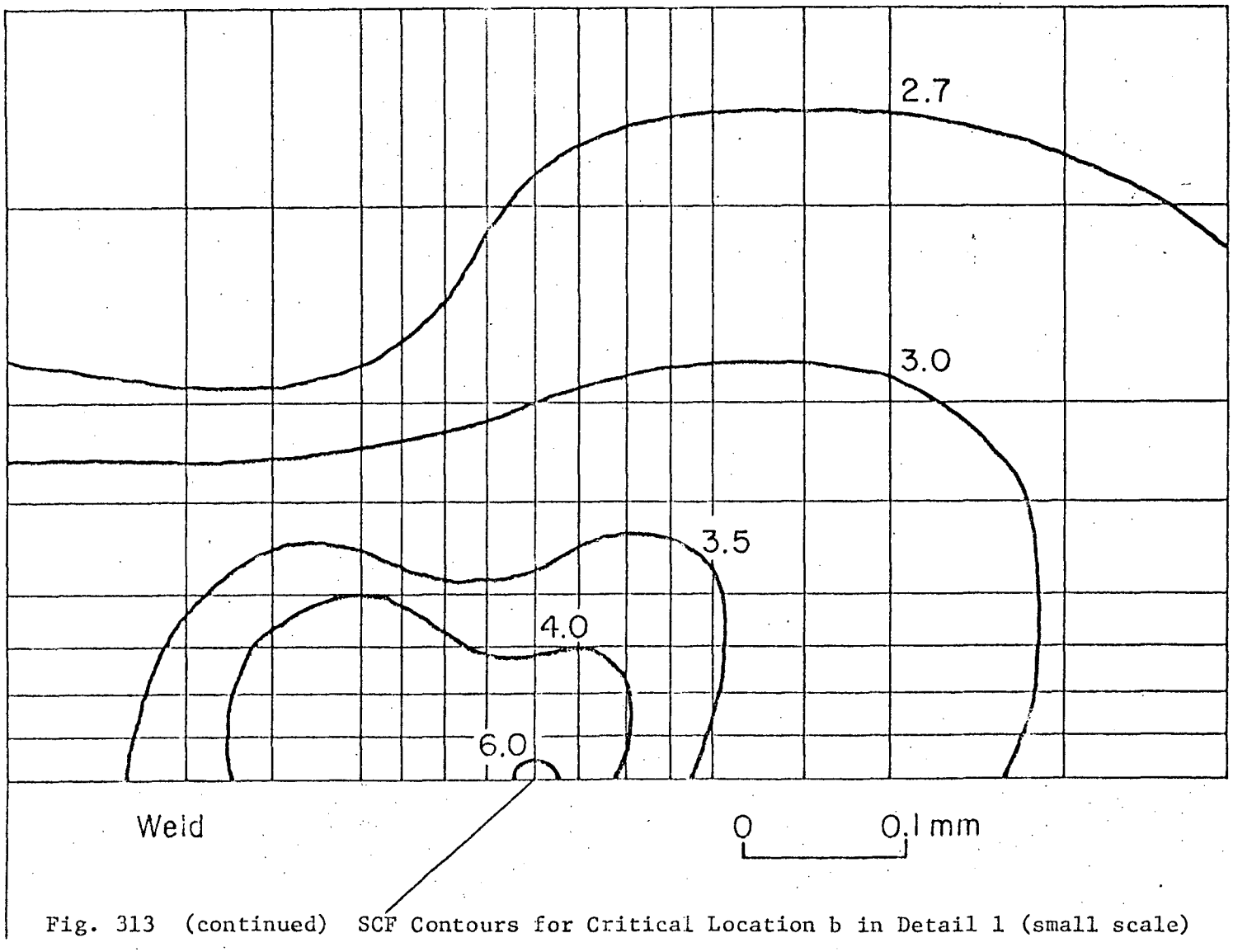

Fig. 313 (continued) SCF Contours for Critical Location b in Detail 1 (small scale)

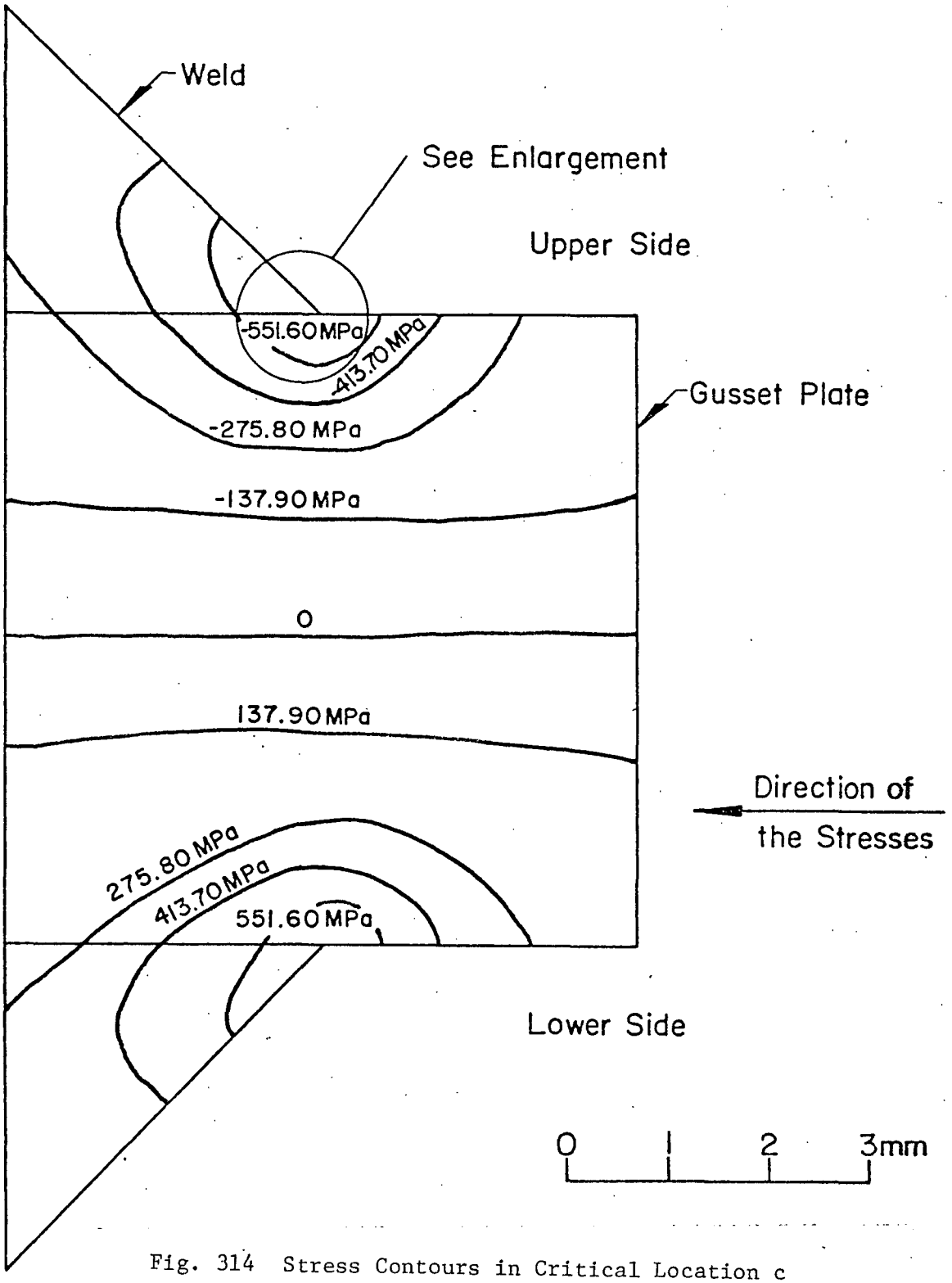

Fig. 314 Stress Contours in Critical Location c in Detail 1 (large scale)

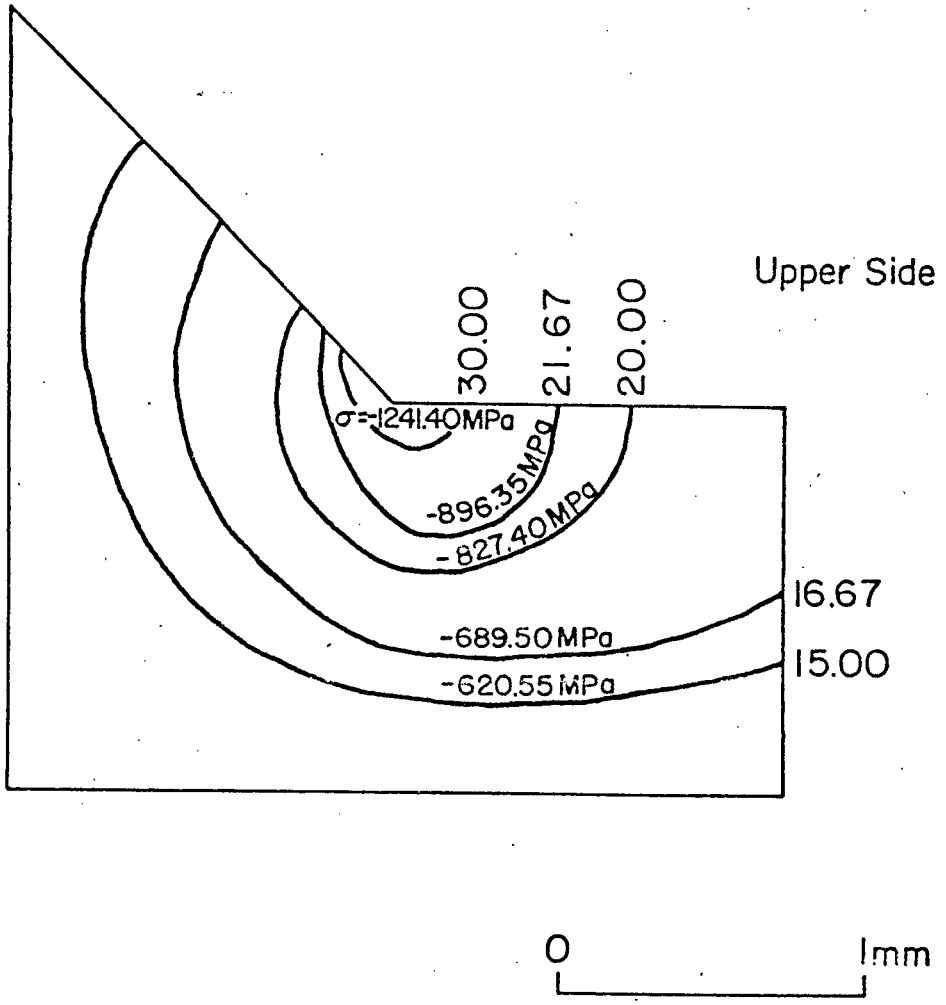

Fig. 314 (continued) Stress Contours in Critical Location c in Detail 1 (small scale)

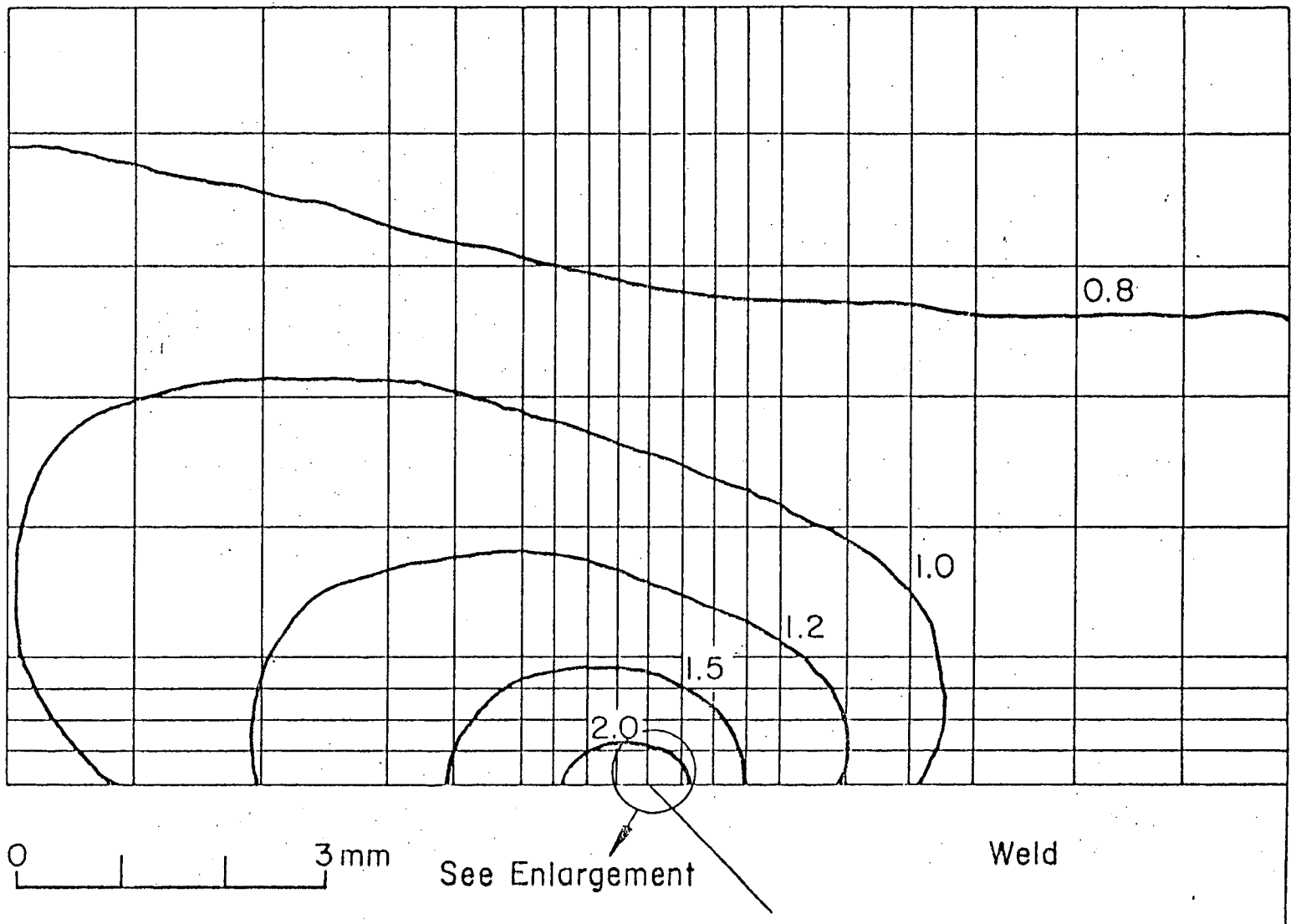

Fig. 315 SCF Contours for Critical Location a in Detail 2 (large scale)

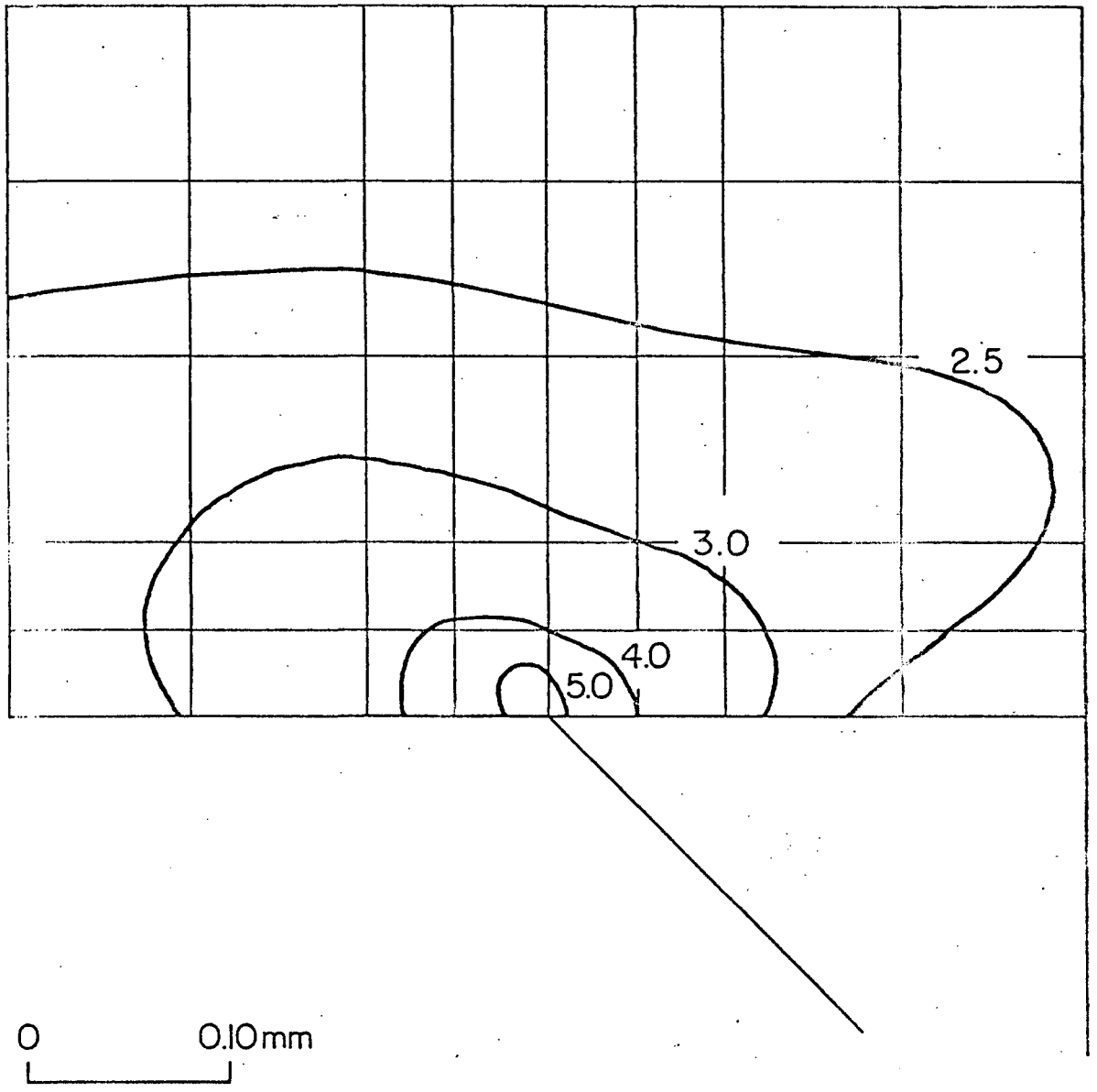

Fig. 315 (continued) SCF Contours for Critical Location a in Detail 2 (small scale)

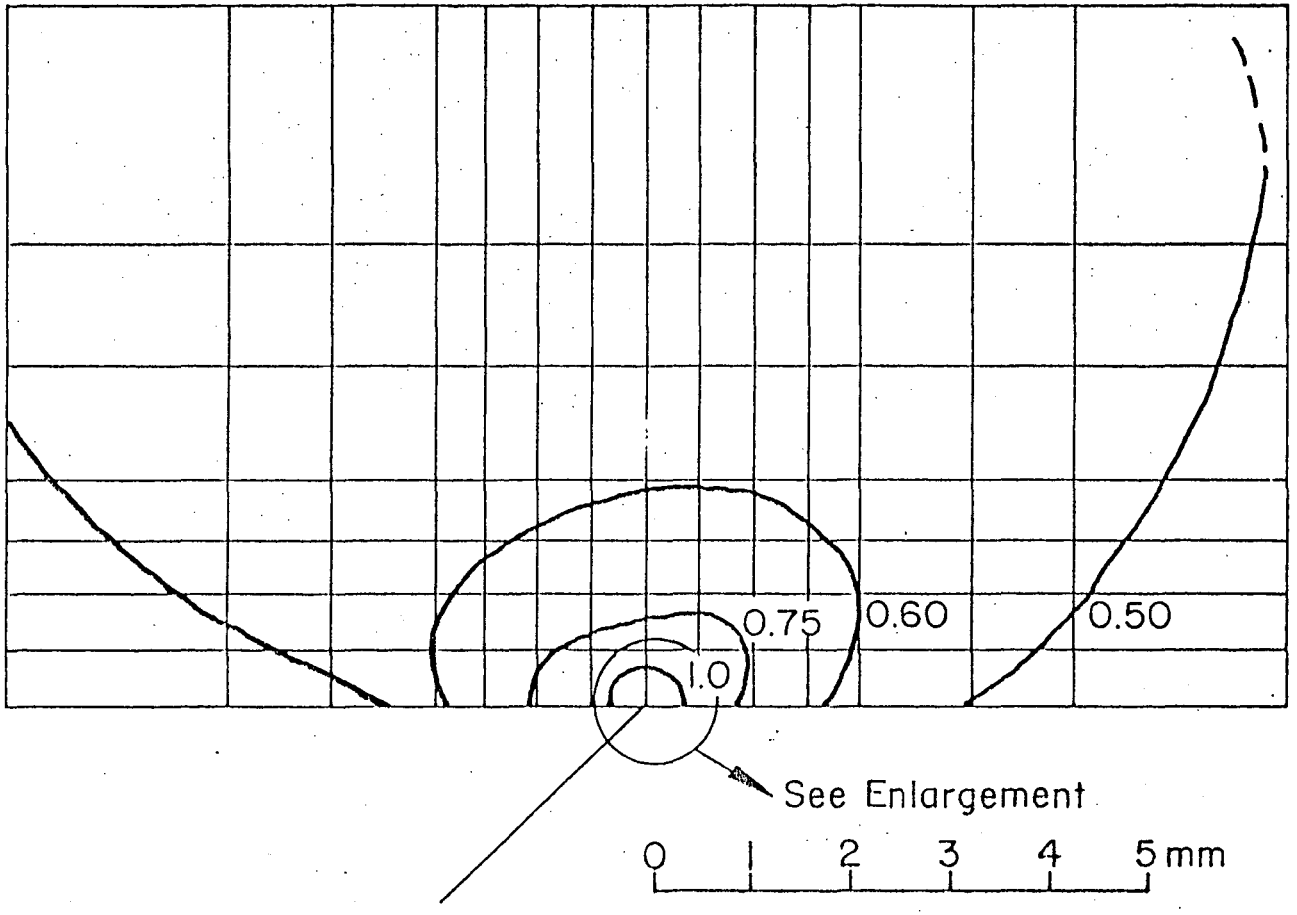

Fig. 316 SCF Contours for Critical Location b in Detail 2 (large Scale)

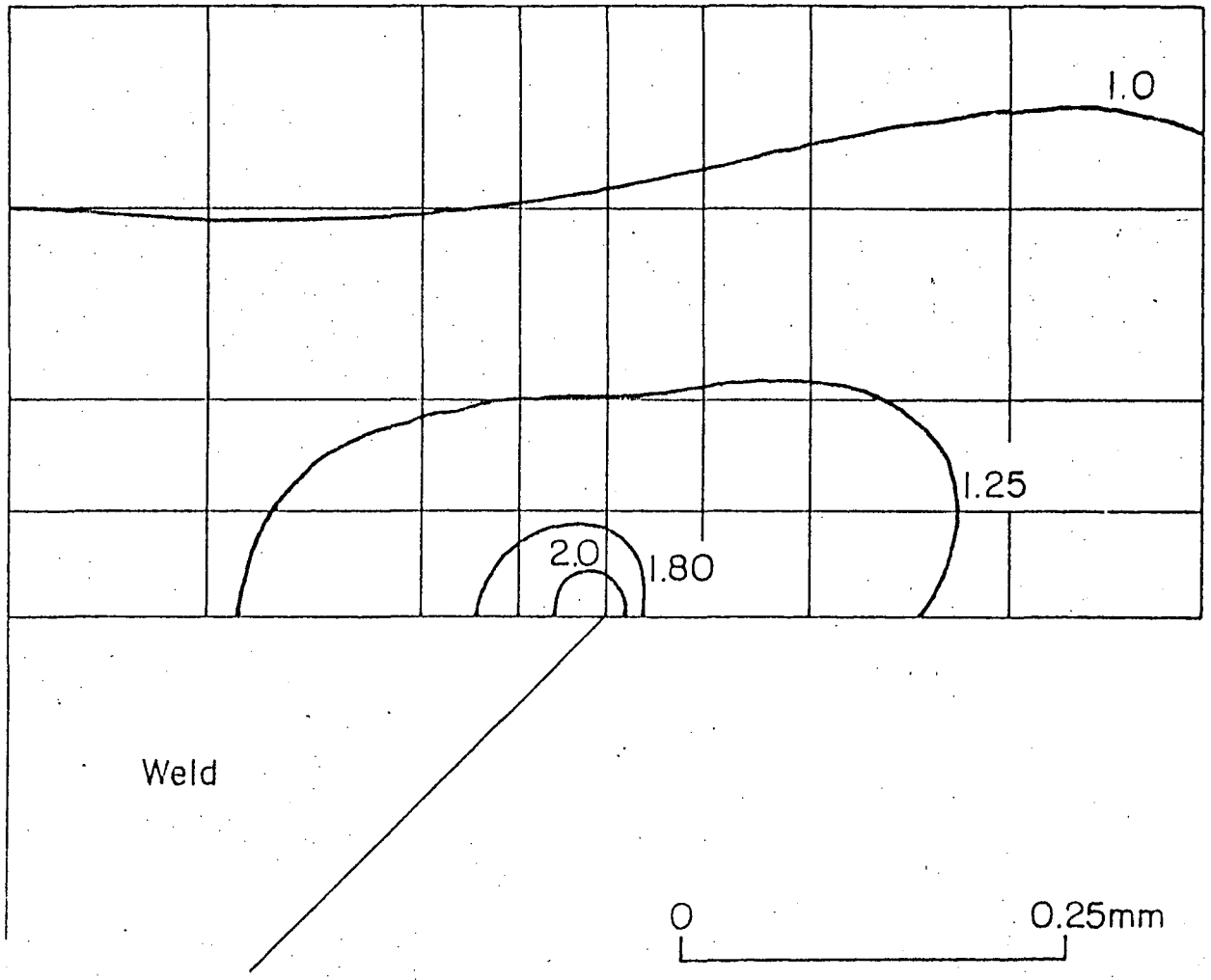

Fig. 316 (continued) SCF Contours for Critical Location b in Detail 2 (small scale)

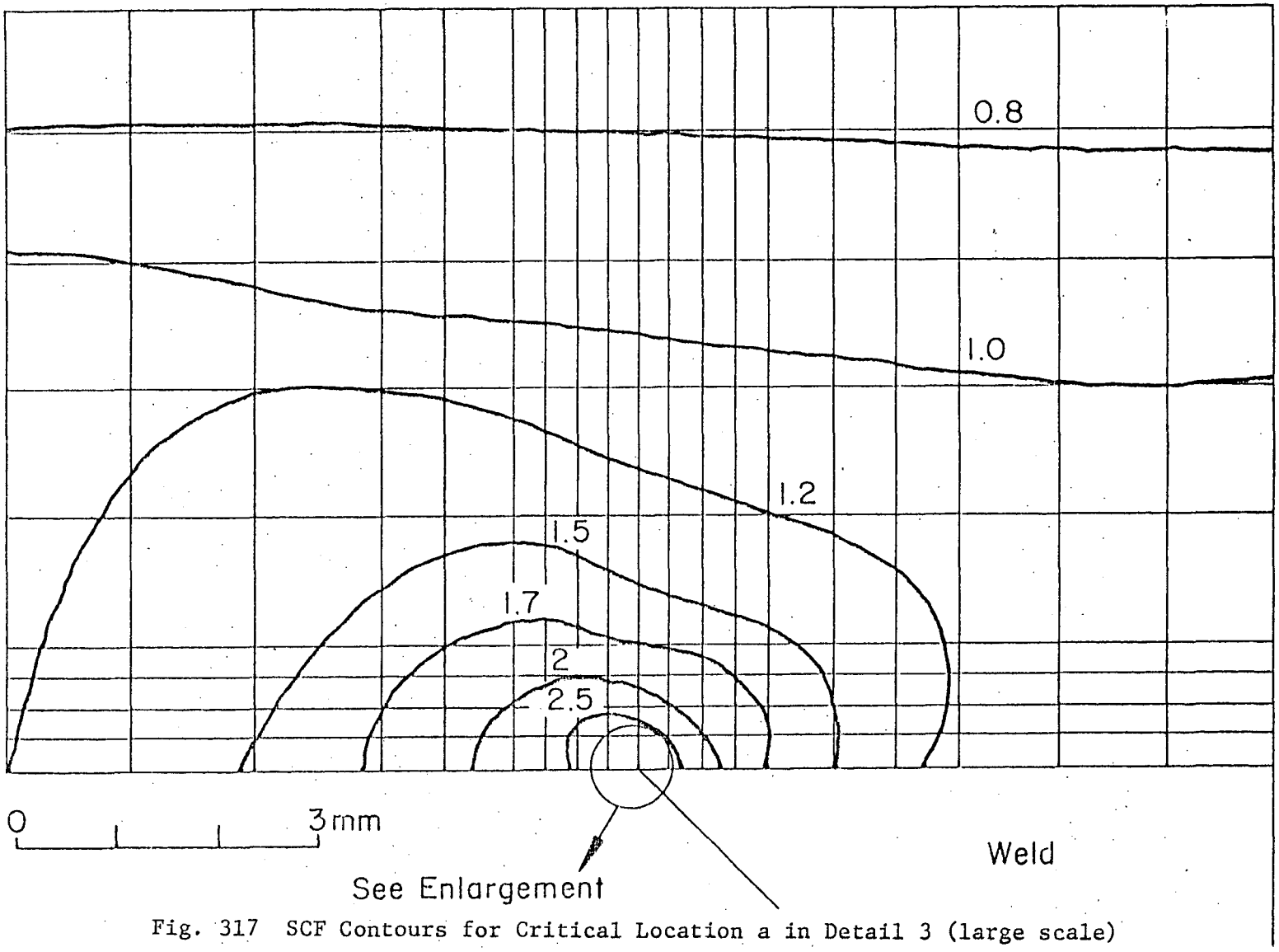

Fig. 317 SCF Contours for Critical Location a in Detail 3 (large scale)

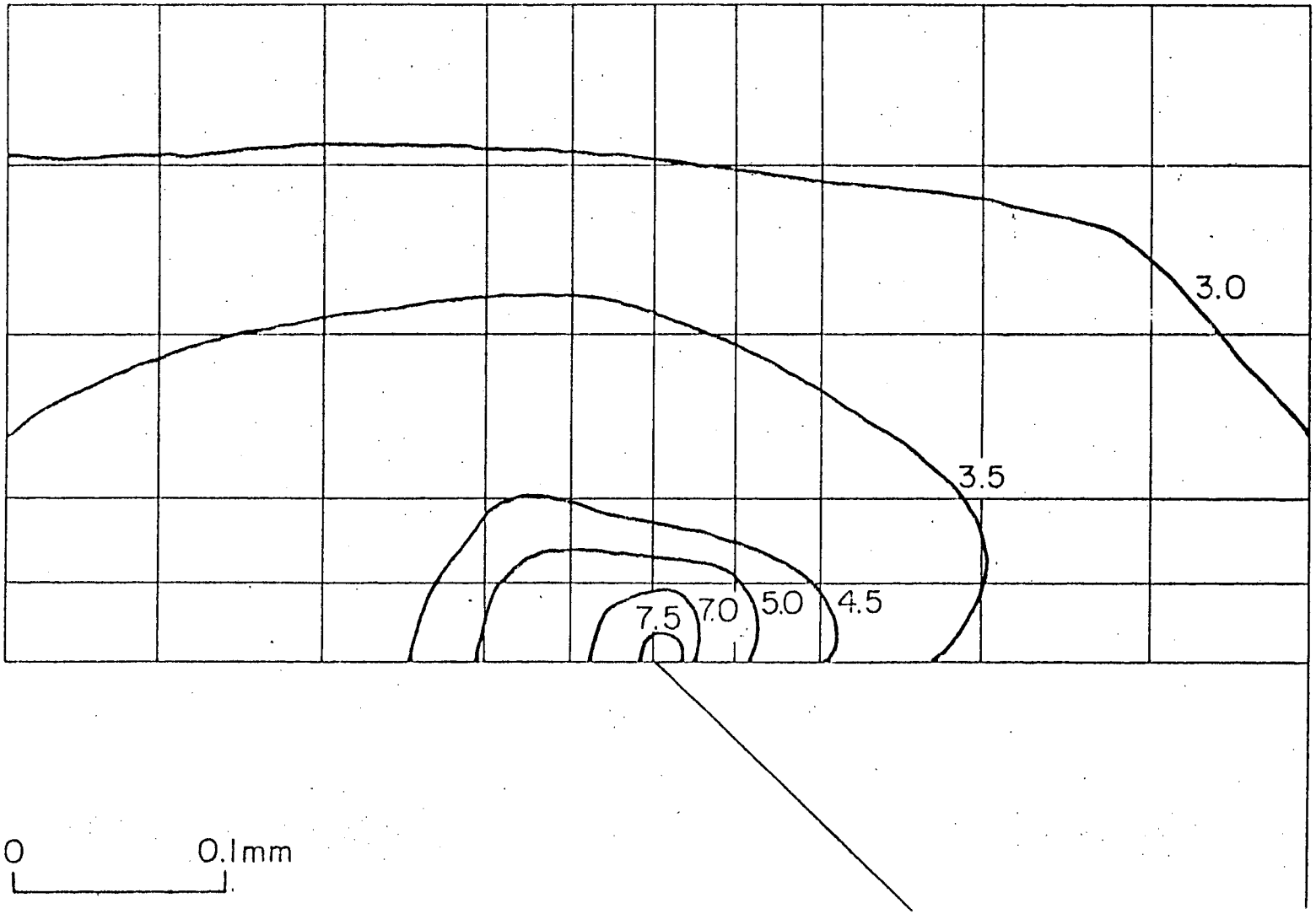

Fig. 317 (continued) SCF Contours for Critical Location a in Detail 3 (small scale)

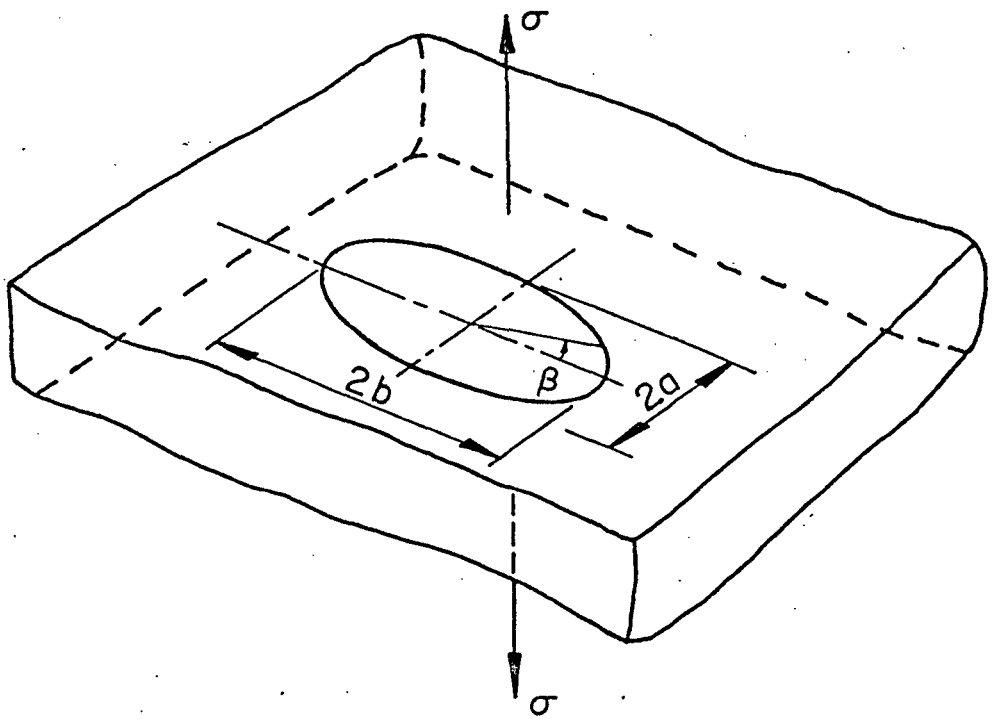

Fig. 318 Elliptical Crack Embedded in an Infinite Body Subjected to Uniform Tensile Stress

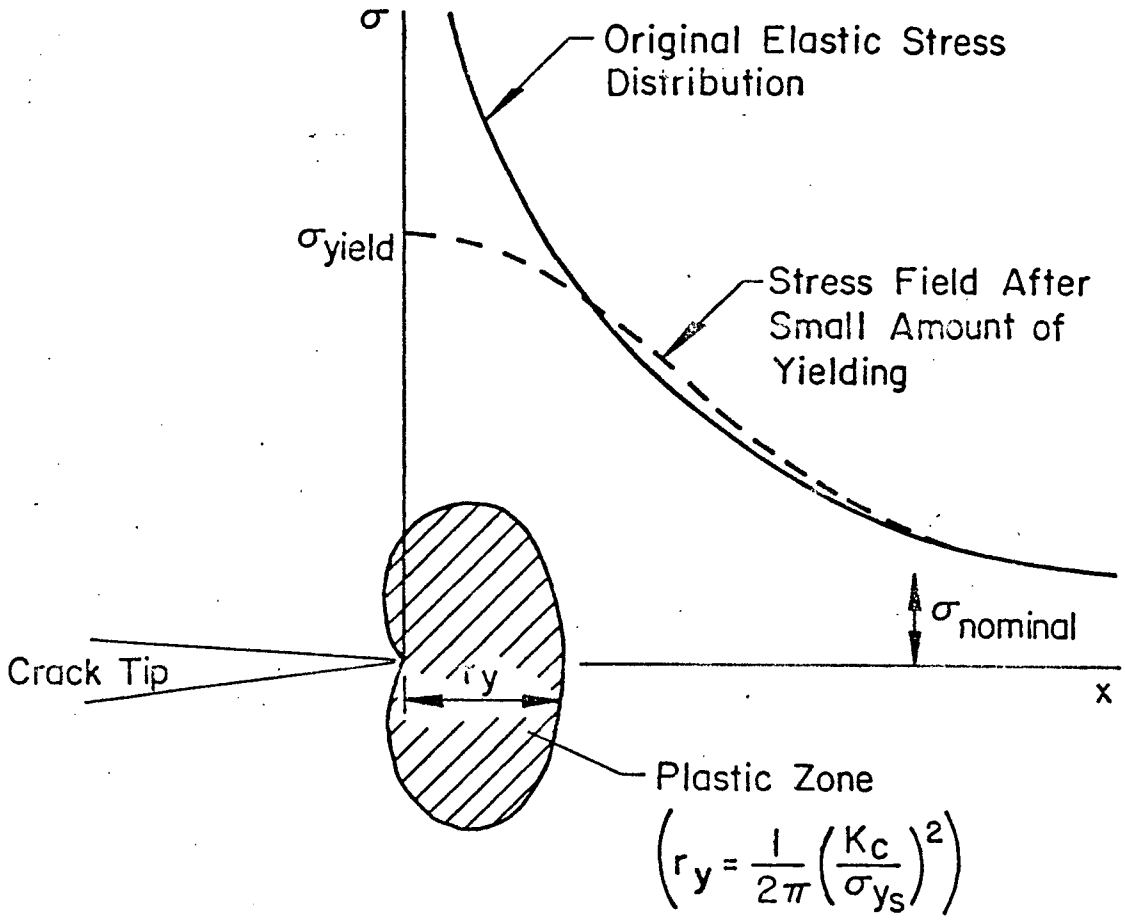

Fig. 319 Stress Distribution at Crack Vicinity

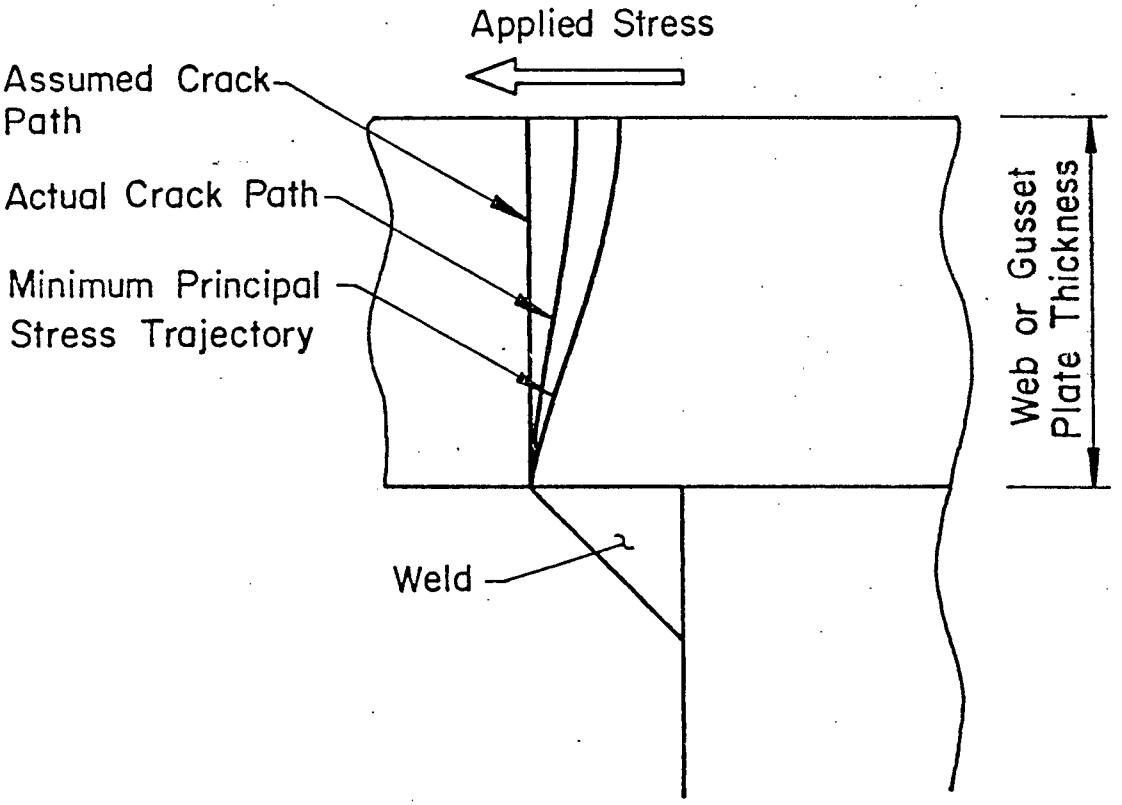

Fig. 320 Crack Path

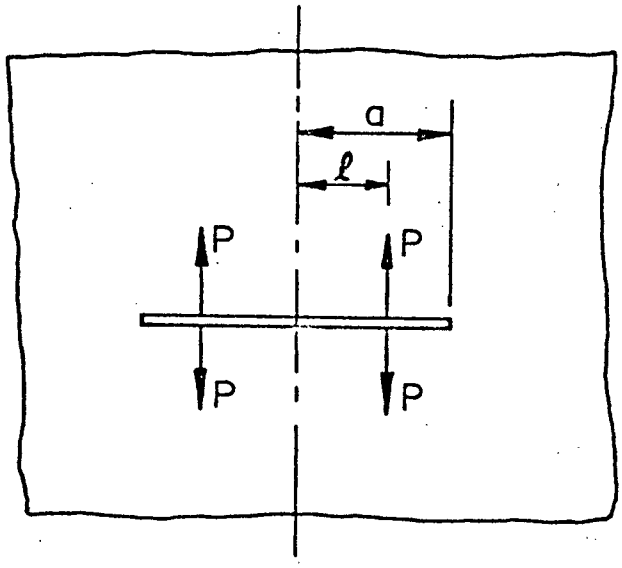

Fig. 321 Albrecht's Crack Loading

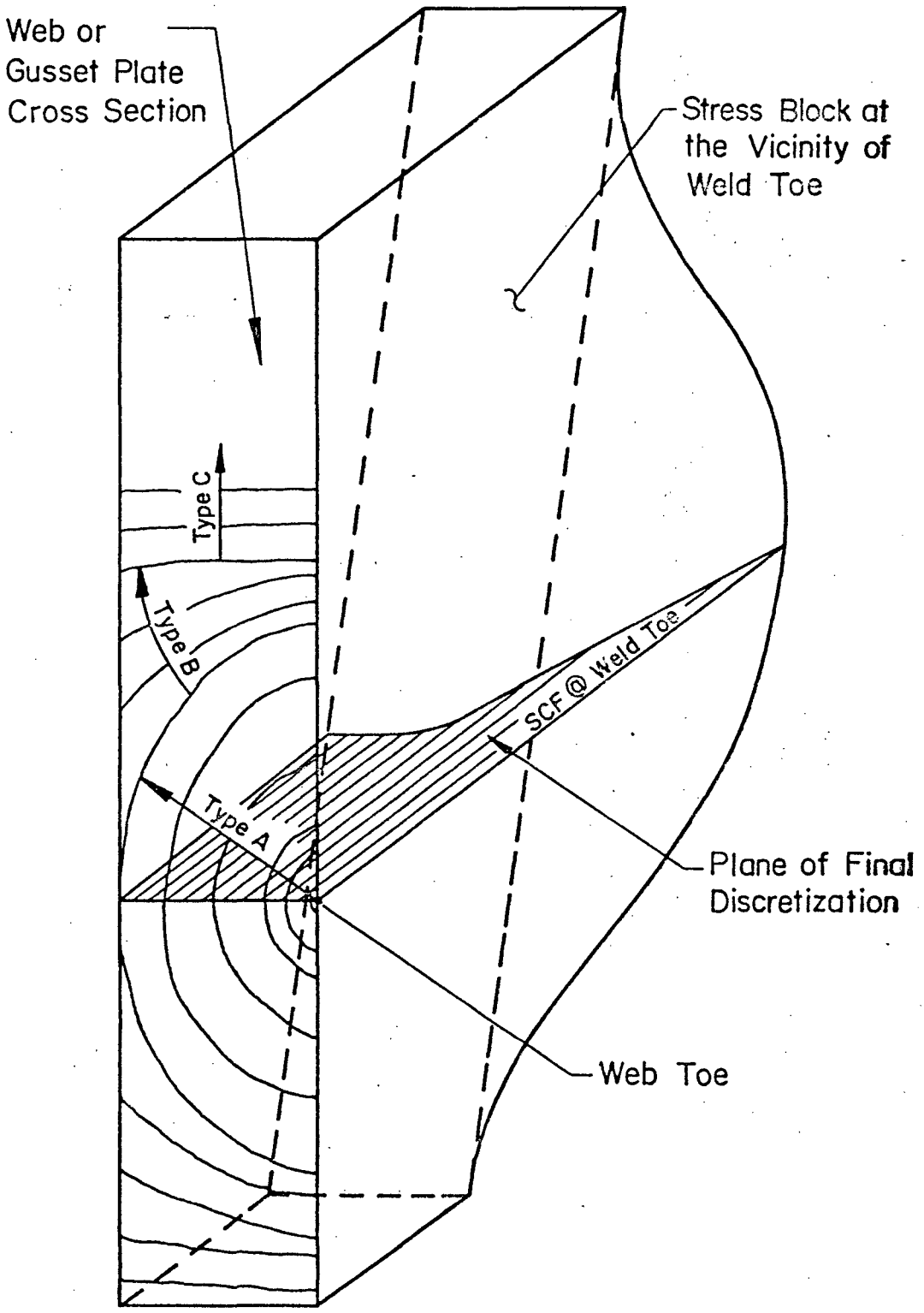

Fig. 322 Stress Block and Crack Propagation Scheme through Web or Gusset Plate Thickness

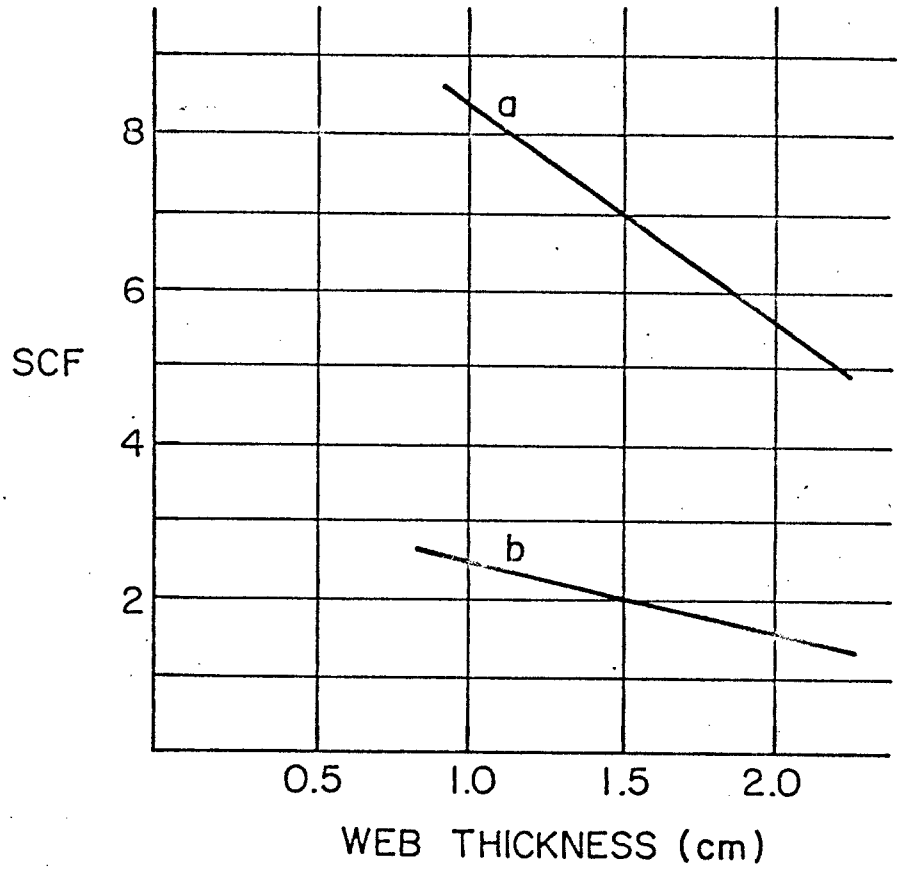

Fig. 323 Effect of Web Thickness on Maximum SCF at Critical Locations a and b

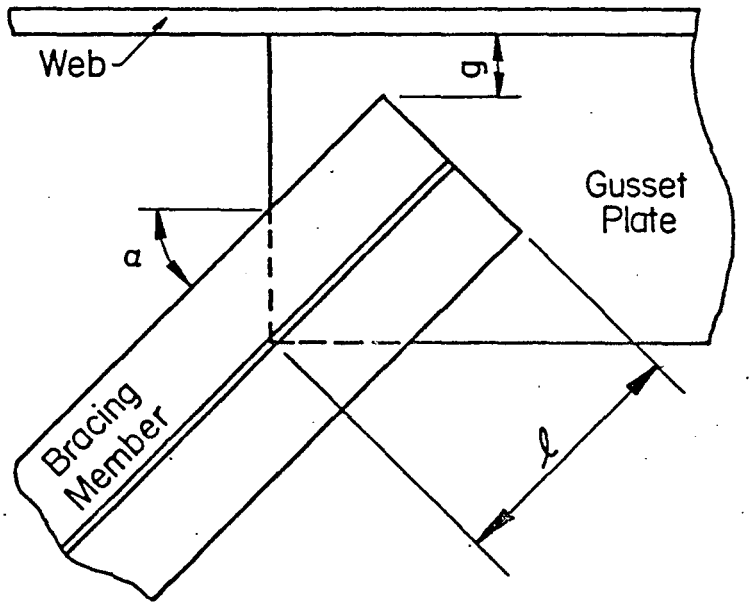

Fig. 324 Parameters of the Gusset-to-Bracing Members Connection

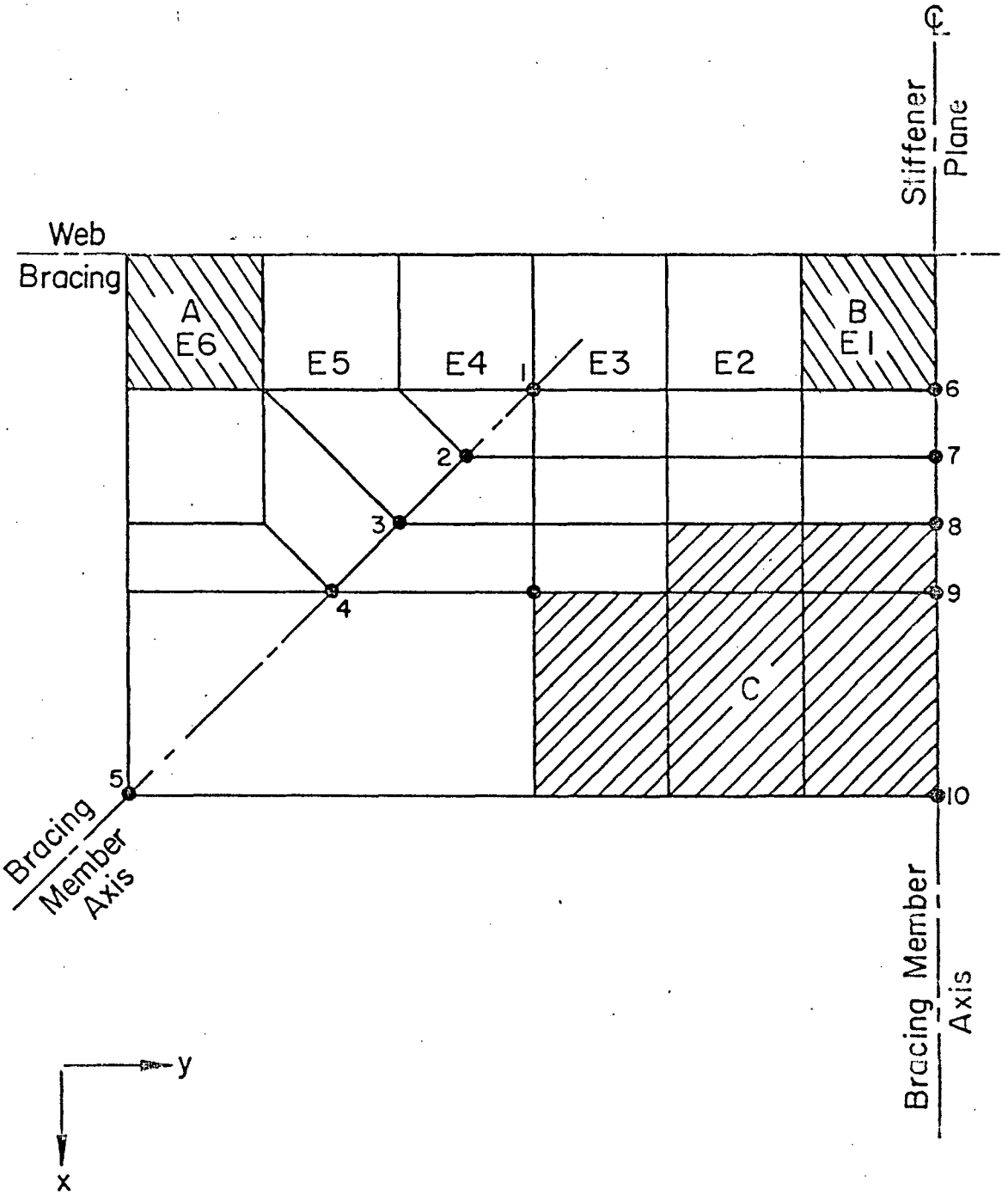

Fig. 325 Discretization used in the Study of the Effect of the Bracing-to-Gusset Connection Length

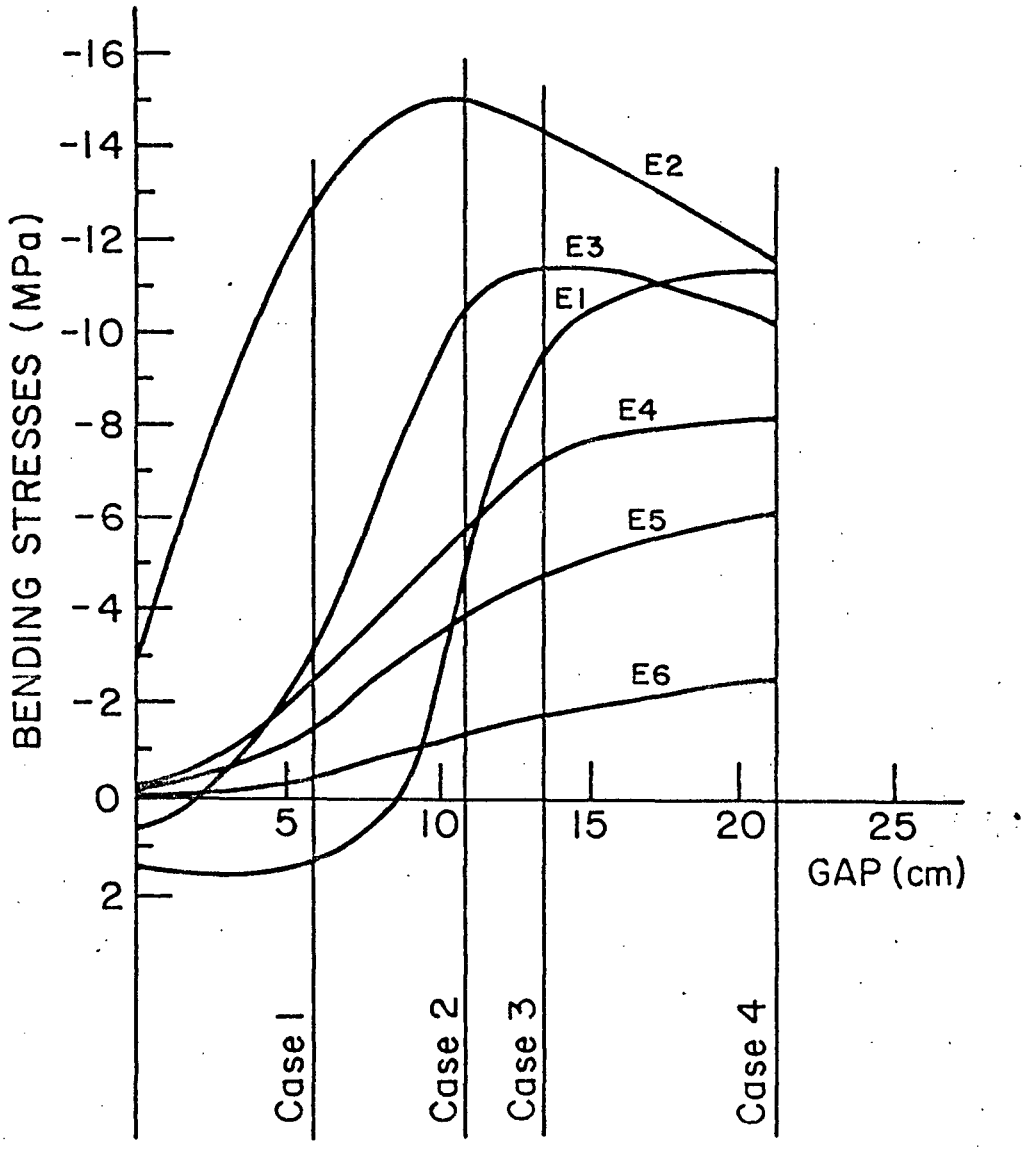

Fig. 326 Out-of-Plane Bending Stresses along Web-to-Gusset Weld (type 1)

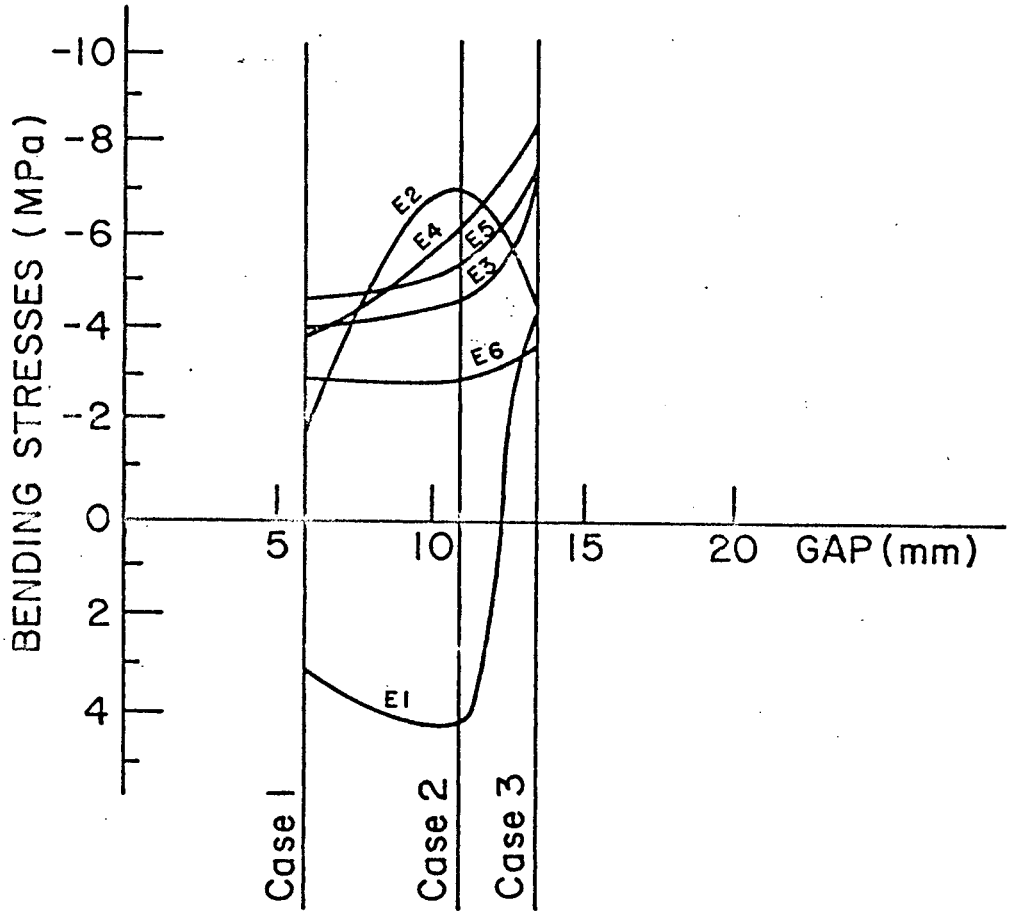

Fig. 326 (continued) Out-of-Plane Bending Stresses along Web-to-Gusset Weld (type 2)

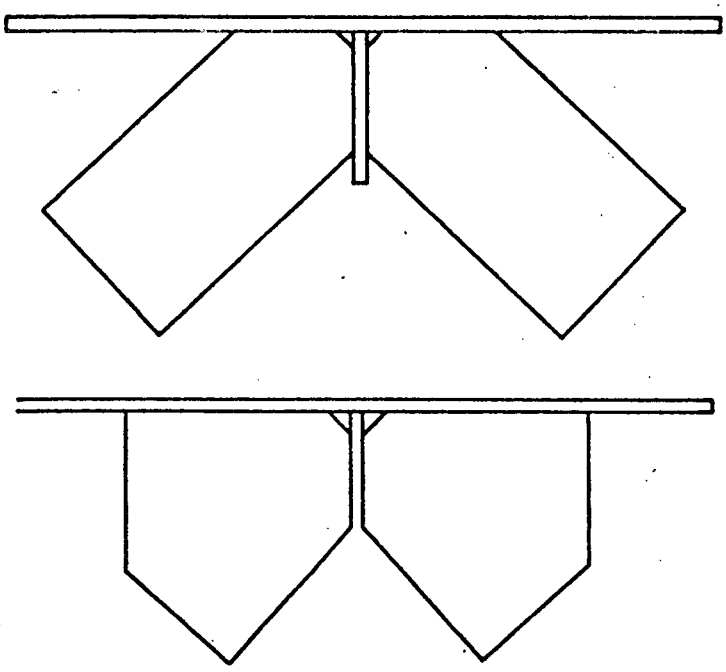

Fig. 327 Special Gusset Plates

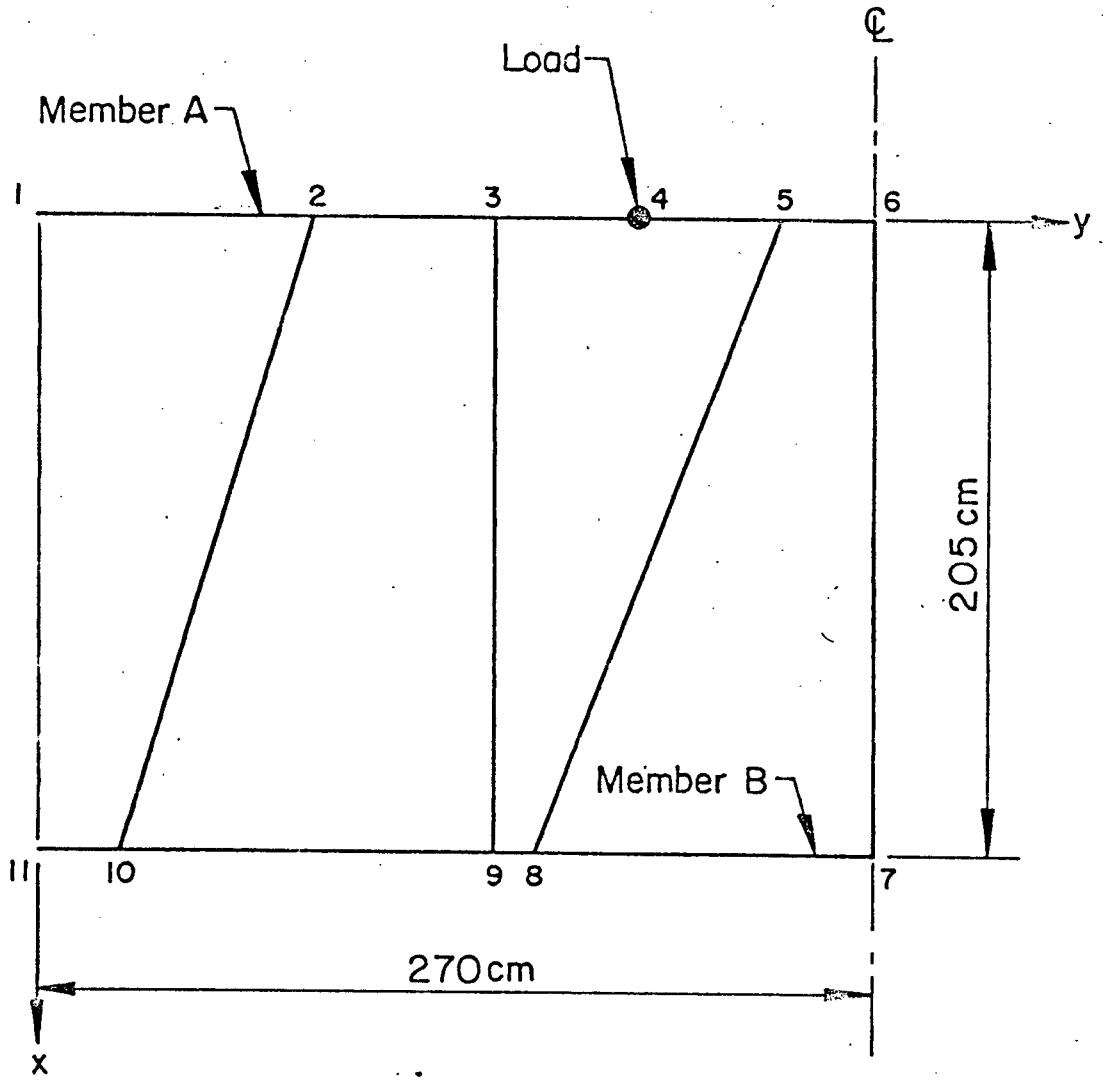

Fig. 328 Discretization used in the Study of the Effect of Relative Stiffness of the Two Parallel Girders

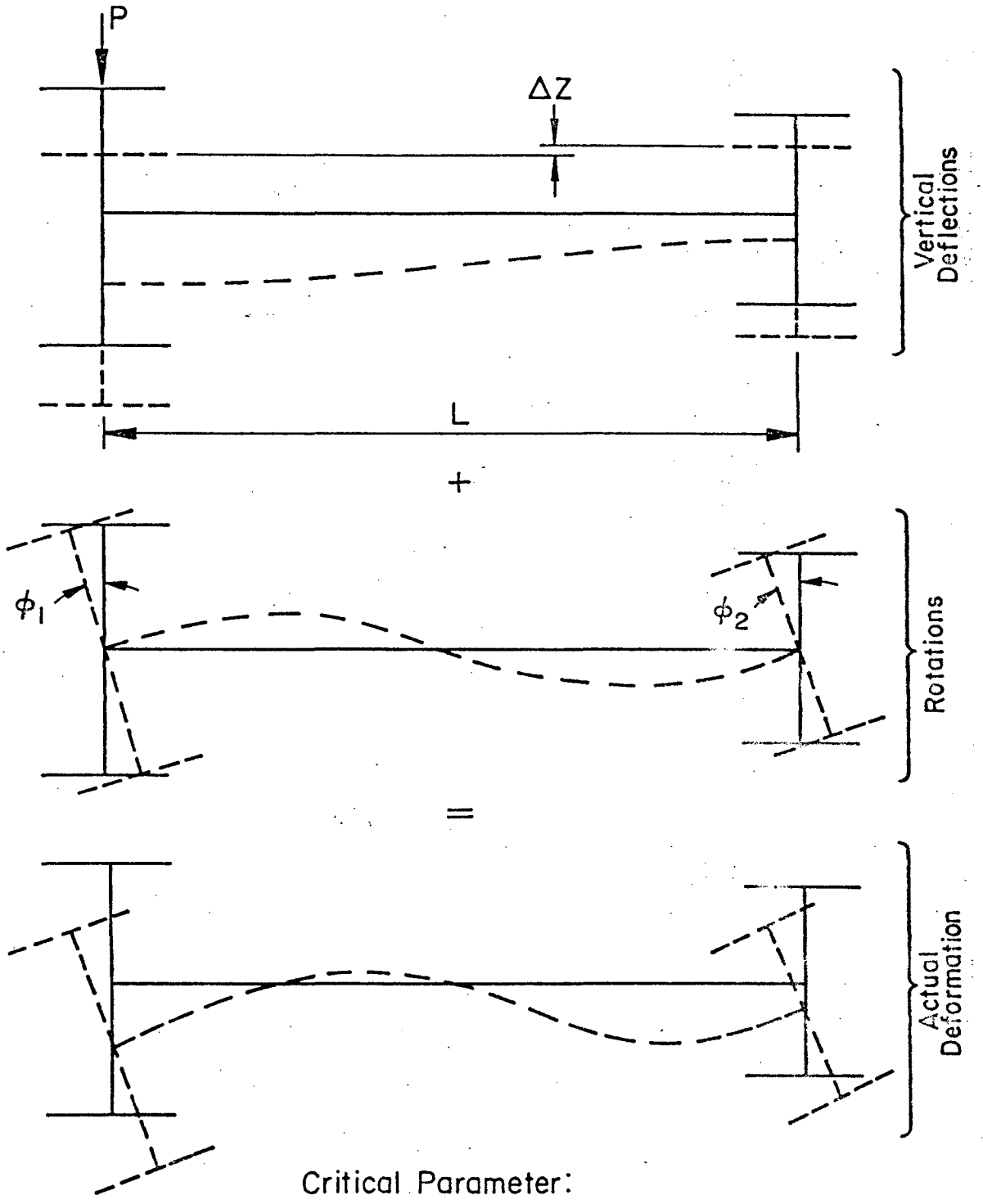

Critical Parameter:

$$\phi = \left|\frac{\Delta Z}{L}\right| - \left|\phi_1\right| - \left|\phi_2\right|$$

Fig. 329 Definition of Critical Parameter φ

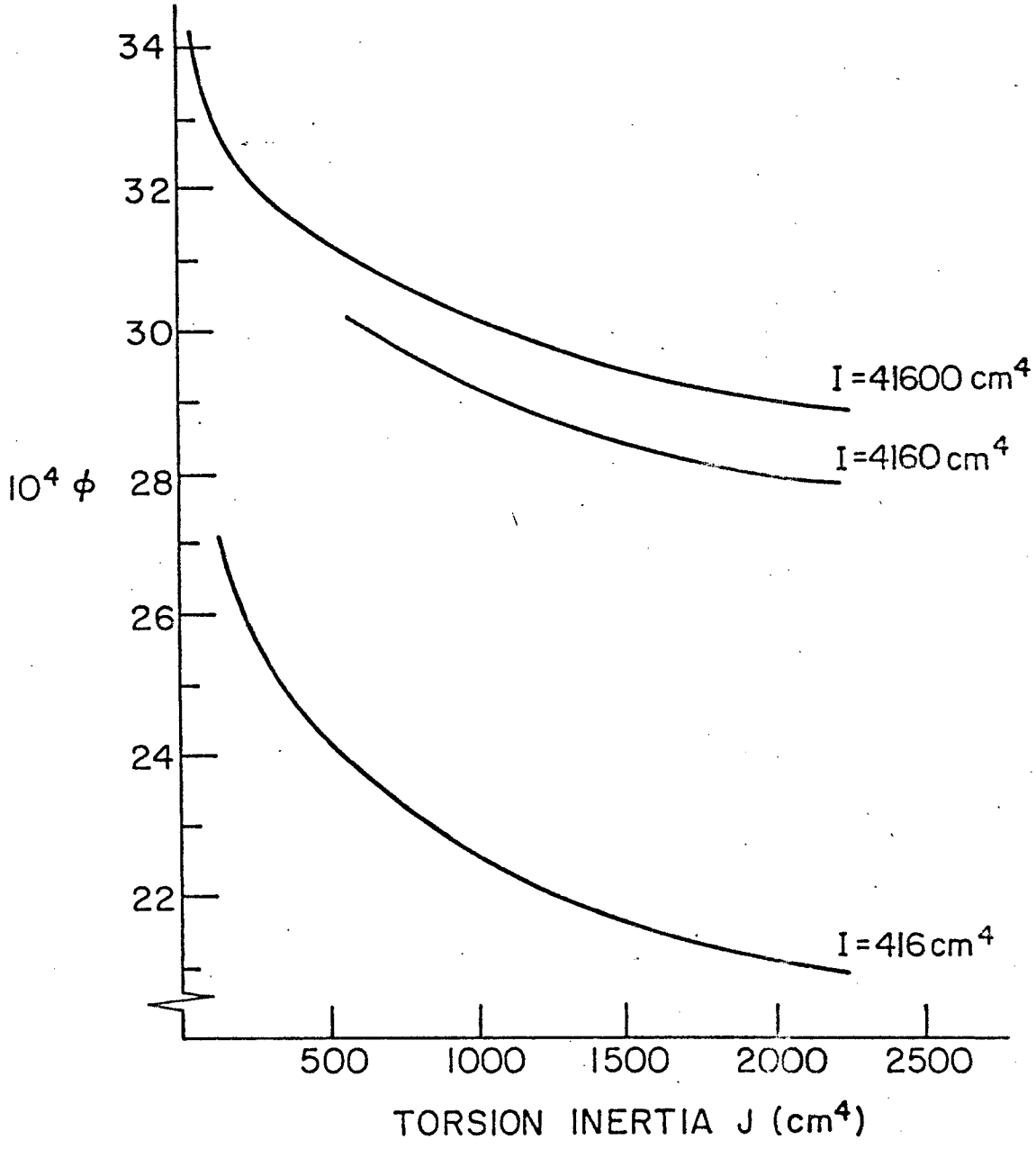

Fig. 330 Effect of Relative Stiffness of the Two Parallel Girders

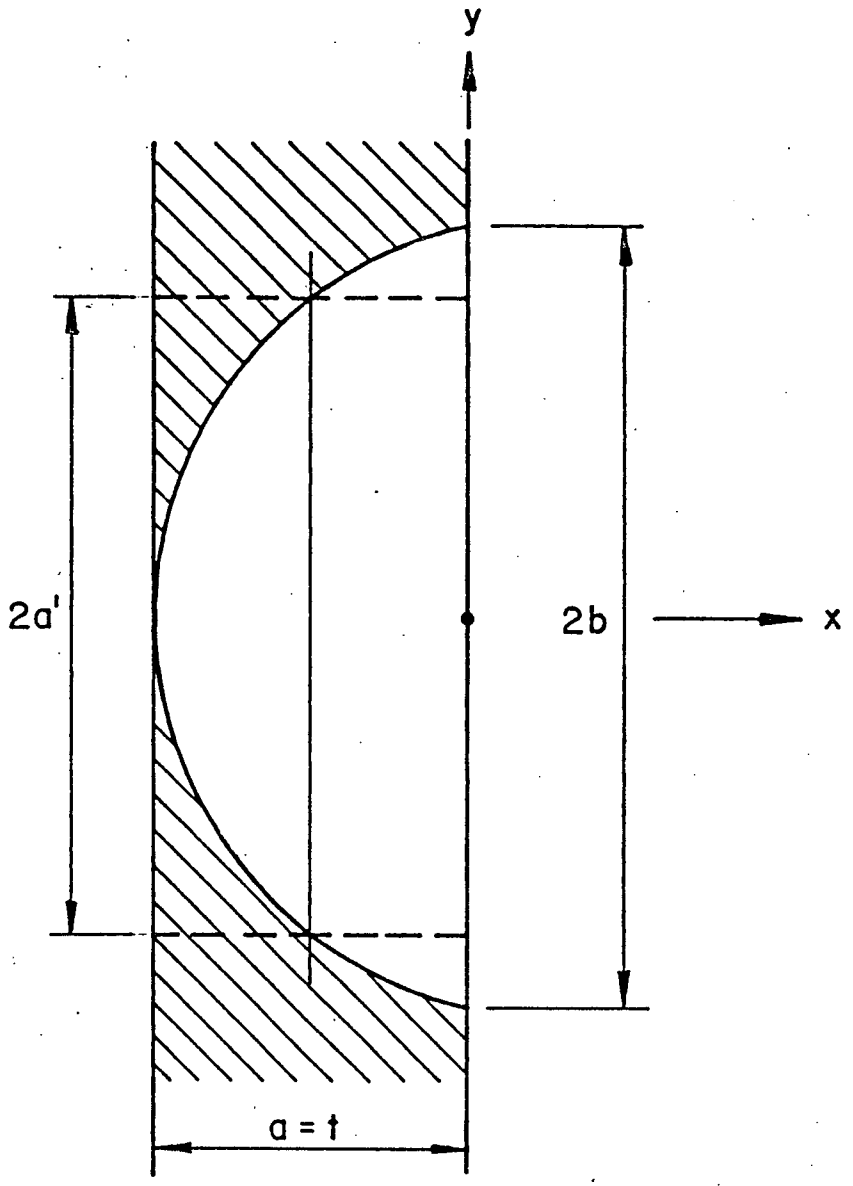

Fig. 331 Assumed Through-Thickness Crack Shape

6. REFERENCES

1. Fisher, J. W., Frank, K. H., Hirt, M. A. and McNamee, B. M. EFFECT OF WELDMENTS ON THE FATIGUE STRENGTH OF STEEL BEAMS, NCHRP Report No. 102, Highway Research Board, National Academy of Science, National Research Council, Washington, D. C., 1970.

2. Fisher, J. W., Albrecht, P. A., Yen, B. T., Klingerman, D. J. and McNamee, B. M., FATIGUE STRENGTH OF STEEL BEAMS WITH WELDED STIFFENERS AND ATTACHMENTS, NCHRP Report No. 147, Transportation Research Board, National Research Council, Washington, D. C., 1974.

3. Standard Specifications for Highway Bridges AASHTO, Washington, D. C., 1978.

4. Fisher, J. W. BRIDGE FATIGUE GUIDE - DESIGN AND DETAILS, AISC, 1977.

5. Paris, P. D., Gomez, M. P. and Anderson, W. E. A RATIONAL ANALYTICAL THEORY OF FATIGUE, The Trend in Engineering, University of Washington, Vol. 13, No. 1, January 1961.

6. Zettlemoyer, N. STRESS CONCENTRATION AND FATIGUE OF WELDED DETAILS, Ph.D. Dissertation, F.E.L., Lehigh University, 1976.

7. Albrecht, P. and Yamada, K. RAPID CALCULATION OF STRESS INTENSITY FACTORS, Paper submitted for publication in the Journal of the Structural Division, ASCE.

8. Bathe, K-J., Wilson, E. L. and Peterson, F. E. SAP IV - A STRUCTURAL ANALYSIS PROGRAM FOR STATIC AND DYNAMIC RESPONSE OF LINEAR SYSTEMS, Earthquake Engineering Research Center, Report No. EERC 73-11, June 1973; revised April 1974, College of Engineering, University of California, Berkeley.

9. Irwin, G. R. THE CRACK EXTENSION FORCE FOR A PART THROUGH CRACK IN A PLATE, Transactions, ASME, Journal of Applied Mechanics, Vol. 29, No. 4, 1962.

10. Shah, R. C., Kobayashi, A. S. ON THE SURFACE FLAW PROBLEM, Proceedings, Winter Annual Meeting of the American Society of Mechanical Engineers, New York, N. Y., November 1972.

11. Boyer, K. D., Fisher, J. W., Irwin, G. R., Roberts, R., Krishna, G. V., Morf, U. and Slockbower, R. E.
FRACTURE ANALYSES OF FULL SIZE BEAMS WITH WELDED LATERAL ATTACHMENTS, Federal Highway Administration, FHWA-RD-77-170, December 1977.

12. Maddox, S. J.
AN ANALYSIS OF FATIGUE CRACKS IN FILLET WELDED JOINTS, International Journal of Fracture Mechanics, Vol. 11, No. 2, April 1975, p. 221.

13. Tada, H. and Irwin, G. R.
K-VALUE ANALYSIS FOR CRACKS IN BRIDGE STRUCTURES, Fritz Engineering Laboratory Report No. 399-1, Lehigh University, Bethlehem, Pa., June 1975.

14. Rolfe, S. T. and Barsom, J. M.
FRACTURE AND FATIGUE CONTROL IN STRUCTURES - APPLICATIONS OF FRACTURE MECHANICS, Prentice-Hall, Inc., Englewood Cliffs, New Jersey, 1977.

15. Tada, H., Paris, P. C. and Irwin, G. R.
THE STRESS ANALYSIS OF CRACKS HANDBOOK, Del Research Corporation, Hellertown, Pa., 1973.

16. McEvily, A. J., Jr.
ON THE ROLE OF DEFECTS IN CRACK INITIATION IN WELDED STRUCTURES, Proceedings, Japan-U.S. Seminar on Significance of Defects in Welded Structures, Tokyo, 1973.

17. Signes, E. G., Baker, R. G., Harrison, J. D. and Burdekin, F. M.
FACTORS AFFECTING THE FATIGUE STRENGTH OF WELDED HIGH STRENGTH STEELS, British Welding Journal, Vol. 14, March 1967.

18. Watkinson, F., Bodger, P. H. and Harrison, J. D.
THE FATIGUE STRENGTH OF STEEL JOINTS AND METHODS FOR ITS IMPROVEMENT, Proceedings, Fatigue of Welded Structures Conference, The Welding Institute, England, July 1970.

19. Fisher, J. W. and Irwin, G. R.
FRACTURE ANALYSIS OF FLAWS IN WELDED BRIDGE STRUCTURES, Proceedings, Japan-U.S. Seminar on Significance of Defects in Welded Structures, Tokyo, 1973.

20. Barsom, J. M.
FATIGUE CRACK PROPAGATION IN STEELS OF VARIOUS YIELD STRENGTHS, U. S. Steel Corporation, Applied Research Laboratory, Monroeville, Pa., 1971.

21. Bardell, G. R. Kulak, G. L.
FATIGUE BEHAVIOR OF STEEL BEAMS WITH WELDED DETAILS, Structural Engineering Report No. 72, Department of Civil Engineering, the University of Alberta, Edmonton, Alberta, September 1978.

22. Hirt, M. A. and Fisher, J. W.
FATIGUE CRACK GROWTH IN WELDED BEAMS, Engineering Fracture Mechanics, Vol. 5, 1973, p. 415.

23. Maddox, S. J.
FATIGUE CRACK PROPAGATION DATA OBTAINED FROM PARENT PLATE, WELD METAL AND HAZ IN STRUCTURAL STEELS, Welding Institute Report No. E/48/72, Cambridge, England, 1972.

24. Maddox, S. J.
ASSESSING THE SIGNIFICANCE OF FLAWS IN WELDS SUBJECT TO FATIGUE, Welding Journal, Vol. 53, No. 9, September 1974.

25. Maddox, S. J.
AN ANALYSIS OF FATIGUE CRACK IN FILLET WELDED JOINTS, International Journal of Fracture, Vol. 11, No. 2, April 1975.

26. Popov, E. P.
MECHANICS OF MATERIALS, Prentice-Hall, Englewood Cliffs, New Jersey, 1952.